

**MATERIALS, DESIGN AND PROCESSING OF AIR
ENCAPSULATED MEMS PACKAGING**

A Dissertation
Presented to
The Academic Faculty

by

Nathan T. Fritz

In Partial Fulfillment
of the Requirements for the Degree
Doctor of Philosophy in the
School of Chemical & Biomolecular Engineering

Georgia Institute of Technology
May 2012

**MATERIALS, DESIGN AND PROCESSING OF AIR
ENCAPSULATED MEMS PACKAGING**

Approved by:

Dr. Sue Ann Bidstrup Allen, Advisor
School of Chemical & Biomolecular
Engineering
Georgia Institute of Technology

Dr. Paul A. Kohl, Advisor
School of Chemical & Biomolecular
Engineering
Georgia Institute of Technology

Dr. Samuel Graham
School of Mechanical Engineering
Georgia Institute of Technology

Dr. Dennis W. Hess
School of Chemical & Biomolecular
Engineering
Georgia Institute of Technology

Dr. Michael Filler
School of Chemical & Biomolecular
Engineering
Georgia Institute of Technology

Dr. Peter Hesketh
School of Mechanical Engineering
Georgia Institute of Technology

Date Approved: December 15, 2011

In dedication to my loving parents Maynard and Peggy Fritz

ACKNOWLEDGEMENTS

I would like to express sincere gratitude to my thesis advisors, Prof. Paul Kohl and Prof. Sue Ann Bidstrup Allen for their advice, support, and encouragement during my time at Georgia Tech. I would also thank my thesis committee members Prof. Dennis Hess, Prof. Michael Filler, Prof. Samuel Graham, and Prof. Peter Hesketh for their helpful input during my Ph.D. I would also give a very special thank you to all my current and past group members who have helped make my time at Georgia Tech such a wonderful experience. Thank you in particular to Dr. Rajarshi Saha, Dr. Yu-Chun Chen, Dr. Venmathy Rajarathinam, Greg Ostrowicki, and Dr. Hyo-Chol Koo for all their help with the work presented in this thesis and my undergraduate research assistants Huy Dao, Zachary Wilson, Felice Yeow and Lisa Thornsberry for their assistance with running experiments. I would also like to thank Daphne Perry who goes above and beyond her duty to ensure that everything in the Kohl Group runs smoothly.

Thank you to the MiRC Cleanroom staff Gary Spinner, Charlie Suh, Tran-Vinh Nguyen, Devin Brown, William Kimes, Ben Hollerbach, John Pham, Walter Henderson, Eric Woods, Gregory Book, and Mikkel Thomas for all their assistance throughout my time in the cleanroom. Thank you to Dr. Farrokh Ayazi and Xin Gao for their insight and work on fabrication and testing MEMS devices. Thank you also to Promerus LLC and Sumitomo Bakelite for their insight and support. Finally I would like to thank my family for all of their encouragement.

TABLE OF CONTENTS

	Page
ACKNOWLEDGEMENTS	iv
LIST OF TABLES	vii
LIST OF FIGURES	viii
SUMMARY	xiii
<u>CHAPTER</u>	
1 Project Motivation	1
1.2 Introduction	1
1.2 Research Objectives	6
2 Packaging Background	9
2.1 Wafer-level Package	9
2.2 Chip-level Package	11
2.3 Packaging Materials	13
2.4 Metallization in Packaging	16
3 Wafer-level MEMS Package	19
3.1 Introduction	19
3.2 Experimental and Material Selection	19
3.3 Results and Discussion	24
3.4 Conclusion	35
4 Chip-level MEMS Package	36
4.1 Introduction	36
4.2 Experimental	37
4.3 Results and Discussion	38

4.4 Conclusion	48
5 Photodefineable Epoxycyclohexyl Polyhedral Oligomeric Silsesquioxane: Properties and Characterization	49
5.1 Introduction	49
5.2 Experimental	51
5.3 Results and Discussion	54
5.4 Conclusion	70
6 Polycarbonates as Temporary Adhesives	71
6.1 Introduction	71
6.2 Experimental and Material Selection	72
6.3 Results and Discussion	74
6.4 Conclusion	86
7 Electroless Deposition of Copper and Silver	87
7.1 Introduction	87
7.2 Experimental and Material Selection	90
7.3 Results and Discussion	91
7.4 Conclusion	103
8 Microfabrication Challenges and Summary	104
8.1 Feasibility and Challenges	104
8.1.1 MEMS Packaging	104
8.1.2 Packaging Materials and Processes	107
8.2 Summary and Conclusions	110
REFERENCES	113

LIST OF TABLES

	Page
Table 1.1 Approximate size of the mechanical portion of a MEMs device.	3
Table 3.1 A list of cavity-sizes and metal overcoats used in this work.	23
Table 3.2 Cavity deflection under nano-indentation. Cavity strength (low deflection) can be improved by using thicker metal overcoats. (40% solvent) could be used.	33
Table 4.1 Numerical values for the bulge equation (4.1) for a 20 μm wide cavity and a 0.7 μm Al overcoat.	43
Table 5.1 POSS etch rates and selectivity in 250 W O_2 plasma with different CHF_3 concentrations. The Selectivity is for a polypropylene carbonate etch rate of 0.66 $\mu\text{m}/\text{min}$.	65
Table 6.1 Solubility chart for polycarbonates. D= Dissolved, S=Swelled, and I=inert.	79
Table 6.2 Average adhesive strengths for bonded polycarbonates and tapes.	82
Table 6.3 Average adhesive strengths in wafer debonding for polycarbonate residues and UV exposed tapes.	86
Table 7.1 Bath formulations for electroless silver.	94
Table 7.2 Bath formulations for electroless copper.	95

LIST OF FIGURES

	Page
Figure 1.1 The market growth for MEMS technologies 2007-2012 by device.	2
Figure 1.2 Example devices by shape. (a) gyroscope (circle), (b) accelerometer (square), (c) piezoresonator (rectangle).	4
Figure 1.3 Schematics of traditional wafer level packages. (a) Cap-and-seal package using a wafer lid and a getter for sealing. (b) Canopy-and-seal package using a patterned silicon oxide, followed by a deposited canopy, the oxide is then etched out using HF and the cavity is sealed with a getter.	5
Figure 2.1 Schematics of epoxy molding processes. (a) Injection molding. (b) Compression molding.	12
Figure 2.2 The chemical structure of epoxycyclohexyl POSS cage $(C_8H_{13}O_2)_n(SiO_{1.5})_n$ when $n=8$.	15
Figure 3.1 Dynamic TGA at 5°C/min showing the effect of a 3 wt.% PAG loading on PPC.	21
Figure 3.2 Schematic of the fabrication process for a MEMS package cavity. (a) Fabricated MEMS device. (b) Spin coat PPC and POSS layers. (c) Pattern POSS mask. (d, e) Pattern PPC using the POSS mask in RIE. (f) Apply Overcoat material. (g) Decompose PPC and cure polymers. (h) Evaporate Al layer.	22
Figure 3.3 Air-cavities formed on smaller simulated devices show debris-free decomposition. (a) Diced sample. (b) focused ion beam cross-sectioned sample.	26

Figure 3.4	Cracked overcoat after decomposition for large cavities (a). Prevent overcoat thermomechanical failure, (b) a thicker overcoat (40% solvent) or (c) multiple (X5) spin-coats of conventional (60% solvent) could be used.	28
Figure 3.5	Decomposition of PPC to form air-cavities. (a) Incomplete decomposition through thick overcoat reveals presence of PPC. (b) Higher decomposition temperature causes overcoat cracking due to pressure build-up. (c) Optimized time and temperature leads to mechanically robust, stable and clean cavities.	30
Figure 3.6	Large air-cavities to package piezoelectric devices. These simulated devices have wider trench-widths and uneven topography. The overcoat after decomposition remains stable and the air-cavities are clean.	31
Figure 3.7	Nanoindentation of cavities show complete collapse at 4 mN for a 20 μm wide cavity with a 1 μm aluminum overcoat (inlay shows nanoindentation spot on the cavity). The deflection of the overcoat decreases as the Al thickness increases or if its replaced by copper (Table 3.2).	32
Figure 3.8	A packaged capacitive resonator device. (a) Device shows clean sensing electrode. (b) Device performance was measured successfully.	34
Figure 4.1	(a) A 20 μm wide with 1 μm Al overcoat cavity stays intact under 4 MPa compression molding. (b) A 50 μm wide cavity completely collapses under 10 MPa compression molding but (c) sustains the same pressure with a 3 μm copper overcoat undergoing 0.5 μm deflection.	39

Figure 4.2	Normalized stress profiles of compressed cavities with a 0.7 μm Al overcoat.	41
Figure 4.3	Schematic of a standard rectangular bulge test. (Equation 4.1)	42
Figure 4.4	(a) FEM simulation of a 3 μm Cu overcoated 40 μm cavity under 10 atm of pressure. (b) FEM simulation of a 3 μm Cu overcoated 40 μm cavity with 30° slanted side walls under 10 atm of pressure.	44
Figure 4.5	Isothermal TGA of polycarbonates to be decomposed in 8 hours.	46
Figure 4.6	Cross-sectioned in-situ decomposition/cure chip level packages. (a) 2 mm diameter, 18 μm tall cavity formed by PPC decomposition at 190°C. (b) 2 mm diameter, 12 μm tall cavity formed by PEC decomposition at 185°C.	48
Figure 5.1	Spin speed curves for POSS films from 40 and 60 wt% of POSS in solution.	55
Figure 5.2	Contrast curve for photodefined epoxycyclohexyl POSS of 1 μm thickness.	56
Figure 5.3	Changes in the absorption coefficient for the POSS film over the wavelengths 225-500 nm.	58
Figure 5.4	SEM images of 10 μm thick photodefined POSS. (a) Arrays of photodefined POSS lines ranging from 5 to 50 μm width with equal lines and spaces. (b) Array of 50 μm wide POSS lines.	60
Figure 5.5	Thermal gravimetric analysis of POSS film to 500 °C at a ramp rate of 1 °C/min.	62

Figure 5.6	(a) SEM image of a 3 μ m thick line of polypropylene carbonate with a 1 μ m patterned POSS mask after an O ₂ plasma RIE. (b) A schematic of the patterned PPC/POSS line.	66
Figure 5.7	(a) SEM image of a cavity utilizing a POSS mask with an Avatrel 200P overcoat. The width of the cavity is 50 μ m and has a height of 3 μ m. (b) A close up of the corner of the cavity in (a). The POSS mask, Avatrel 2000P overcoat and aluminum cap have been identified and measured.	68
Figure 5.8	An all POSS overcoat cavity designed for a resonator. A 1 μ m Al layer is on top of the 2 μ m POSS overcoat. The trenches in the wafer show where the resonator would be located.	69
Figure 6.1	Structure of polycarbonates. (a) Polyethylene carbonate, PEC. (b) Polypropylene carbonate, PPC. (c) Polycyclohexene carbonate, PCC.	73
Figure 6.2	Dynamic thermal gravimetric analysis of polycarbonates ramped at 1°C/min.	77
Figure 6.3	Dynamic TGA showing the effects of PAG on decomposition temperature.	78
Figure 6.4	Spin speed curves for PCC and PPC/PCC formulations.	80
Figure 6.5	Result of a single PPC 90 degree peel test.	81
Figure 6.6	Peel test results from optimization of bonding temperature for PPC adhesive.	83
Figure 6.7	Peel test results from optimization of bonding pressure for PPC adhesive.	84

Figure 7.1	Mechanism of phenol-novolac etching prior to Sn-Pd activation.	88
Figure 7.2	Electroless copper deposition on the treated POSS surface and a portion of the cross hatch test.	99
Figure 7.3	SEM of electroless copper deposited on the sidewalls of TSVs. The copper on the top surface was polished off.	102

SUMMARY

This work uses a three-dimensional air cavity technology to improve the fabrication, and functionality of microelectronics devices, performance of on-board transmission lines, and packaging of micro-electromechanical systems (MEMS). The air cavity process makes use of the decomposition of a patterned sacrificial polymer followed by the diffusion of its by-products through a curing polymer overcoat to obtain the embedded air structure. Applications and research of air cavities have focused on simple designs that concentrate on the size and functionality of the particular device. However, a lack of guidelines for fabrication, materials used, and structural design has led to mechanical stability issues and processing refinements.

This work investigates improved air gap cavities for use in MEMS packaging processes, resulting in fewer fabrication flaws and lower cost. The identification of new materials, such as novel photo-definable organic/inorganic hybrid polymers, was studied for increased strength and rigidity due to their glass-like structure. A novel epoxy polyhedral oligomeric silsesquioxane (POSS) material was investigated and characterized for use as a photodefineable, permanent dielectrics with improved mechanical properties. The POSS material improved the air gap fabrication because it served as a high-selectivity etch mask for patterning sacrificial materials as well as a cavity overcoat material with improved rigidity. An investigation of overcoat thickness and decomposition kinetics provided a fundamental understanding of the properties that impart mechanical stability to cavities of different shape and volume. Metallization of the cavities was investigated so as to provide hermetic sealing and improved cavity strength. The improved air cavity, wafer-level packages were tested using resonator-type devices

and chip-level lead frame packaging. The air cavity package was molded under traditional lead frame molding pressures and tested for mechanical integrity. The development of mechanical models complimented the experimental studies. A model of the overcoat materials used the film properties and elastic deformations to study the stress-strain behavior of the suspended dielectric films under external forces. The experimental molding tests and mechanical models were used to establish processing conditions and physical designs for the cavities as a function of cavity size. A novel, metal-free chip package was investigated combining the in-situ thermal decomposition of the sacrificial material during post-mold curing of the lead frame molding compound. Sacrificial materials were characterized for their degree of decomposition during the molding cure to provide a chip package with improved mechanical support and no size restrictions.

Improvements to the air cavities for MEMS packaging led to investigations and refinements of other microfabrication processes. The sacrificial polycarbonate materials were shown to be useful as temporary bonding materials for wafer-level bonding. The release temperature and conditions of the processed wafer can be changed based on the polycarbonates formulation. The electroless deposition of metal was investigated as an alternative process for metalizing the air cavities. The deposition of silver and copper using a Sn/Ag catalyst as a replacement for costly palladium activation was demonstrated. The electroless deposition was tested on polymer and silicon dioxide surfaces for organic boards and through-silicon vias.

CHAPTER 1

PROJECT MOTIVATION

1.1 Introduction

Traditional semiconductor microelectronic components, e.g. integrated circuits (IC), are thin-film, planar devices. High-aspect ratio, three-dimensional (3D) structures can provide new functionality, such as in micro-electromechanical systems (MEMS). Such 3D structures perform functions other than logic and memory, such as sensing. A particular area of interest is the fabrication of 3D air cavity structures by means of a sacrificial, place-holder material [1-3]. An air-cavity can be constructed by using processes involving the patterning of a thermally or photochemically decomposable sacrificial material followed by the application of a gas permeable, overcoat layer. When the sacrificial polymer is decomposed, the reaction by-products permeate through the overcoat leaving an enclosed air cavity. This process allows one to use standard photolithography and relatively low-temperature processes to fabricate structures in a cost-effective manner. These 3D structures can be incorporated into the design of on-chip and/or on-board components. The processes can be changed easily to tailor unique geometric structures such as bridges, tunnels, channels, arches, boxes, and bubbles. The air cavity structures could be used in applications such as low dielectric transmission lines [4], microfluidic channels [5-7], and encapsulation packaging [8-11].

One particular application of the air-cavity approach to packaging that would benefit from this research is in the packaging of 3D MEM devices. MEMs devices have

become an important technology. Figure 1.1 shows how the market growth of MEMs will increase over the next few years such as resonators, accelerometers, and gyroscopes [12].

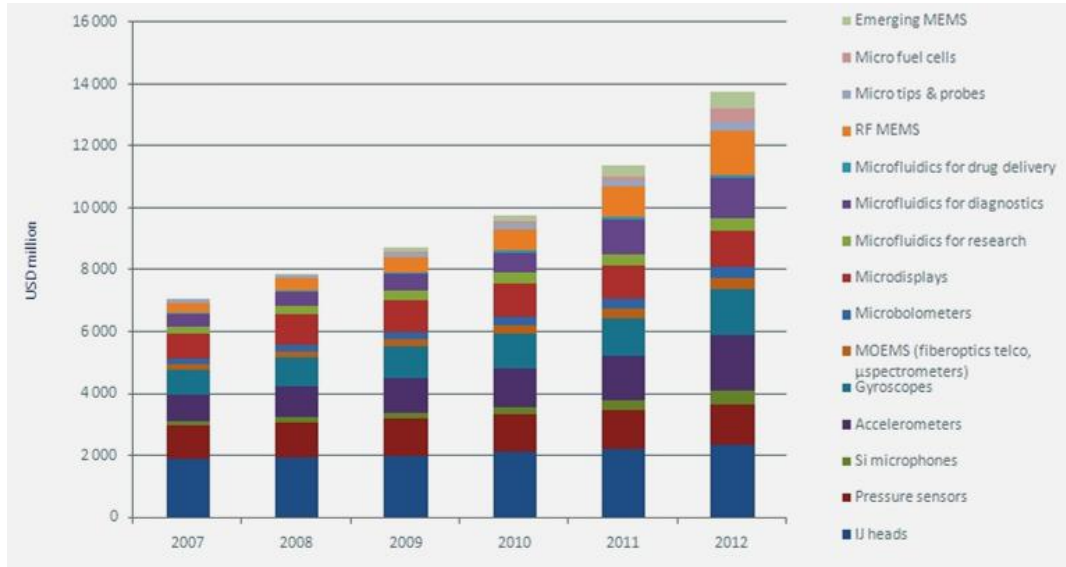


Figure 1.1: The market growth for MEMs technologies 2007-2012 by device [12].

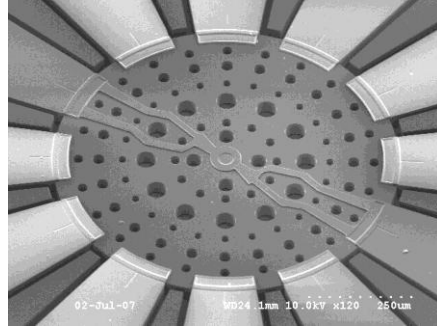
This growth will require improvements on current MEMs technologies and the development of new devices. There is a critical need for high-quality, low-cost packaging for these MEMS devices, analogous to how plastic packaging became a critical enabling technology for commodity integrated circuits. MEMs devices can range in size (Table 1.1) and can require specific environments based on the device. The device size may be adjusted for fabrication purposes such as ease of release or for operational purposes such as adjustment of size for frequency of resonation and capacitance. A piezoresistive device requires a low stress package because the device operation can drift from the designed response with the application of suitable forces [13]. A device designed to operate based on a change in capacitance generally has low electrical signal strength, small device features, and narrow trenches. The small signal requires the device to be in close proximity to the integrated circuits it works with. The devices often require vacuum

packaging to maintain that signal that would be influence by molecular dampening of the device due its small features, other devices may require only a hermetic seal to protect from humidity or corrosive materials that may dampen the device mechanics or destroy the device. The devices listed in Table 1.1 may be made using capacitive, piezoresistive, or other technologies. All of these devices generally require hermetic sealing.

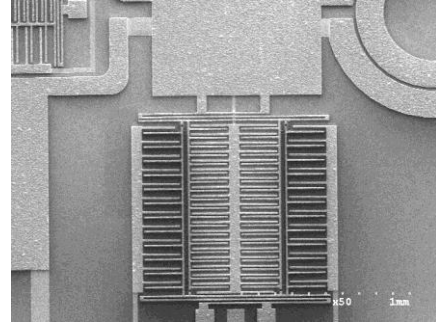
Table 1.1: Approximate size of the mechanical portion of a MEMs device [9, 11, 14-19].

Device type	Size range
Resonators	10 μm – 500 μm
Accelerometers	250 μm – 3 mm
Gyroscope	750 μm – 1cm

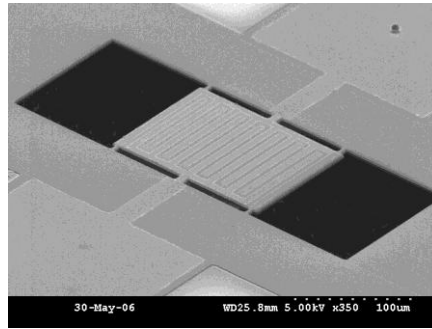
The shapes of devices (Figure 1.2) can also vary widely. For example, gyroscopes are generally circles and accelerometers are rectangles. The size and shape of the devices are determined during the design of the device for optimal performance. However, few considerations are made for the package dimensions and requirements.



(a)



(b)



(c)

Figure 1.2: Example of MEMS devices by shape. (a) gyroscope (circle), (b) accelerometer (square), (c) piezoresonator (rectangle) [19].

Traditional electronic packaging approaches are not used to encapsulate 3D structures and are often not appropriate because of cost and spatial constraints. For typical MEMS-based products, packaging expense can be as high as 20% to 40% of the products total material and assembly cost [20]. The package requires increased functionality such as low stress packaging for piezoelectric functioning devices, hermetic sealing for vacuum sealing, or preventing atmosphere contamination. The device functionality requires additional packaging attributes provided by the materials and construction that can limit the device performance and testing for the finished package. The harsh effects of dicing may also cause damage before device testing [13]. These constraints have led to single chip packaging methods, rather than low-cost batch

packaging. Developing a wafer-level package using low-cost integrated circuit packaging would decrease the cost by allowing the devices to be tested before chip-level packaging. Several types of wafer-level packages (Figure 1.3) using cap-and-seal methods have been developed and are used in industry [13, 17, 21].



Figure 1.3: Schematics of traditional wafer-level packages. (a) Cap-and-seal package using a wafer lid and a getter for sealing. (b) Canopy-and-seal package using a patterned silicon oxide, followed by a deposited canopy, the oxide is then etched out using HF and the cavity is sealed with a getter.

These packaging methods are usually mechanically robust due to the rigid materials used in their construction. However, wafer-to-wafer alignment, high temperature deposition, and aggressive etching processes cause these approaches to be overly complex and expensive. The use of an air cavity approach would help solve these problems in wafer-level MEMS packaging. If an encapsulating air cavity can be employed to protect the MEMS structure, then the MEMS device can be treated like a commodity, low-cost 2D electronic device, and high-volume integrated circuit packaging can be employed. However, it is very important that the protecting air cavity maintain its shape during an injection molding process for chip level packaging in order to avoid impairment of the mechanical component of the MEMS device.

1.2 Research Objectives

MEMs packaging is an ideal test-bed for studying new materials and mechanical reliability of air cavity structures. The testing of several different device designs will allow testing of structures of different geometries (circles and rectangles) and size (micrometers to millimeters). Devices of different shapes and sizes may be fabricated on the same wafer, increasing the need for mechanical stability over a variety of shapes and sizes. Air cavities can be tested for collapse under pressure in traditional chip level packaging processes not typically seen in air cavity board technology.

An in-depth study into the materials, processing and air cavity design could provide a broader architectural approach to solving the chemical and mechanical problems. Development and characterization of new materials and structure will help to improve the mechanical reliability. The properties of the overcoat materials can be important in the design and ultimate function of the structure by providing hermeticity, hydrophobicity, low dielectric constant, and rigidity, to name a few properties. However, the mechanical strength of the structures is critical, especially when pressure is applied to the device either during fabrication or use. Mechanical rigidity is a function of size, geometry, and material properties. The dimensions of the overcoat material are highly dependent on the size and design of the air cavity as well as the material itself.

One example of a possible material is the development and use of a spin-coated, photosensitive, hybrid inorganic/organic dielectric. Such a material could combine the desirable deposition and processing aspects of organic materials and the hardness and etch resistance of inorganic overcoat materials. The use of an epoxy polyhedral oligomeric silsesquioxane (POSS) as a cross-linked film will provide a mechanically

rigid overcoat. This novel POSS material provides a rigid overcoat material ideal for cavity fabrication.

The MEMS package fabrication process was optimized to not only protect the appropriate MEMS functionality but also to maximize the support during processing and minimize stress points and defects in the package structure. The thicknesses of the sacrificial and overcoat material were optimized for thin, rigid structures. The decomposition was set for a stepwise approach to avoid rupture of the cavity. Air cavities needed testing to withstand chip level packaging molding conditions. The development of a mechanical model with appropriate experimental verification of cavity properties provided a means of designing the correct dimensions, geometry, materials, and processing limitations (ex. maximum pressure load) for particular applications. Wafer level package functionality testing on capacitance resonator devices provided assessment of the package for its intended use.

It is important to recognize general advancements in microfabrication technologies that occur through the optimization of the air cavity process. Investigation of the sacrificial materials demonstrated that polycarbonates provided a high quality film and could be decomposed at different temperatures depending on the formulation. While polycarbonates play an important role as a place holder in 3D packaging structures, their film properties and decomposition allow for them to be tested for use as temporary adhesives in wafer-wafer bonding. The temporary adhesives can be used for wafer thinning processes used in MEMS, solar cells, and IC chip packaging. Thin silicon substrates have improved heat dissipation, flexibility, reduced electrical resistance and 3D stacking capabilities. The development of the POSS material provided a new rigid

dielectric material for board applications. However, cost effective metallization practices are important in its use. The development of a palladium-free, silver and copper electroless deposition process can lower the cost of board processes, through silicon via (TSV) processes, and metallization of the air cavity MEMs packages. Improvements can be made by determining the optimal electroless deposition and adhesion of copper and silver on epoxy board, silicon dioxide and POSS for metallization in the air cavity process as well as general microelectronic packaging processes.

CHAPTER 2

PACKAGING BACKGROUND

2.1 Wafer-level Package

Recent applications in MEMS technology have expanded its applications and potential market use [22]. While certain MEMS devices require special conditions for operation, a cost efficient, IC-compatible packaging process would significantly improve the cost and application for a variety of MEMS devices.

There are various wafer level packaging methods available commercially. Wafer level packaging methods include interfacial bonding of a pyrex glass lid, which has a similar coefficient of thermal expansion to silicon [21]. The lid is anodically bonded to the MEMS wafer at approximately 400°C by applying a negative voltage to the glass. Other interfacial bonding methods include plasma-activated bonding. Electrical feed-throughs are made through a via in the lid wafer. Bonding with intermediate melting materials, such as low melting temperature glass and solder have also been used [21]. These bonding techniques can be applied to a non-planar surface and hence lateral electrical feed-through, which results in a non-planar surface, can be used. MEMS devices can also be encapsulated using surface micromachining [21]. The cavity surrounding the MEMS device can be formed by wet etching a sacrificial layer, and the openings needed for removal of the temporary placeholder material are plugged by deposition of a sealing material. A vacuum cavity is required for some MEMS devices, such as resonators and infrared sensors. Electrical feed-through structures required for

electrical interconnection are indispensable for wafer level packaging and must be considered when designing the hermetic packages [21].

Air gap structures have been used in micro and nanosurface micromachining processes for fabricating MEMS and nanoelectromechanical systems (NEMS) capable of in-plane and through-plane motion [23]. These cavity structures use a low temperature, thermally decomposable sacrificial material, especially desirable for isolating electrical and mechanical parts. The overcoat material on these structures should be tolerant of stress and temperature effects and offer a convenient diffusion path for the decomposition by-products. Furthermore, a metal overcoat is often necessary for hermetic sealing and increased mechanical strength of the air cavity [24]. Overall, the materials for sacrificial layer, overcoat and hermetic seal should be compatible with existing processes and offer good layer-to-layer adhesion.

Numerous reports of wafer level packaging of MEMS structures using air-cavity technology have been published. Joseph et al. used the decomposition of Unity^R 2303 polymer (a commercial sacrificial material, Promerus LLC) through a thin SiO₂ film to fabricate an air cavity and package MEMS resonators [9]. The processing protocol is complex because an oxide mask is first used to pattern the Unity layer. An oxide/Avatrel (polynorbornene dielectric, Promerus LLC) overcoat was used for mechanical strength and to expose the bond pads. Similar methods were used to package varactors and accelerometers. An improvement in the performance of the MEMS devices was observed after packaging with this air-cavity approach [25]. Monajemi et al. successfully packaged a wide range of MEMS devices using both photodefinable and non-photodefinable Unity to form the air cavity. However, photodefinable Unity was found to leave a residue from

the photo-active compound after decomposition which could affect the performance of the device [26]. Raeis-Zadeh et al. packaged a tunable inductor using Unity and Avatrel (overcoat); however, a separate material was used to pattern the sacrificial polymer [27]. Reed et al. developed a compliant wafer-level process containing air-cavities that offer high on-chip current and enable terabit/s bandwidth [28].

2.2 Chip-level Package

Current chip-level MEMS packaging can be costly. The packages usually consist of large, bulky, metal packages to account for environmental conditions required for device operation. These packages tend to be costly with expensive materials, one-by-one packaging and testing not seen in the IC industry. The wafer level packaging technology for MEMS devices discussed previously is crucial for transforming the MEMS device into a form compatible with IC packaging processes. Once the MEMS device is compatible with lead frame or other IC packages, it could be packaged at commercial chip packaging houses and receive all the cost and scale benefits they offer. Utilizing the IC packaging industry would vastly improve the cost and expand the application for a large variety of MEMS devices. Standard packaging techniques would more easily allow the heterogeneous integration of MEMS devices with ICs because MEMS devices could be handled and treated just like an IC in multi-chip ball grid array (BGA) packages. Lead frame packaging is an ideal test bed for chip level testing as a mature cost efficient technology in IC packaging. The lead frame package has been used to package a wide variety of types and sizes of microelectronic devices and undergoes similar processes necessary for advanced chip packaging such as ball grid arrays and chip stacking. Lead

frame package is accomplished by attaching the device to a wire frame and using epoxy molding at high pressure to encapsulate it. Schematic drawings of compression and injection (transfer) molding of air cavity packages are shown in Figure 2.1. The injection molding process forces the epoxy molding compound (EMC) around the device in the mold. This is the traditional process for low-cost chip packaging and uses high molding pressures (e.g. 10 MPa). The compression molding process molds only the top side of the device and uses lower pressure than injection molding (e.g. 4 to 10 MPa). Compression molding is commonly used in chip stacking packages.

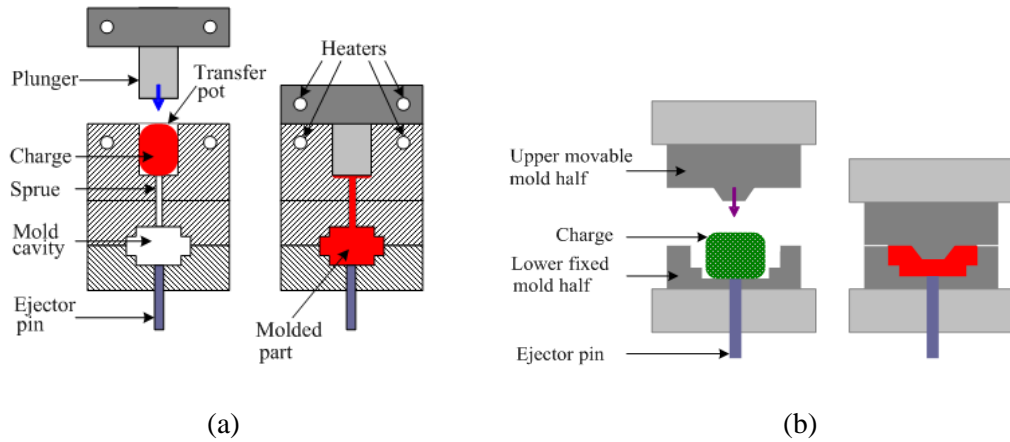


Figure 2.1: Schematics of epoxy molding processes [29]. (a) Injection molding. (b) Compression molding.

2.3 Packaging Materials

Determining the optimal material for a packaging process is necessary to reduce processing and cost as well as maximizing the necessary properties for the functionality. Many traditional materials can meet the demands of current devices, but new materials are required for next generation packaging to optimize strength, patterning, and dielectric constant. In general, there are three classifications of materials that can be used as a barrier film or layer in microelectronics and these include organic materials, inorganic materials, and hybrids.

Organic materials (polymers) can provide low impact deposition (usually spin coating). These materials can be functionalized to obtain some properties (i.e., hydrophobicity). Many organic films can be easily patterned through photodefinition for easy processing. However, many organic films have insufficient mechanical properties with modulus of less than 3 GPa. The films usually have trade-offs with low chemical resistance and thermal degradation depending on chemical structure. When used as a dry etch mask, the organic films have high selectivity with respect to inorganic compounds. For these reasons organic, films are limited in most top film applications.

Inorganic materials can be divided into two categories of electrically insulating or conducting. These materials have high elastic modulus, usually greater than 50 GPa, and excellent thermal stability properties. These materials have high plasma etch selectivity with respect to most organic materials. Inorganics can easily be etched by the appropriately chosen acid systems or by plasma conditions different from organic materials. Organic materials are plasma etched usually using an oxygen plasma producing carbon dioxide and water. The disadvantage of inorganic barriers is often cost.

Most inorganic films require costly plasma-assisted deposition systems. These systems require specialized high temperature, gaseous environments that could damage the underlying film. Deposited films are often brittle and under high residual stress, which results in cracks and poor adhesion. Inorganic materials can be difficult to pattern. In some cases, a photodefineable organic material can be used to transfer the pattern to the inorganic material, which limits pattern transfer to the bottom film to a tri-layer pattern system.

Some hybrid materials take advantage of both organic and inorganic materials. Depending on the combination and amount of organic components and glass components the material can have attributes of each material. Care must be taken when dealing with hybrids to obtain the required properties. Examples include sol-gel, spin on glasses, and functionalized POSS materials.

Sol gel materials tend to be monomers or low molecular weight oligomers that can crosslink into networks with low to moderate SiO_x content. These polymers can be deposited by spin coated and can be functionalized. The modulus can be varied over wide ranges. However, high modulus often results in films which are brittle or stressed with poor crack resistance. Dry etch selectivity is moderate but inconsistent with organic materials. The starting material can be a liquid at room temperature or a solid dissolved in a solvent. The low crack resistance limits the film thicknesses values, sometimes less than 1 μm . For this reason, most sol-gel materials are poor candidates for more than just coating materials.

Spin-on-glasses include materials such as hydrogen silsesquioxane (HSQ) and methyl silsesquioxane (MSQ). HSQ and MSQ have ladder-type or cage-type sheets of

SiO_x with methyl or hydrogen terminated corners. As a low-k material with good adhesion and thermal properties, they have played an important role in the microelectronics industry. These materials require advanced patterning techniques (they are not photosensitive) and can only be used in ultra thin form (less than 1 μm) since the internal stress causes cracks and mechanical failure.

One example of a possible material was the development and use of a spin-coated, photosensitive, hybrid inorganic/organic dielectric that combined desirable deposition and processing aspects of organic materials and the desirable aspects of inorganic overcoat materials. POSS is commonly used as a property enhancing additive in organic films. However, the use of the epoxy POSS as a pure film provides a mechanically rigid chemically resistant material. An example of the 8 cornered POSS functionalized with an epoxy group is shown in Figure 2.2.

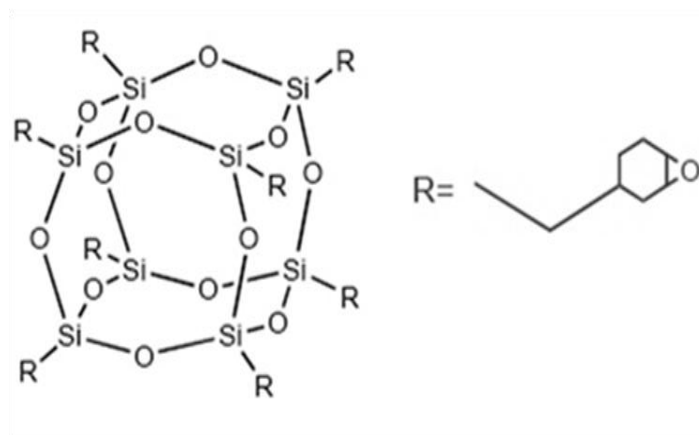


Figure 2.2: The chemical structure of epoxycyclohexyl POSS cage $(\text{C}_8\text{H}_{13}\text{O}_2)_n(\text{SiO}_{1.5})_n$ when $n=8$.

The POSS films investigated here would be similar to, but an improved version of the current spin-on-glasses. POSS can provide some of the same benefits as spin-on-glass,

but would be photo-patterned in thicker film due to the organic groups at the corners which could be used for 3D cross-linking at edge of the silicon oxide cage structure.

2.4 Metallization in Packaging

The major research focus for ICs has been on the increase in transistor integration density and its performance enhancement. However, now packaging is a bottleneck of overall system performance and cost [30]. One of the functions of electronic packaging is the electrical connection of multiple devices. Conventional packages usually have many conducting lines and inter-level vias within the structure separated by a dielectric material. Organic packaging is based on epoxy and Cu conducting lines formed by electroless deposition and/or electrodeposition.

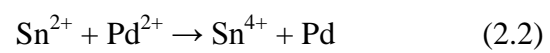
The interface between polymer and metal usually has high interfacial energy, and may have poor adhesion strength. The surface of the FR-4 board is modified by various methods to enhance adhesion. There are two major approaches: physical and chemical methods. The chemical method involves modification of the surface chemical groups to those that can form covalent or ionic bonds between the two materials. Physical adhesion methods increase of surface roughness of the substrate by swelling and chemical etching to induce anchoring between the metal film and the surface. This results in high surface roughness between the FR-4 board and Cu film, which is undesirable. High-frequency signals operating in the gigahertz range travel in the skin of the conductor due to the interaction with its own magnetic field [30]. The depth of the skin used for high frequency signal transfer can be estimated by Equation 2.1 [31].

$$\delta = \sqrt{\frac{2\rho}{\omega\mu}} \quad (2.1)$$

Where δ is skin depth, ρ is the resistivity of the conductor, ω is the angular frequency of current, and μ is the magnetic permeability of the conductor. At frequencies above a few GHz, the skin effect has significant impact if the surface is rough. The roughness could generate unacceptable loss and noise [30]. Therefore, the control of the surface roughness of the polymer board without losing adhesion strength is an important topic for packaging research.

Another serious issue is substrate warpage due to the difference in thermal expansion coefficient between polymer and chips [32-34]. Many thermal processes, including polymer curing and soldering could twist the structure and induce significant stress value to the interconnection part. The failures due to thermal stresses are the subject of many studies [32-34]. Also, the high dielectric constant of the FR-4 board would be a source of dielectric loss in high-frequency signals [30], which could be a serious issue and requires low-k dielectric substrates for high-performance applications.

Electroless deposition is based on the electron transfer between metal ion and reducing agent in the electrolyte. This is facilitated by catalyst particles on the substrate. The process is generally autocatalytic since the metal film itself acts as a catalyst for the reaction, so that continuous deposition can occur. In this deposition method, the most important point is how to form high density, catalytic particles which are adherent to the substrate. Sn-sensitization and Pd activation is the major technology for the formation of the catalyst on a variety of substrates. This technology uses adsorption of Sn (II) colloids followed by Pd activation. The replacement reaction between this Sn^{2+} and Pd^{2+} , results in the formation of Pd metal particles, Equation 2.2.



Pd has excellent catalytic activity for most electroless processes however, it is expensive.

CHAPTER 3

WAFER-LEVEL MEMS PACKAGE

3. 1 Introduction

In this work air cavities were fabricated for use as wafer-level MEMS packaging. Air cavities allow for a photolithography process capable of fabricating air/vacuum encapsulated structures over the entire wafer. This technology provides a cost efficient, low profile, wafer-level MEMS package that allows the device to be treated as an IC type device for further packaging. New materials and processing steps allow for the design of the air cavity technology to be used over a large range of MEMS device sizes. An improved overcoat material allowed for a non-photodefineable sacrificial material to be patterned using reactive ion etching for cleaner cavities. The overcoat thickness and decomposition recipe was optimized for a crack free and rigid cavity. Cavities were tested for mechanical strength as well as cleanliness before packaging a capacitance resonator.

3.2 Experimental and Material Selection

Polypropylene carbonate, PPC, was used as the sacrificial material. It is a copolymer of carbon dioxide and propylene oxide, polymerized at high pressure in the presence of catalyst [35]. High-purity forms of the PPC exist in regular, alternating units without ether-linkage impurities in the backbone. PPC decomposes by chain scission and unzipping mechanisms [36]. Decomposition proceeds via chain unzipping at low temperatures because the cyclic monomer is thermodynamically favored over the

straight-chain polymer [37]. At higher temperature, chain scission competes with the unzipping decomposition mechanism. PPC is an attractive sacrificial material for microelectronics because it decomposes cleanly into low-molecular-weight products with little residue in inert and oxygen-rich atmospheres [38]. Air cavities were formed by encapsulating PPC in a polymer dielectric and decomposing the PPC layer allowing the products to diffuse through the overcoat, thus leaving a gaseous void [22]. Several other polycarbonate systems were investigated for lower or higher decomposition properties. Additives, such as a photo acid generator (PAG), can be added to PPC to lower decomposition temperature. Figure 3.1 shows a dynamic thermal gravimetric analysis (TGA) of pure PPC and a 3 wt% PAG loaded PPC. The PAG material thermally decomposes into an acid decreasing the decomposition temperature of the PPC. When exposed to ultraviolet radiation, the acid is generated at a lower temperature catalyzing the PPC decomposition at temperatures as low as 100°C. Polyethylene carbonate (PEC) was investigated as a low temperature sacrificial material. PEC has similar physical properties to PPC and decomposes at 180°C.

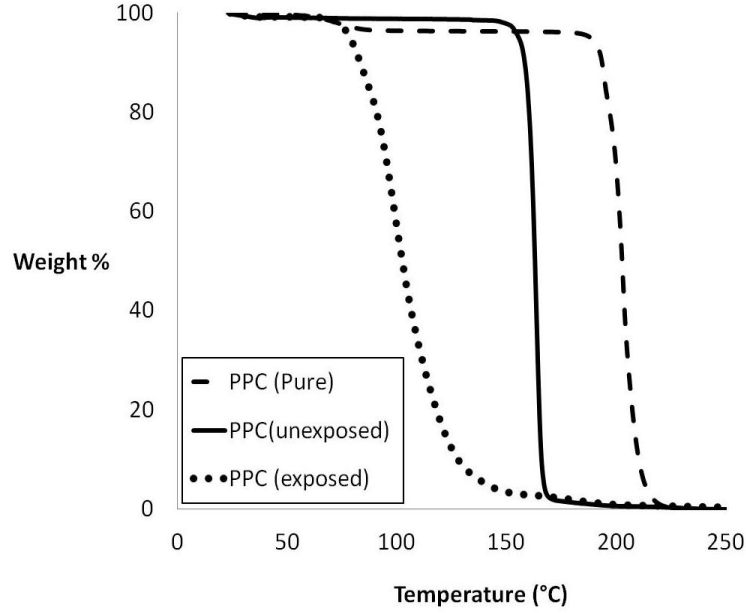


Figure 3.1: Dynamic TGA at 5°C/min showing the effect of a 3 wt.% PAG loading on PPC.

The properties of the overcoat material are important in the design of the air-cavity structure. The use of a spin-coated, photosensitive, hybrid inorganic/organic dielectric has been previously shown to be an effective overcoat material [22, 23, 39]. In this work, a photodefineable form of POSS was created by the addition of a photo-initiated catalyst to POSS. POSS was dissolved in mesitylene making a 40 wt% or 60 wt% solution. An iodonium photo-acid generator was added at 1 wt% of POSS and sensitizer at 0.33 wt% of POSS so as to make the formulation photosensitive at 365 nm. Deep trenches in 100 mm diameter (100) silicon wafers were etched using the Bosch process. These trenches resemble actual capacitive and piezoelectric MEMS devices that were fabricated. Trench widths varied between 2 and 6 μm , and the trench-depth was approximately 6 μm . Each device had in 2 to 6 trenches depending on the type of device and each wafer had several hundred devices. Wafer-level packaging was then carried out using the PPC/POSS material system. After completing the packaging steps, the wafers

were diced with a diamond saw and characterized using scanning electron microscopy (SEM), nano-indentation, and tape test for metal adhesion. A complete process flow is shown in Figure 3.2.

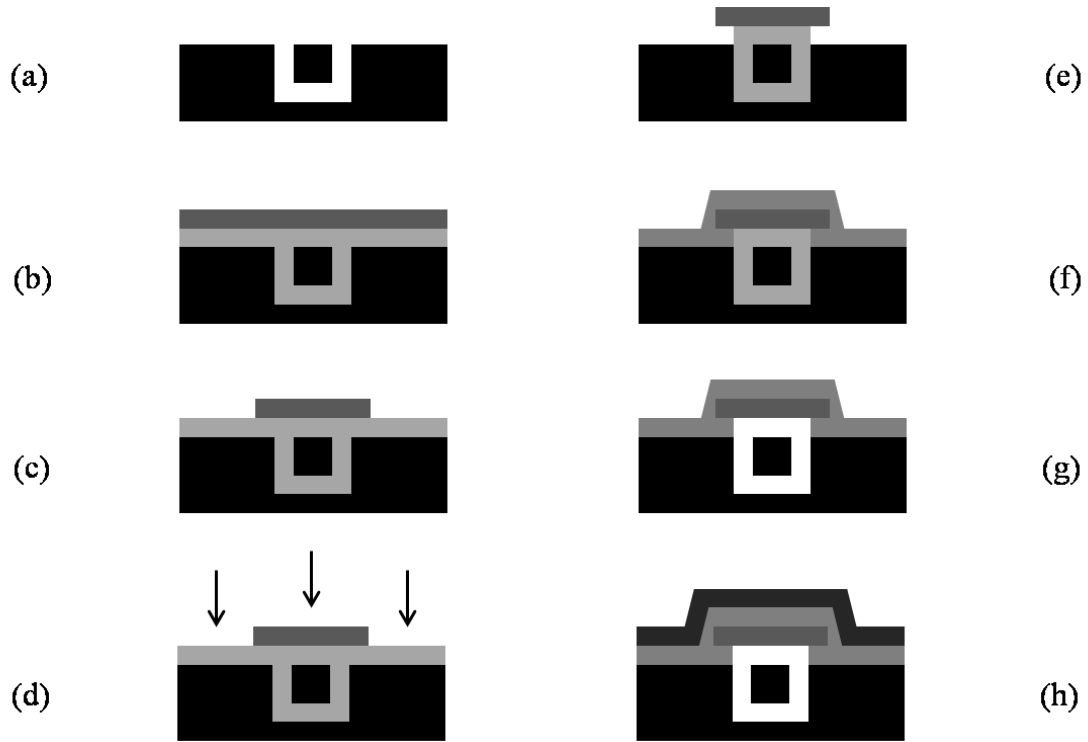


Figure 3.2: Schematic of the fabrication process for a MEMS package cavity. (a) Fabricated MEMS device. (b) Spin coat PPC and POSS layers. (c) Pattern POSS mask. (d, e) Pattern PPC using the POSS mask in RIE. (f) Apply Overcoat material. (g) Decompose PPC and cure polymers. (h) Evaporate Al layer.

PPC was initially spin-coated on the silicon trenches and soft-baked on a hot-plate at 100°C for 5 min. Several spin-coating steps were required for deeper and wider trenches. The PPC thickness varied between 3 and 4 μm after baking. For patterning the PPC, POSS was spin-coated at 4000 rpm resulting in a 0.6 μm thick film (Fig 3.2(b)). POSS was pre-baked at 85°C for 5 minutes, patterned at 365 nm and post-baked at 85°C for 5 min. POSS was spray developed using isopropyl alcohol (Fig. 3.2(c)) [39]. PPC was

reactive ion etched using a 6% CHF₃ and 94% O₂ plasma that resulted in a PPC/POSS etch rate selectivity of 24 (Fig. 3.2(d)). The PPC etch rate was 0.66 µm/min. The overcoat POSS was then spin coated to a thickness of 3 to 6 µm and patterned (Fig. 3.2(f)). Finally, the PPC was decomposed at 240°C for 4 to 10 hrs in a N₂ environment using a step-wise ramp-rate described elsewhere [1]. The wafers were subjected to a short duration oxygen plasma prior to metallization to improve metal-to-POSS adhesion. Aluminum was evaporated to a thickness of 0.7 µm and patterned to expose the electrode areas (Fig. 3(h)). For more rigid overcoats, Ti (50 nm) and Cu (1 to 3µm) were used instead of aluminum. Ti was the adhesion promoter for the copper metal overcoat. Different cavity-types with dimensions and overcoat thickness are tabulated in Table 3.1.

Table 3.1: A list of cavity-sizes and metal overcoats used in this work

Simulated devices	Width (µm)	Length (µm)	Metal overcoat (µm)
Capacitive (small) resonator	10-50	300-400	Al: 0.7µm, Cu: 1.5µm
Capacitive (large) resonator	50-150	300-400	Al: 0.7µm, 2µm, Cu: 1.5µm
Piezoelectric resonator	150-200	300-400	Cu: 1.5µm

After fabrication, the individual packages were inspected for thermo-mechanical cracking at the edges using a Hitachi FE3500 SEM. Close inspection of the trenches was done using a focused ion beam (FIB) (FEI Nova Nanolab) sectioning tool. The wafer was diced, and the shape and cleanliness of the cross-section examined. The small and large devices were diced and inspected. Nano-indentation was carried out to assess the mechanical strength of the cavities. A pressure test was developed using a Hysitron nano-indenter and a previous protocol for a bubble test used in sea-of leads fabrication [40].

The nano-indenter used a 20 μm diameter conospherical tip. The test location at the center of 30 to 50 μm wide cavities did not encounter resistance from the side-walls during experimentation. The cavities were indented at room temperature to a force of 8.5 mN. A cross-hatch tape test was used to determine the adhesion strength of thicker metal overcoats [41]. After the tape has been applied and pulled off, the cut area was then inspected and rated.

The packaging protocol thus developed has been successfully verified on an actual capacitive resonator approximately 100 X 400 μm in size. The electrical performance of the device was evaluated after packaging.

3.3 Results and Discussion

The first samples studied were smaller devices packaged using 40% POSS as the masking material for patterning the PPC sacrificial material and the cavity overcoat material. The cavity width was varied between 20 and 50 μm and the length varied between 200 and 600 μm . To prevent cavity cracking or rupture, the PPC decomposition process was modified from a constant thermal ramp rate to a constant weight percent decomposition rate [1]. The constant rate of decomposition allows for the more orderly diffusion of decomposition products through the overcoat avoiding high internal pressures. Thermogravimetric analysis of the polymer was used to determine the parameters for the constant rate of decomposition [1]. The reaction kinetics can be expressed as the nth order Arrhenius relationship, as shown in Equation 3.1.

$$r = Ae^{\frac{-Ea}{RT}}(1 - rt)^n \quad (3.1)$$

Where r is the decomposition rate, A is pre-exponential factor, E_a is the activation energy (kJ/mol), T is the temperature (K), and t is time (s). The decomposition reaction was determined to be first order ($n=1$) with a pre-exponential factor (A) and activation energy (E_a) of $9 \times 10^{12} \text{ min}^{-1}$ and 120 kJ/mol, respectively. Eq. 3.1 can be rearranged for temperature (T) vs. decomposition time (t) as shown in Equation 3.2. A rate of 0.25 wt.%/min for the decomposition was used to decompose the PPC. No degradation of the cavities was observed.

$$T = \frac{E_a}{R} \left[\ln \frac{A(1-rt)^n}{r} \right]^{-1} \quad (3.2)$$

The SEM cross-sections are shown in Figure 3.3(a) and 3.3(b) and exhibit debris-free cavities with robust, sturdy overcoats. The overcoat stability allowed the cavity to retain the shape of the original PPC structure under the overcoat. Close inspection of the trenches using FIB, Fig. 3.3(b), also showed clean cavities.

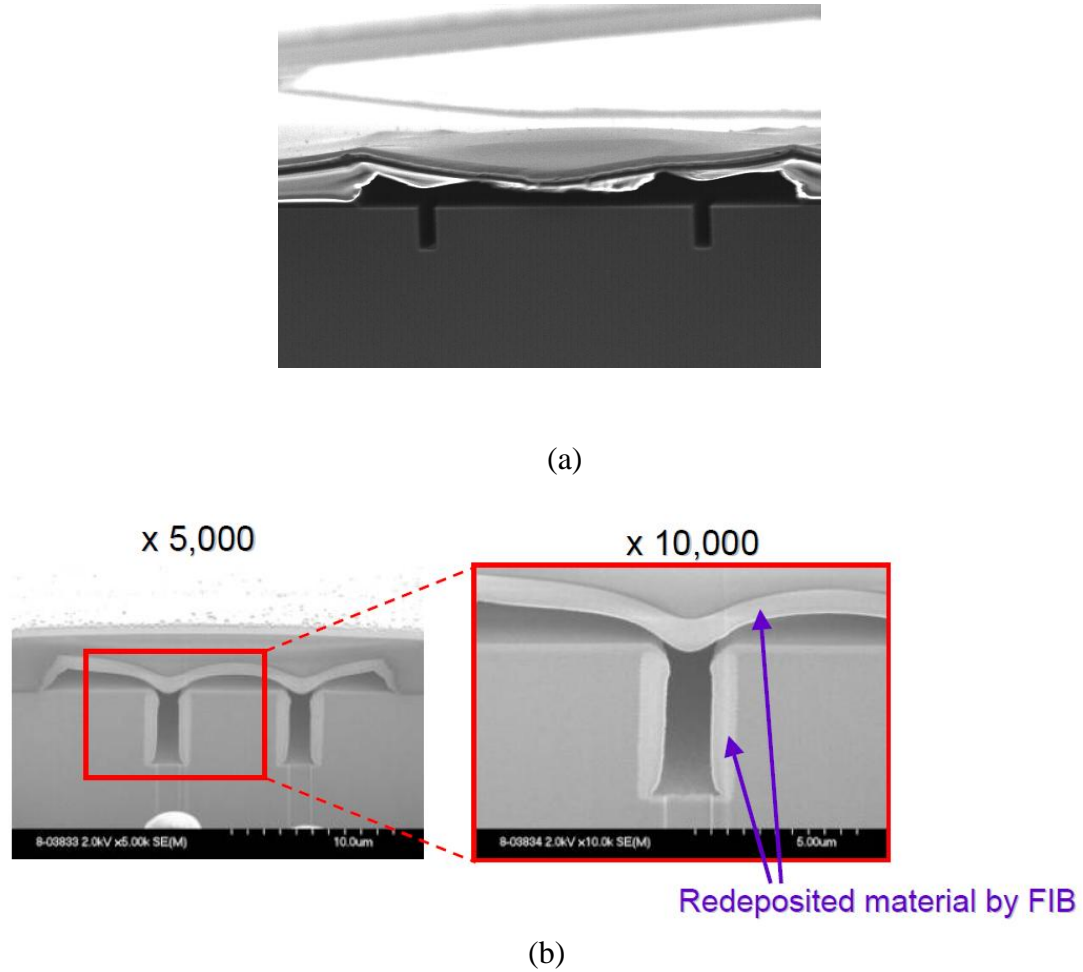


Figure 3.3: Air-cavities formed on smaller simulated devices show debris-free decomposition. (a) Diced sample. (b) Focused ion beam cross-sectioned sample.

Apart from the inadvertent deposition of material from the FIB, the trenches were debris-free. PPC can form non-uniform shapes during spin-coating which leads to occasional dips within the overcoat just above the trench. Such dips will not affect the functionality of the MEMS devices as long as the overcoat does not come in contact with the device area. However; since the cavity height is reduced above the trench, these areas remain vulnerable during contact or injection molding. Also, these dips become larger if the trench width is increased. Adjusting the PPC thickness by changing the polymer viscosity and spin-coat conditions can mitigate non-planar problems. Spin-coating

multiple layers followed by drying (i.e. soft baking) at room temperature can improve the amount of reflow into the trench. The room temperature soft bake prevents thermal reflow of the PPC into the trench and the multiple layers improve planarization of the device features.

The overcoat formulation was adjusted for different cavity dimensions to provide better uniformity. For large cavities ($>100\text{ }\mu\text{m}$ wide), thin overcoat layers tend to crack during PPC decomposition, and the overcoat is unable to provide the mechanical strength necessary to support the cavity, as shown in Figure 3.4(a).

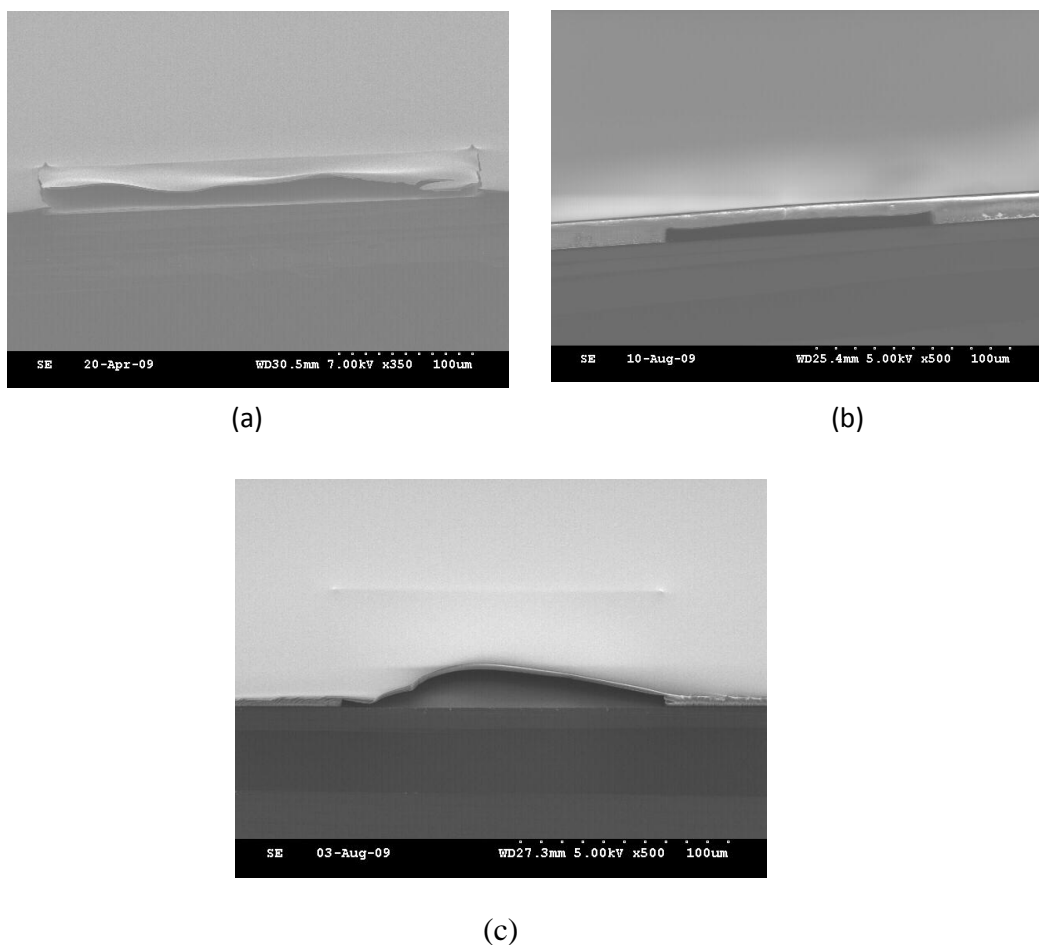


Figure 3.4: Cracked overcoat after decomposition for large cavities (a). To prevent overcoat thermomechanical failure, (b) a thicker overcoat (40% solvent) or (c) multiple (X5) spin-coats of conventional (60% solvent) could be used.

Changing the POSS-to-solvent ratio helps tune the properties of the overcoat. The polymer concentration was raised from 40% to 60% for better control of overcoat uniformity and thickness. The 60% POSS formulation results in a lower degree of film cracking (compared to 40% formulation) during thermal decomposition. The thicker film improves coverage and planarization on the edges of the cavity, as shown in Fig. 5(b). Alternatively, spin coating of multiple layers of the 40% POSS formulation produced a crack-free cavity with similar edge coverage to the 60% POSS while maintaining an overall thinner film as shown in Fig. 3.4(c). The decomposition ramp rate was lowered

when thicker overcoats were used so as to lower the pressure build-up. As shown in Figure 3.5(a), a 4 hr decomposition recipe is not long enough to fully decompose the PPC. Higher decomposition temperatures lead to cracking of the overcoat due to pressure build-up during decomposition, as shown in Fig. 3.5(b). A slow ramp-rate followed by a long temperature hold is necessary to form near-perfect air-cavities with sharp side-walls. In our experiments, a $0.5^{\circ}\text{C}/\text{min}$ ramp-rate and 6 to 8 hr hold at 240°C was necessary for cavities with widths from 50 to $150\text{ }\mu\text{m}$, Fig. 3.5(c).

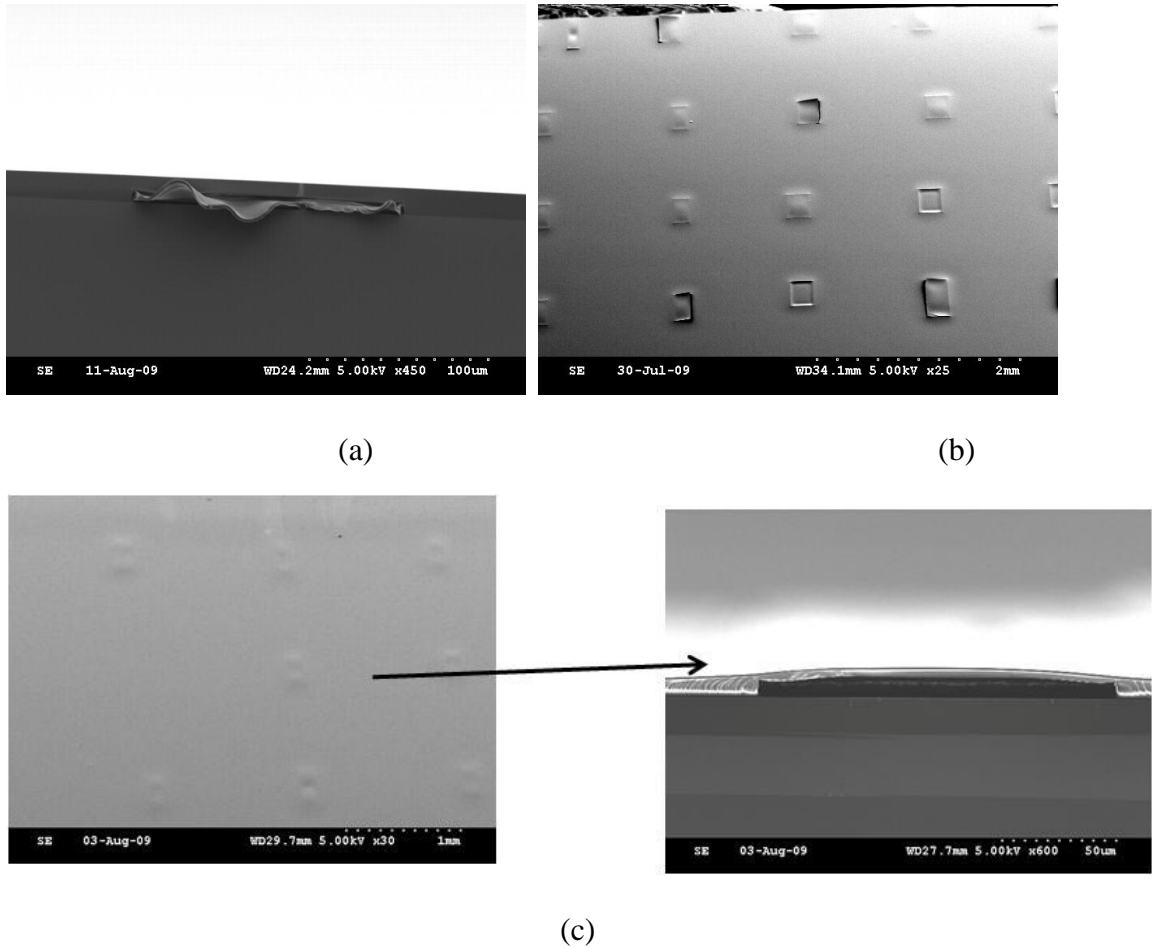


Figure 3.5: Decomposition of PPC to form air-cavities. (a) Incomplete decomposition through thick overcoat reveals PPC. (b) Higher decomposition temperature causes overcoat cracking due to pressure. (c) Optimized time and temperature leads to mechanically robust, stable and clean cavities.

The protocol for packaging capacitive resonators (~ 50 to $150 \times 400 \mu\text{m}$) had to be modified slightly to carry out wafer-level packaging of devices larger than 150 to $300 \times 400 \mu\text{m}$. Besides being quite large ($\sim 200 \mu\text{m}$ wide and 500 - $600 \mu\text{m}$ long), these devices had complex topography. By using a thicker overcoat (60% polymer) and multiple spin-coats we were able to successfully package such complex geometries after a 10 hour decomposition regime for the sacrificial polymer. The resulting cavities (Fig. 3.6) were found to be clean and mechanically stable. Hence, for smaller devices (less than $150 \mu\text{m}$ wide), multiple spin coats of 40% polymer with 6 to 8 hr decomposition times were adequate. However, devices with widths larger than $150 \mu\text{m}$ require multiple spin-coatings of 60% polymer mixtures with longer decomposition times. The decomposition time depends on the thickness of PPC. Wider cavities require thicker PPC films to prevent cavity collapse during decomposition or molding.

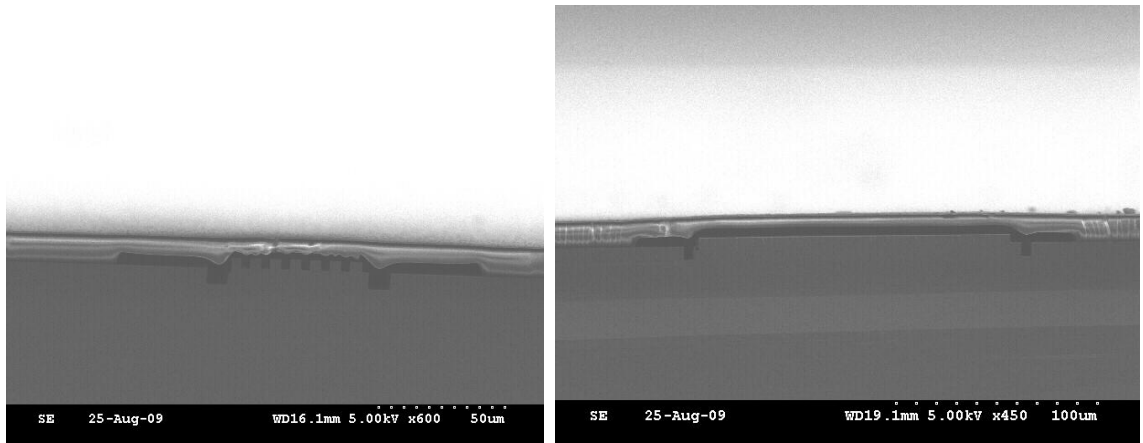


Figure 3.6: Large air cavities to package piezoelectric devices. These simulated devices have wider trench-widths and uneven topography. The overcoat after decomposition remains stable and the air-cavities are clean.

The robustness of the cavity overcoats was evaluated using nano-indentation. For a 3 μm POSS overcoat (40% POSS formulation) and 0.5 μm thick aluminum metallization, complete collapse for a 3.5 μm tall cavity was observed at 4 mN as shown in Figure 3.7.

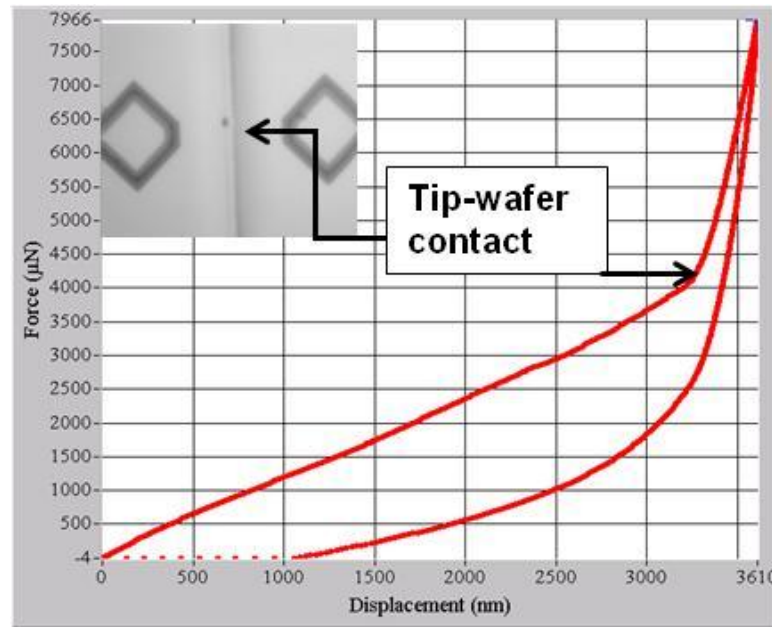


Figure 3.7: Nano-indentation of cavities show complete collapse at 4mN for a 20 μm wide cavity with a 1 μm aluminum overcoat (inlay shows nano-indentation spot on the cavity). The deflection of the overcoat decreases as the Al thickness increases or if replaced by copper (Table 3.2).

This translates to a cavity-strength of 51 MPa. Cavities with widths from 10 to 40 μm were tested. The tip was placed in the middle of the cavity to minimize side-wall effects. The nano-indentation results have been tabulated in Table 3.2. If the aluminum were replaced by 1.5 μm thick copper; the rigidity increases due to the higher elastic modulus of copper compared to aluminum. As shown in Table 3.2, the cavity deflects 1.3 μm at 8.46 mN. The deflection is similar to a 2 μm aluminum overcoat. The increase in rigidity can be analyzed using the analytical beam deflection equation where the force per unit

length (P) is uniformly distributed across a beam with width (w), thickness (t), and an effective modulus (E_{eff}), Equation 3.3 [42].

$$d = \frac{5Pw^3}{32E_{\text{eff}}t^3} \quad (3.3)$$

Eq. 3.3 was used to model the deflection of the overcoat on a rectangular cavity without sealed ends to estimate the air cavity deflection with respect to size and pressure. Table 3.2 shows that for an air cavity design with a large deflection, the air cavity collapse can be prevented by increasing the modulus of the overcoat material and/or increasing overcoat thickness.

Table 3.2: Cavity deflection under nano-indentation. Cavity strength (low deflection) can be improved by using thicker metal overcoats. (40% solvent) could be used.

Metal	E (GPa)	t (μm)	F_{max} (mN)	d_{max}(μm)
Al	70	0.7	4	3.5
Al	70	2	8.5	1.1
Cu	128	1.5	8.5	1.3

High-performance, high-frequency single-crystal silicon capacitive resonators have been fabricated using the high-aspect ratio poly and single crystalline silicon (HARPSS) fabrication process on silicon-on-insulator substrates [43]. These devices are the same cavity size as the structures shown in Figure 3.3, except for the fact that the

trenches were fabricated in an SOI wafer and the oxide was etched, thus releasing the cantilevers to form a functioning device with metal bond-pads. Wafer-level packaging was carried out on these devices using the POSS/PPC/Al system. After packaging, the devices were electrically tested for package integrity and subsequently diced for SEM analysis. Figure 3.8(a) shows SEM micrographs of the device cross section. A debris-free cavity was observed. The device performance was measured, as shown in Fig. 3.8(b). Since the device performance could not be measured prior to packaging, it was not possible to analyze the effect of packaging on performance. However, a clean sensing electrode surface was observed after dicing which shows negligible effect of packaging on device performance. The device performance was measured and a loss of 29 dB was observed at a resonant frequency of 141 MHz, which is typical of companion devices. The losses are similar to published values on these devices [44].

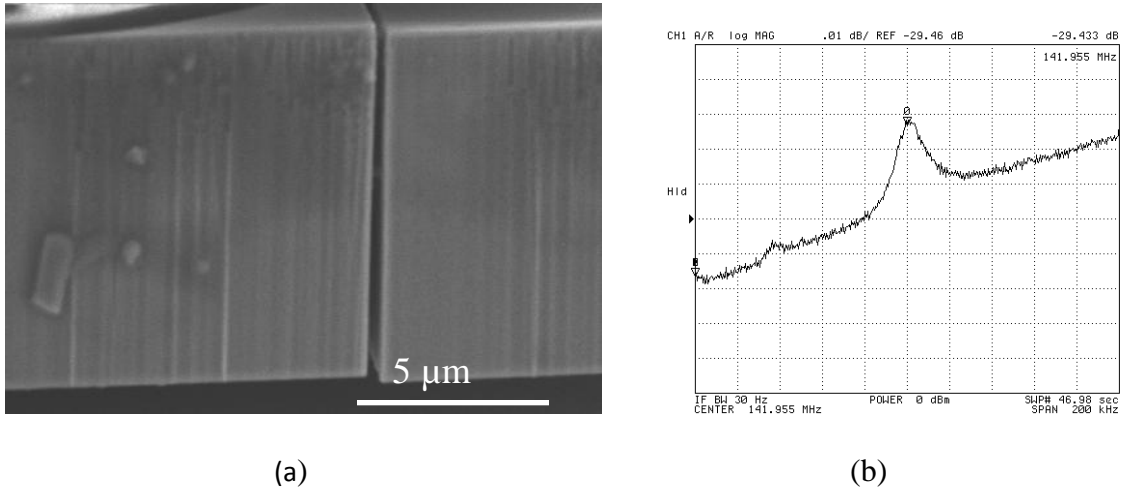


Figure 3.8: A packaged capacitive resonator device. (a) Device shows clean sensing electrode. (b) Device performance was measured successfully.

3.4 Conclusion

In this work, we have used a novel tri-material system comprising of PPC/POSS/metal to successfully fabricate air-cavities to package MEMS devices on a wafer-level. The sacrificial material was deposited in a manner to mask and planarize the topography of the MEMS device. The overcoat and decomposition recipe was optimized for a crack free overcoat after the decomposition. The air-cavities are flexible in size and shape, mechanically robust, and debris-free. Nano-indentation was carried out to estimate the mechanical strength of the cavities. Further, a set of capacitive resonator devices were successfully packaged and characterized using this process.

CHAPTER 4

CHIP-LEVEL MEMS PACKAGING

4. 1 Introduction

In this chapter, a wafer-level air cavity package is tested for compliancy in chip level package. Wafer-level packages, without an active device, as described in the previous chapter, were tested in transfer and compression molding processes used in lead frame packaging. In order for the air cavity to be an acceptable package, it must avoid collapse during thermal and pressure conditions used for epoxy molding. To prevent collapse (roof contact with device surface) adjustments were made to the metal overcoat to strengthen the roof structure. The cavity height was adjusted to account for any deformation to the roof. Finite element modeling and analytical solutions were used to design air gaps and analyze the deformation from cross-sectioned chip cavities.

A second novel packaging approach demonstrated in this study is the in-situ decomposition of the sacrificial material during the epoxy molding process. This is especially useful for large, semi-hermetic lead frame packages. The new, chip-level package retains the sacrificial material during the molding process and performs the decomposition step (cavity formation) during the epoxy cure step once the epoxy over molding material is rigid, preventing cavity collapse. Sacrificial materials were chosen for complete decomposition of the material in the cavities. This in-situ method allows molding and release of very large channels and cavities for a range of packaged devices where hermetic sealing is not necessary.

4.2 Experimental

Wafer-level packaging of dummy MEMS devices was completed through metallization using the processing steps described in chapter 3. A metal-free undecomposed package was also completed for a simultaneous decomposition of the sacrificial material during the lead frame package epoxy curing. The wafers were diced and individual packages bonded to a lead frame. The epoxy molding compound was applied by either transfer molding or compression molding. Transfer molding consisted of injecting the epoxy molding around the device into the desired shape. Transfer molding was carried out at 175°C for 105 s at 10 MPa and then post mold cured at 175°C for 8 hrs, unless otherwise noted. Compression molding was completed on several packages as well. Compression molding places the molding compound on the device and applies a relatively low pressure (e.g. 4 MPa) to form the packaged shape. Samples were cross-sectioned to evaluate the extent of damage. Raman spectroscopy was carried out to investigate debris found in the cavity after cross-sectioning. Focused ion beam images confirmed debris-free cavities prior to molding. Furthermore, to prevent collapse during molding due to the high pressure, large cavities were metallized with a thicker copper coat. Titanium was used as the adhesion layer. Subsequent packages were molded and observed for cavity damage.

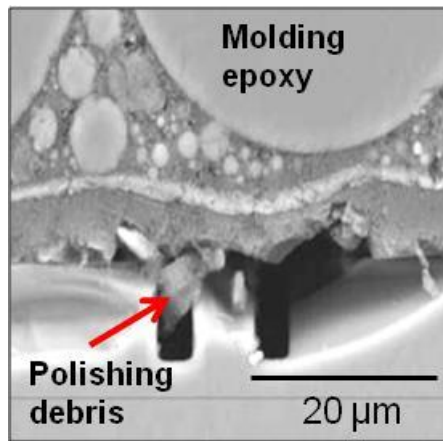
Two-dimensional mechanical analysis of air-cavity packages was carried out using ANSYS 13.0 finite element modeling. A linear, elastic isotropic model was used in addition to the assumption of perfect adhesion existed between polymer and metal layers. A rough, frictional contact (with no slip; infinite coefficient of friction) between overcoat and wafer under high pressure was assumed as a boundary condition. Modeling of all

layers was done with PLANE42 elements: a 2D structure with 4 nodes. Contact between POSS and the wafer was modeled using CONTAC171 and TARGE169 elements compatible with PLANE42. CONTAC171 is used to represent contact and sliding between 2-D "target" surfaces, defined by TARGE169, and a deformable surface, defined by this element. This element has two degrees of freedom at each node: translations in the nodal x and y directions. In this model nodes on CONTAC171 and its respective nodes on TARGE169 are tied together representing a no-slip condition. Both are line elements and demonstrated realistic contact physics in the model. During the simulation, the molding pressure was applied from the top and the cavity deflection was calculated and compared to experimental conditions. A comparison was also made with a standard analytical solution. The effect of different metals and thicknesses on the deformation and stress distribution within the cavity was studied. Conclusions drawn from simulations helped in the design of stronger overcoats for larger cavities.

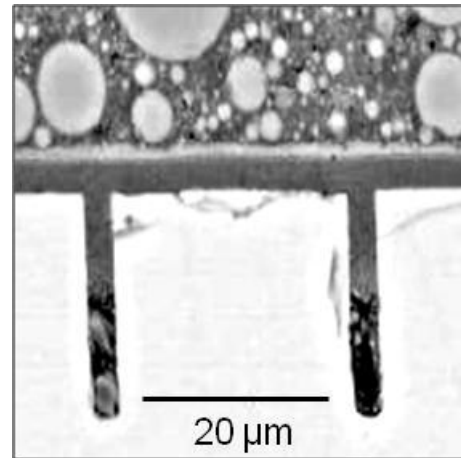
4.3 Results and Discussion

Once the wafer level package cavities (chapter 3) were created they can then be diced and molded for lead frame packaging. Cavities were molded using an epoxy molding compound (EME-G700E, Sumitomo Bakelite Co.). It was observed that the initial cavities with 0.7 μm aluminum overcoat and 20 μm width, were able to withstand a molding pressure of 4 MPa, Fig. 4.1(a). However, they collapsed completely at 10 MPa pressure, Fig. 4.1(b). The debris inside the cavity in Fig 4.1(b), was studied using Raman spectroscopy and the spectra shown to be polishing material. Larger cavities (75 μm wide) were observed to completely collapse at both pressures. If we replace the

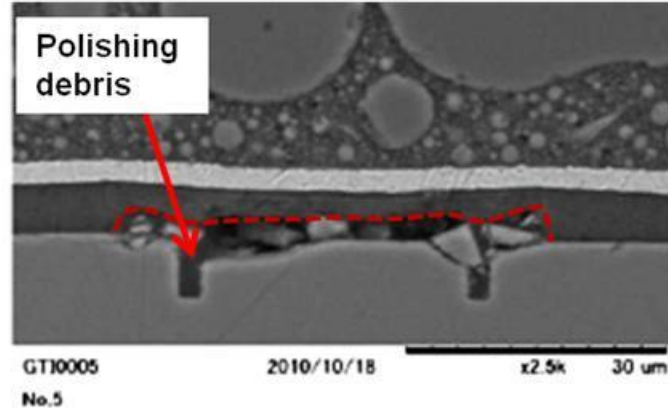
aluminum overcoat with a 3 μm thick copper overcoat, the cavities were able to withstand higher pressure. It was observed that cavities as wide as 100 μm were able to withstand 10 MPa pressure and deform only slightly, Fig. 4.1(c).



(a)



(b)



(c)

Figure 4.1: (a) A 20 μm wide with 1 μm Al overcoat cavity stays intact under 4 MPa compression molding. (b) A 50 μm wide cavity completely collapses under 10 MPa compression molding but (c) sustains the same pressure with a 3 μm copper overcoat undergoing 0.5 μm deflection.

In order to increase the cavity strength, for a specific cavity-width, one needs to increase the metal thickness or the elastic modulus. Increasing the cavity height would

also be an advantage because a larger deformation would be necessary for device failure. However, this would require thicker PPC coatings and subsequently thicker POSS overcoats for conformal coverage. The cavity deflections at a certain molding pressure closely match the FEM and analytical models as explained later. Increasing the POSS overcoat thickness will affect the cavity strength; however the elastic modulus of POSS is approximately 4 GPa which is much lower than either aluminum or copper. Thick metal layers can also be problematic due to residual stresses.

The 2D FEM model was used to understand the pressure limits in cavity deflection during molding. The normalized Von Mises stress was calculated for specific configurations. As seen from Figure 4.2, the FEM model shows the deflection of a 40 μm wide cavity with 0.7 μm thick aluminum at 4 and 10 MPa pressure. At 4 MPa pressure, the measured deflection is 1.5 to 2 μm which is essentially the same as the simulated value of 1.5 μm . At 10 MPa atm pressure, the experimental cavity, Fig 4.1(b) completely collapsed to the surface showing no presence of a cavity. However, the 10 MPa simulation, Fig 4.2, shows collapse in the center of the cavity. The simulation included only elastic properties. The full collapse may involve the plastic deformation of the overcoat.

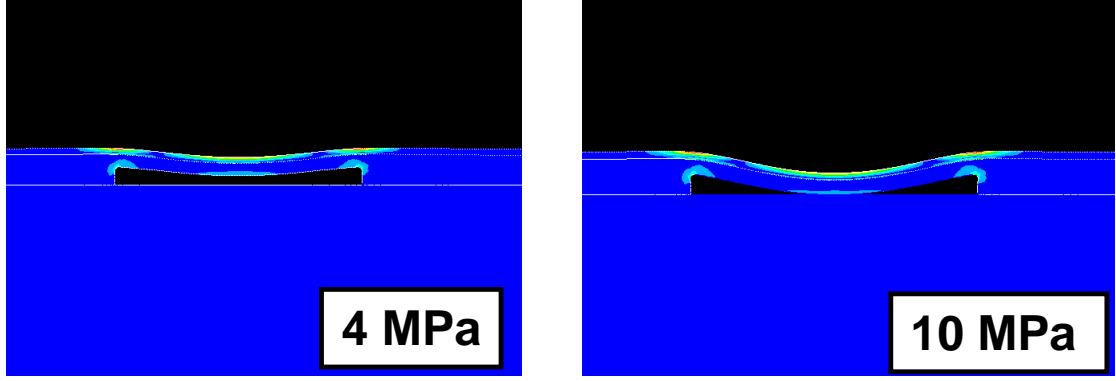


Figure 4.2: Normalized stress profiles of compressed cavities with a 0.7 μm Al overcoat.

The FEM results were compared to a previously derived analytical model, the rectangular bulge equation, to correlate the deflection values obtained from the finite element technique, as shown in Equation 4.1 [45].

$$P = \frac{2ht\sigma_0}{a^2} + \frac{4h^3Et}{3a^4(1-\nu^2)} \quad (4.1)$$

Where, P is the molding pressure. The overcoat material properties are accounted for with E being the elastic modulus, ν is the Poisson ratio, and σ_0 is the initial film stress. The variables a , t and h refer to the geometry of cavity. The value a is the half of the width of the cavity, t is the thickness of the overcoat, and h the the height of the maximum deflection of the overcoat from its intial location.

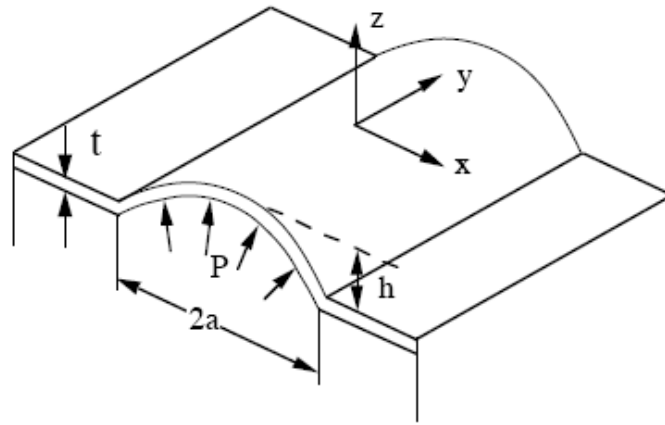


Figure 4.3: Schematic of a standard rectangular bulge test. (Equation 4.1)

The elastic modulus of the overcoat was assumed to be dominated by the metal portion of the metal-polymer composite because the modulus of the metal is about 30 times greater than that of the polymer. The initial film stress, σ_0 , of the annealed, electrodeposited copper film was found to be approximately 30 to 100 MPa depending on thickness of the film used from the literature [46]. When the initial calculations were made the first term of the equation was significantly smaller than the second term using the literature range. Therefore, first term was assumed to be negligible for further calculations in estimating the deflection of the cavity. The two controllable factors for design of the package is the metal overcoat thickness and adjustment of the cavity height to prevent total deflection.

Table 4.1: Numerical values for the Bulge equation (4.1) for a 20 μm wide cavity and a 0.7 μm Al overcoat.

P(atm)	a(μm)	t(μm)	h(μm)
40	10	0.7	2
100	10	0.7	2.8

As shown in Table 4.1, the corresponding deflection values were 2 μm and 2.8 μm for 40 and 10 MPa pressure, respectively. These values match both experimental and FEM values. The 0.7 μm Al overcoat was replaced by a 3 μm Cu overcoat to provide improved mechanical stability. The total deflection of a 3 μm copper overcoat at 10 MPa pressure was found to be 0.56 μm from Eq. 4.1 and FEM simulation (Figure 4.4(a)), which is the same as the experimental deflection in Fig. 4.1(c).

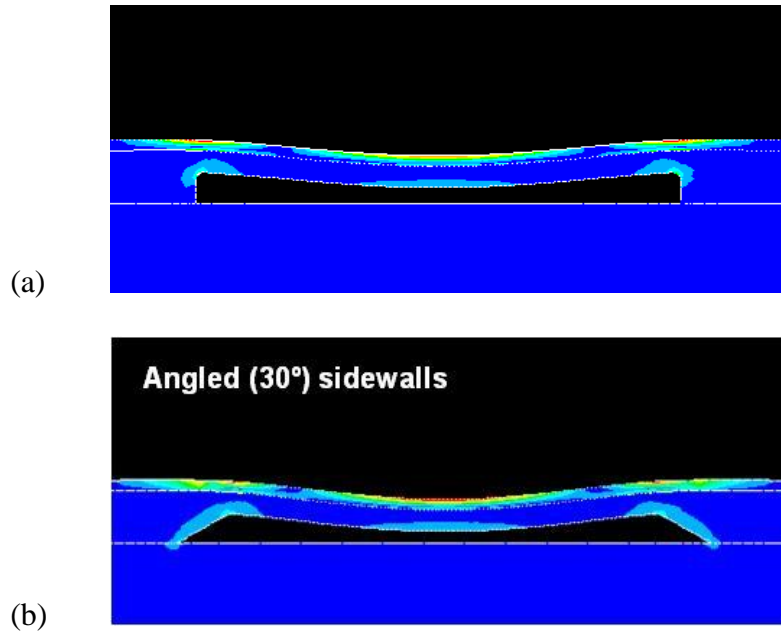


Figure 4.4: (a) FEM simulation of a 3 μm Cu overcoated 40 μm cavity under 10 atm of pressure. (b) FEM simulation of a 3 μm Cu overcoated 40 μm cavity with 30° slanted side walls under 10 atm of pressure.

The overall stress in the overcoat and deflection of the air-cavity could be further reduced through optimization of the cavity design, thicknesses, and annealing conditions. For example, a 10% decrease in the maximum stress along the cavity sidewalls was calculated by forming a 30° slope in the side-walls, and simulated in Figure 4.4(b). Changing the cavity from a straight side-walled structure to a sloped sidewall through the patterning and reflow of the PPC will help optimize a cavity that is more resistant to stress as has been published earlier [1].

The adhesion between POSS and the substrate and POSS the metal overcoat was found to be excellent. However, in order to increase the cavity strength, a thicker metal overcoat was required. When thicker metal overcoats were used, e.g. 2 μm aluminum, the residual stress during e-beam deposition was great enough to cause adhesive failure between the aluminum and the POSS. An oxygen plasma clean was used prior to metal

deposition to improve the adhesion. For thicker copper overcoats, copper was electroplated at low current density on the sputtered seed layer followed by annealing at 180°C for 1 hr to reduce the internal stress. After annealing, the metal film exhibited excellent adhesion.

The results presented above show that there are numerous methods to strengthen the overcoat and fabricate ever wider cavities. However, there is a limit to the metal thickness (e.g. loss of metal adhesion due to residual stress) and optimization of the cavity shape has a limited benefit. In order to fabricate significantly wider cavities, a new approach to creating semi-hermetic chip level packages was developed which prevents collapse of the cavity during molding. In the process described above, the PPC was slowly decomposed prior to injection molding. The overcoat was designed to withstand the molding pressure. During molding, the epoxy encapsulant quickly hardens. The new approach leaves the sacrificial polymer in the cavity during the initial molding step. Once the encapsulant has hardened, the sacrificial polymer in the cavity can be decomposed creating a cavity during post mold curing of the encapsulant. Since the encapsulant is rigid during PPC decomposition, there are few size restrictions for the cavity and no metal support is necessary for the molding process.

This in-situ cavity creation process needs to fit within the post mold cure temperature-time cycle. Typical post mold cure conditions are between 175°C to 190°C for eight hours. Thus, the sacrificial material needs to be chosen so as to completely decompose within this temperature-time profile. The sacrificial material must also be stable enough not to decompose in the early stage of molding when the epoxy encapsulant is not rigid.

Isothermal thermal gravimetric analysis, TGA, data was collected for a set of polycarbonates to identify materials that remain intact during molding and yet will decompose during post mold curing. Figure 4.5 shows the weight change of PPC at 190°C and PEC at 185°C. Decomposition occurs slowly with complete decomposition within the target eight hour period. Little decomposition occurs within the first minutes of the isothermal scan which corresponds to the time in the mold at high pressure. The third sacrificial polymer investigated was PPC with a 3 wt.% PAG loading. This mixture decomposes faster than the pure polymer at the target temperature and may leave a residue from the PAG loading [36].

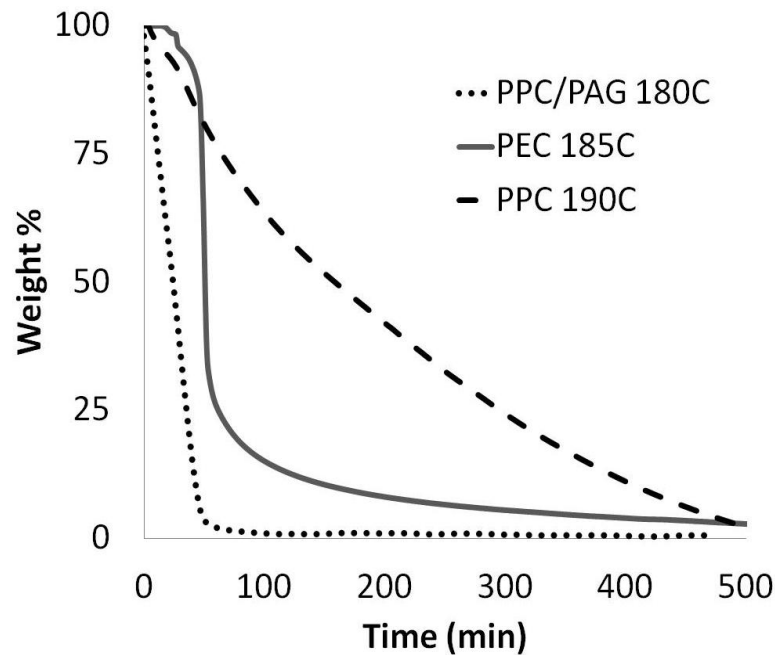


Figure 4.5: Isothermal TGA of polycarbonates to be decomposed in 8 hours.

Each material was patterned using a POSS mask followed by RIE, as described above. The cavities were 1 and 2 mm diameter circles and squares, either 10 and 18 μm

in height. The patterned sacrificial material was coated with a 3 μm POSS overcoat to seal the cavities for dicing and handling. After dicing, the cavities were injection molded at 175°C, 10 MPa for 100 seconds. Sets of cavities were decomposed and cured at 185°C and 190°C for the full eight hours. The cavities were then cross-sectioned for examination. The PPC with PAG cavities collapsed under the molding conditions, as was expected from the TGA data. This is due to the fast decomposition of the sacrificial material before the epoxy compound became rigid. The cavities formed using PPC at 185°C had a small amount of residual PPC after 8 hours decomposition, however the same cavities cured at 190°C producing visibly clean structures, as shown in Figure 4.6(a). The PEC cavities were fully decomposed above 185°C giving visibly clean cavities. The PEC cavity in Figure 4.6(b) was slightly deformed due to reflow of the PEC during the patterning and overcoating. Both PPC and PEC cavities exhibited no size or shape limitations. The yield on forming 1 to 2 mm squares and circles was high, and it is expected that much larger cavities could be formed because little force is exerted on the structure when the sacrificial material decomposes.

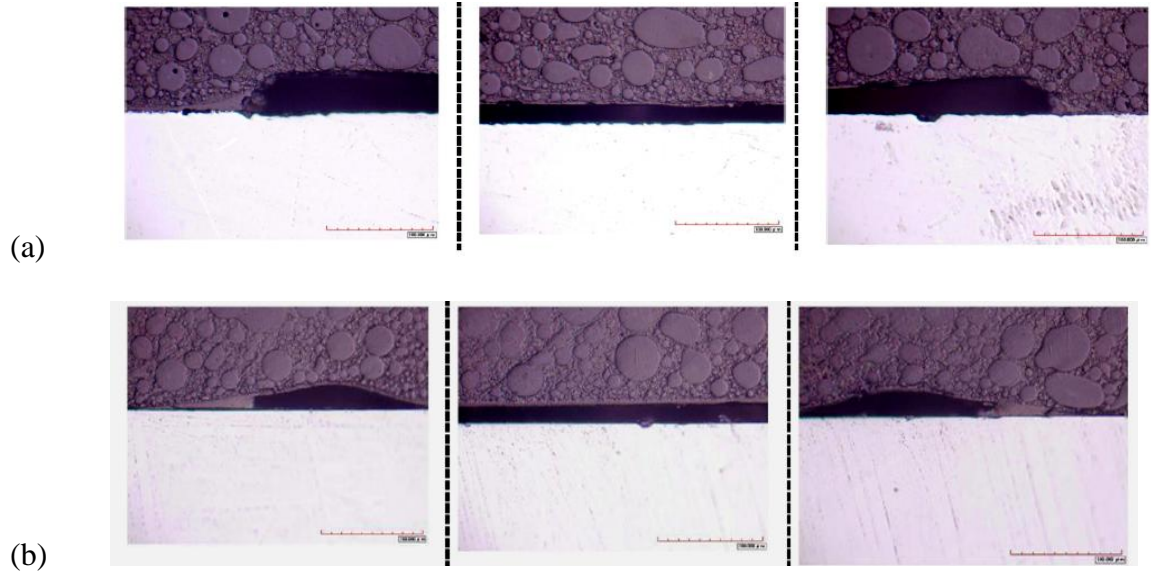


Figure 4.6: Cross-sectioned in-situ decomposition/cure chip level packages. (a) 2 mm diameter, 18 μm tall cavity formed by PPC decomposition at 190°C. (b) 2 mm diameter, 12 μm tall cavity formed by PEC decomposition at 185°C.

4.4 Conclusion

Compression/injection molding was carried out on cavities with different metal overcoats. Stronger and thicker metal overcoats offer better cavity-strength. 2D FEM analysis was used to correlate the experimental observations. Both FEM and analytical equations were able to predict the deformation behavior of the cavities under applied molding pressure. A novel semi-hermetic package was created using an in-situ sacrificial decomposition/epoxy cure molding step for creating large cavity chip packages.

CHAPTER 5

PHOTODEFINEABLE EPOXYCYCLOHEXYL POLYHEDRAL OLIGOMERIC SILSESQUOXANE: PROPERTIES AND CHARACTERIZATION

5.1 Introduction

Polymers are widely used as dielectric materials in microelectronic and microfluidic devices. Epoxy-based materials can be patterned and have appropriate mechanical characteristics for use as overcoats in microelectromechanical systems (MEMS) packaging and microfluidic channels created through the use of sacrificial polymers [9-11, 21]. However, polymer-based epoxy overcoats can deform during thermal processing, lack adequate mechanical strength, and have similar reactive ion etching (RIE) characteristics as sacrificial polymers when used in MEMS packaging [3]. Inorganic materials, such as plasma deposited silicon dioxide, have been used in pattern-transfer to organic films because of their high RIE selectivity (etch rate of the polymer relative to the etch rate of the pattern-transfer material). However, a non-photosensitive pattern-transfer material may require a third, photosensitive layer (i.e. tri-layer process). An inorganic pattern transfer material, such as plasma deposited glass, can be brittle and require relative high deposition temperature. In addition, plasma deposited glass requires costly deposition facilities, and the films can be highly stressed. The use of a spin-coated, photosensitive, hybrid inorganic/organic dielectric could provide processing advantages and can obtain suitable chemical, thermal, plasma, and mechanical properties.

Polyhedral oligomeric silsesquioxane (POSS) is a hybrid inorganic/organic compound with interesting film properties. POSS has a rigid silicon oxide cage with functionalized organic side groups which can be used for cross-linking. POSS has been used in microelectronics as a nanocomposite additive in organic polymers to improve mechanical properties [47, 48]. The functionalized POSS has also been studied in combination with a curing agent or copolymer to form films. The use of a glycidyl ether functionalized POSS cross-linked with a diamine curing agent has been modeled as a potential chip underfill by Lin et al [49]. Asuncion and Laine investigated films formed from an amine functionalized POSS cross-linked using an epoxy based or anhydride based curing agents for an oxygen barrier in electronic packaging [50]. A photosensitive POSS structure functionalized with acrylate and benzocyclobutane moieties has been synthesized and investigated as a flash imprint film [51, 52].

In this study, a novel POSS dielectric has been developed using only epoxy-functionalized POSS as the monomer. The use of epoxy-functionalized POSS allows spin coating and fabrication of a photodefinable, highly cross-linked, dense film with organic/inorganic characteristics. Processing conditions were optimized, and the optical, thermal, mechanical, and chemical properties were evaluated and compared with those of organic-only epoxy dielectrics. POSS was investigated for several MEMS applications, including as a high-selectivity permanent mask for pattern transfer to an organic sacrificial polymer film. An air cavity process using a patterned sacrificial polymer was demonstrated.

5.2 Experimental and Material Selection

Epoxycyclohexyl POSS (Hybrid Plastics Inc.) was used in this study. It consists of a silicon oxide cage structure with an epoxycyclohexyl group on each corner, $(C_8H_{13}O_2)_n(SiO_{1.5})_n$ where $n=8, 10$, or 12 . The formulation is a mixture of 8, 10, and 12 cornered POSS molecules and corresponding epoxy groups. An example of the 8 cornered POSS functionalized with an epoxy group is shown in Figure 2.2.

POSS was dissolved in mesitylene making 40 wt% or 60 wt%, solids solutions. An iodonium photo-acid generator (PAG) was added at 1 wt% of POSS and sensitizer at 0.33 wt% of POSS so as to make the formulation photosensitive at 365 nm.

POSS samples were spin coated onto $\langle 100 \rangle$ silicon wafers and then soft-baked on a hotplate at 85°C for 5 minutes to remove the solvent from the polymer film. A 1 kW Hg-Xe lamp with a broad band filter over 350-380 nm was used for exposure with an optimal dose of 250 mJ/cm². The lamp intensity was calibrated using a broadband detector for the entire range of 350-380 nm. The post-exposure bake (PEB) was performed on a hotplate at 85°C for 5 minutes. The films were developed in an agitated isopropanol bath followed by a deionized water spray rinse. The films were cured in a nitrogen-purged tube furnace. The temperature was ramped at 1°C/min and held at the cure temperature, 240°C, for 1 hour. The furnace was allowed to cool slowly by natural convection to room temperature before the samples were removed.

A Zeiss Ultra 60 scanning electron microscope (SEM) was used to obtain images. Film thicknesses were measured with a Veeco Dektak profilometer. A tape test was used to investigate POSS adhesion. After processing, a cross-hatched was made in the POSS film followed by tape testing. The thermal stability was measured using a TA instruments

Q50 thermal gravimetric analysis (TGA). The POSS film was typically heated to 500 °C, using a 1 °C/min ramp rate.

A variable density optical mask (Opto-line International Inc.) was used to study the effect of dose on contrast and pattern resolution. The mask allowed for the POSS to be exposed to multiple doses on a single wafer. The exposed features were developed and used to measure D_{100} and, D_0 so that the contrast (γ) could be determined, (Equation 5.1). D_{100} is the exposure dose at which all the material remains and D_0 is the exposure dose at which all of the photodefined material is removed.

$$\gamma = \frac{1}{\log_{10}\left(\frac{D_{100}}{D_0}\right)} \quad (5.1)$$

The UV absorption was measured with a Hewlett Packard 8543 UV-vis spectrophotometer using the Beer-Lambert law (Equation 5.2).

$$\frac{I}{I_0} = 10^{-\alpha l} \quad (5.2)$$

Where, I_0 is the incident intensity, I is the intensity at a path length l , and α is the absorption coefficient. The hydrophilic/hydrophobic nature of POSS films was investigated using water contact angle measurements with a Rame–Hart CA goniometer (model 100). For the measurements, 4 μ L water drops were brought into contact with a POSS film and still images were recorded and analyzed.

Quasi-static nano-indentation was conducted on the samples using a Hysitron Triboindenter with a Berkovich tip. The process and characterization necessary to obtain the modulus and hardness followed the procedures of Rajarathinam et al [53].

The reactive ion etching (RIE) of POSS was investigated to study the potential use of POSS as a hard mask for the pattern transfer to other materials such as polypropylene carbonate (PPC) (Novomer, Inc.). The PPC films were made by dissolving it in γ -butyrolactone, typically 18 wt% polymer. PPC samples were spin coated onto <100> silicon wafers and then soft-baked on a hotplate at 100°C for 5 minutes to remove the solvent. Polynorbornene based dielectrics, Avatrel 2000P (Promerus LLC) and Avatrel 8000P (Promerus LLC) were used as organic masks in comparison to a POSS mask. Avatrel 2000P was processed according to the procedures of Bai et al [54, 55]. Avatrel 8000P was processed according to the procedures of Rajarathinam et al [53]. A Plasma-Therm RIE operating at 13.56 MHz was used to measure etch selectivity. The pressure and power were held constant at 310 mTorr and 250 W, respectively. The ratio of O₂ to CHF₃ gas in the RIE chamber was optimized for maximum etch selectivity and minimal residue.

The POSS films developed here also were tested in air cavity fabrication for use in a MEMS packaging application. The POSS build-up was used to form a clean, durable cavity for packaging by using POSS as an overcoat for the PPC sacrificial material. A 3 μ m film of PPC was spun on a silicon wafer and soft-baked. A 2 μ m film of POSS was then spin coated on top of the PPC film and processed. The exposed PPC was reactive ion etched using the optimized etch conditions leaving patterned POSS on top of patterned PPC. The samples were fully encapsulated with an overcoat of POSS or Avatrel 2000P. The samples were then heated and metallized in a Kurt J. Lesker PVD75 filament evaporator. The samples were heated under vacuum to 240°C and held at

temperature for 2 hours to decompose the sacrificial PPC. The samples were allowed to cool under vacuum and 1 μm of aluminum was deposited on the samples.

5.3 Results and Discussion

The optical, mechanical, and chemical properties of photodefined POSS were investigated. Thin POSS films were also studied for use as a masking material for sacrificial organic polymers in MEMS packaging applications.

POSS thin films were deposited by spin coating using mesitylene as the casting solvent. The viscosity of the POSS-solvent mixture and resulting film thickness was adjusted by changing the percent solids in the mixture. A 60 wt% and 40 wt% POSS formulation in mesitylene were prepared and spin-coated onto 100 mm diameter silicon wafers with a 120 nm thermal oxide. Spin speeds from 500 and 4000 revolutions per minute (rpm) were used. The samples were spun at 500 rpm for 10 seconds, ramped to the desired speed, and held at speed for 10 seconds. The samples were then soft-baked on a hot plate at 85°C until the films were tacky. The soft bake time increased with film thickness. The 12 μm film was soft baked for 10 minutes on a hot plate while the 2 μm film was baked for 3 minutes. The wafer was exposed to UV radiation at a dose of 250 mJ/cm^2 and a post exposure bake at 85°C for 5 minutes. The wafers had a visibly even-coat on the wafer except for the edge bead which covered the outermost 4 mm of the wafer coated at 500 rpm. The final film thickness, as measured at two locations on the wafer, is shown in Figure 5.2. The 60 wt% POSS solution had a single-coat thickness of

5 μm to 12 μm whereas the 40 wt% POSS solution produced thickness from 2 μm to 4 μm . Other formulations can be used to expand the thickness range.

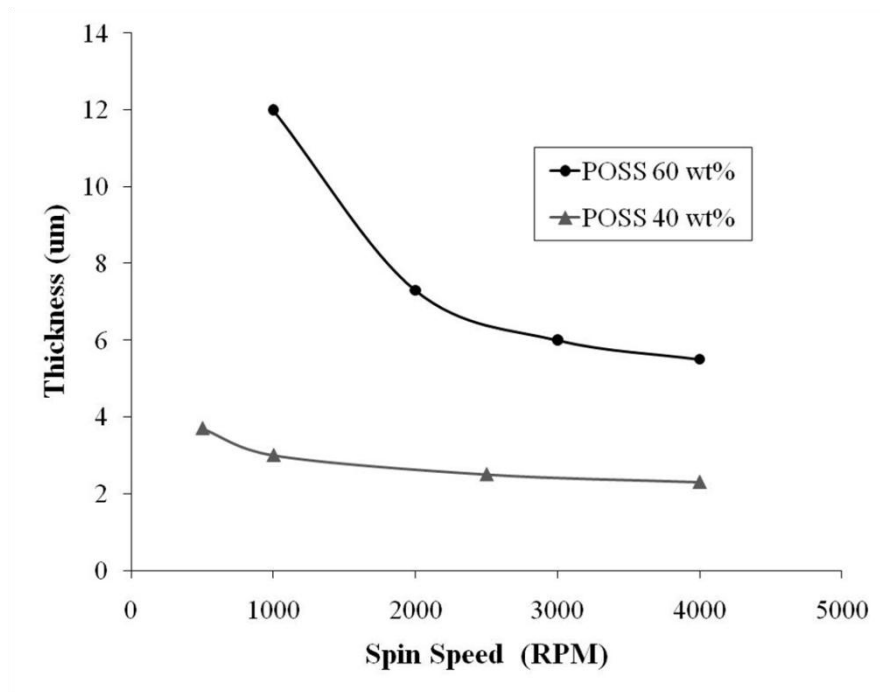


Figure 5.1: Spin speed curves for POSS films from 40 and 60 wt% of POSS in solution.

The photospeed and contrast were evaluated using 1.5 μm thick films of the 40 wt% POSS mixture. The POSS film was softbaked at 85°C and exposed through a variable density optical mask with a broadband wavelength of 350-380 nm. The material is a negative-tone dielectric which crosslinks in the exposed areas. The sample was then post exposure baked at 85°C for 5 minutes. The film was developed in an agitated isopropanol bath for 2 minutes to dissolve the unexposed film. The development time was determined by the appearance of a translucent residue film on the surface, indicating that the unexposed film had cleared. The residual film was removed by using a deionized water spray for 1 minute. The remaining polymer thickness for each dose was measured with a profilometer. The D_0 and D_{100} were found to be 19.4 mJ/cm^2 and 89.4 mJ/cm^2 ,

respectively. The contrast value was calculated from Figure 5.3 to be 1.51. Some of the polymer regions exposed at doses at or near D_0 and D_{100} had undergone some degree of delamination from the silicon surface during development. Delamination was exacerbated by vigorous agitation during the developing process. Features exposed to doses between 29.8 mJ/cm^2 and 58.08 mJ/cm^2 , had less than 25% of the features remaining on the surface. Features exposed to doses above 58.08 mJ/cm^2 showed layered development with a large fraction of the film intact. The sensitivity is similar to SU-8, which had a value of 40 mJ/cm^2 for a $30 \text{ }\mu\text{m}$ film [53]. The contrast is comparable to Novolac-based photoresists, which have contrast values for thin films from 0.7 to 3.6 [56].

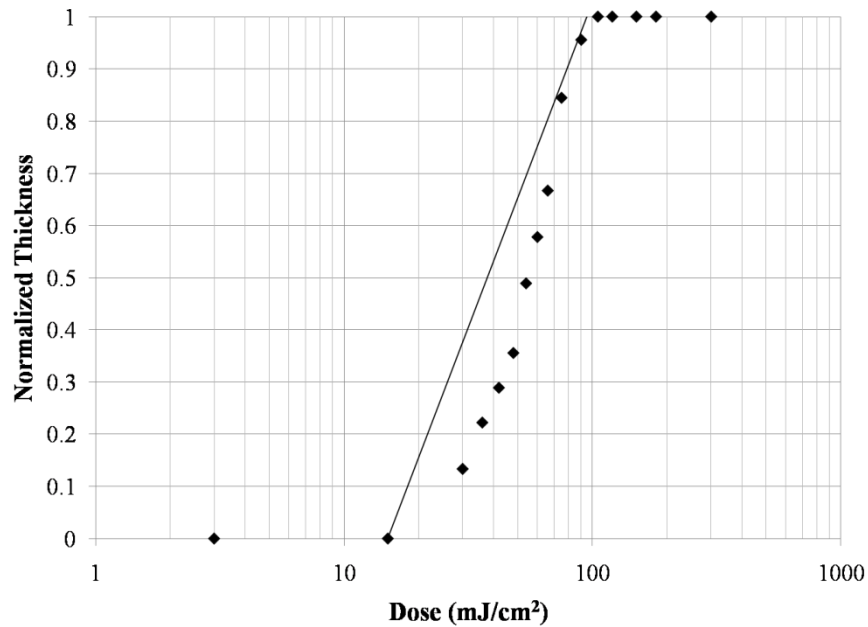


Figure 5.2: Contrast curve for photodefined epoxycyclohexyl POSS of $1 \text{ }\mu\text{m}$ thickness.

The adhesion of the POSS layer was investigated by using a simple pass/fail modification of ASTM D3359 tape test. The POSS layer was scribed with a cross-hatched pattern prior to the tape test. Adhesion of POSS, especially at the edges of the scribe marks, was visually examined. The POSS films were $1.5 \text{ }\mu\text{m}$ thick and cast from a

40 wt% POSS in solvent mixture. The minimum exposure dose to achieve adhesion was investigated. Samples were spun onto a wafer and soft baked at 85°C for 3 minutes. A range of exposure doses were used. The samples were post exposure baked at 85°C for 5 minutes prior to tape testing. Doses greater than 150 mJ/cm² showed good adhesion to the surface for samples on both freshly HF-cleaned wafers and on wafers with a native oxide. When the POSS was deposited on 120 nm of thermally-grown oxide, the adhesion improved. The minimum dose necessary to pass the tape test was 110 mJ/cm².

The effect of post-POSS processing, especially heating, on adhesion was investigated. The exposed and developed POSS samples were heated (i.e. cured) at 240°C for 2 hours in an ambient atmosphere and retested for adhesion. All samples passed the adhesion test after heating to 240°C.

The absorbance of the POSS mixture in the UV-Vis region was investigated. POSS films deposited from the 60 wt% solution were spun on silica glass slides. As shown in Figure 5.4, the absorption coefficient was found to be 63 cm⁻¹ at 365 for a softbaked POSS film. The absorption coefficient at 365nm dropped after the PEB of the POSS to 37.8 cm⁻¹. The decrease in the absorption coefficient can be attributed to the decomposition of the sensitizer and PAG, the main absorbing groups in the film. Soft baked POSS films with a thickness of 4.2 μm, 7.3 μm, and 10 μm, had an absorption coefficient of 60 cm⁻¹, 63 cm⁻¹, and 66 cm⁻¹, respectively. A least squares regression of absorbance vs thickness data showed a linear relationship with a zero x-intercept and slope of 65 cm⁻¹. The absorption coefficient affects sensitivity and contrast, especially for thick films where the optical dose is attenuated in the bulk of the film. For example, in order to achieve a minimum dose at the greatest depths, the surface is overexposed.

Thus, a 15 μm thick film experiences 10% attenuation throughout the film. The 1 μm film passed the tape test with no delamination at a dose of 150 mJ/cm^2 while the 15 μm showed minor delamination due to the lower dose at the bottom of the film.

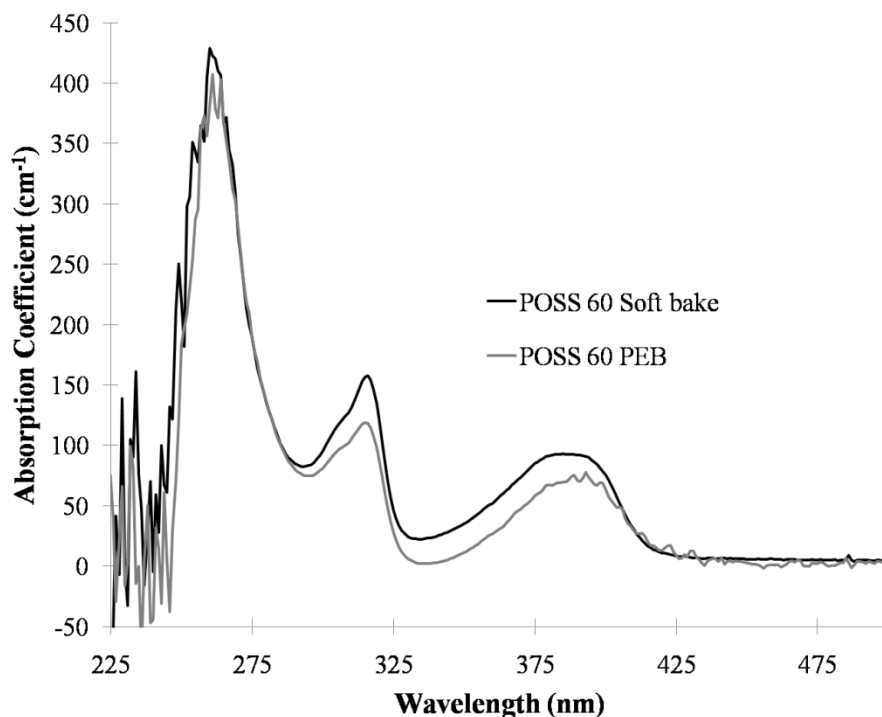


Figure 5.3: Changes in the absorption coefficient for the POSS film over the wavelengths 225-500 nm.

The photosensitivity and pattern fidelity of POSS was investigated. POSS films were spin coated from a 60 wt% solution at 1250 RPM forming a 10 μm thick film and softbaked. The films were irradiated with broadband radiation (wavelength of 350 to 380 nm) through a variable-density mask. The films were PEB, developed in isopropanol, and rinsed to remove cleanly the unexposed film, as described previously. The features with the highest spatial resolution in terms of maintaining size, pitch, and sharp corners/edges were exposed at 250 mJ/cm^2 . Features exposed to doses below 250 mJ/cm^2 delaminated and had poor shape definition. At higher exposure dose, the features had poor pitch fidelity, and rounded edges. Figure 5.5(a) shows an array of 10 μm thick POSS lines

ranging from 5 to 50 μm in width with equal lines and spaces. Features above 10 μm in width had excellent pattern fidelity. These features maintained full pitch and showed clean, sharp corners matching the features on the mask. Figure 5.5(b) shows 50 μm wide lines in more detail. The sidewalls are well defined and vertically straight but have a degree of line edge roughness. Features below 10 μm in width had increased rounding of the edges, poor pitch fidelity, and increased delamination for the smaller structures.

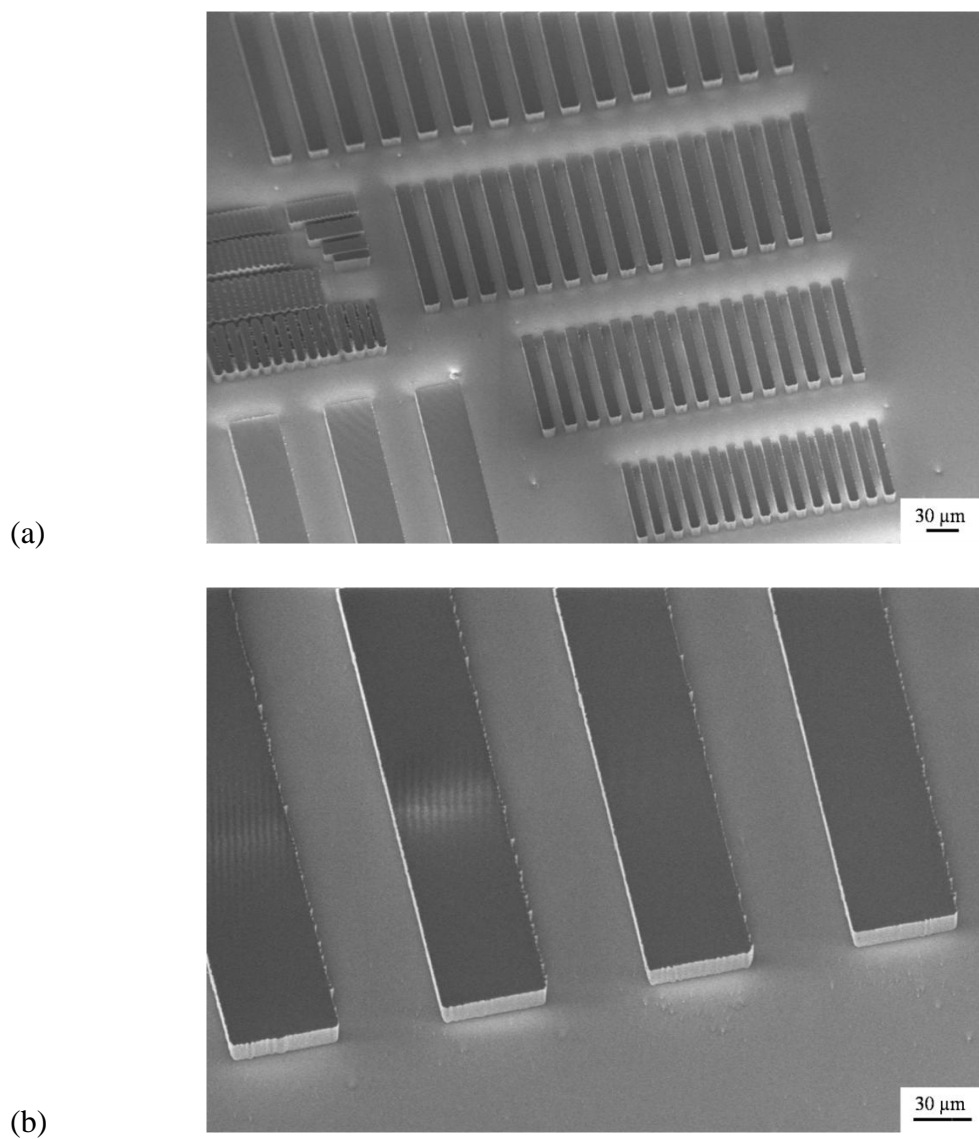


Figure 5.4: SEM images of 10 μm thick photodefined POSS. (a) Arrays of photodefined POSS lines ranging from 5 to 50 μm width with equal lines and spaces. (b) Array of 50 μm wide POSS lines.

The chemical resistance of the POSS films was examined for delamination, cracking, and excessive swelling when exposed to acids and solvents used in fabrication. POSS films (5 μm thick) were immersed in different liquids for 15 minutes. The liquids include isopropanol, acetone, mesitylene, propylene glycol methyl ether acetate, 2-hexanone, hot 3 M sulfuric acid, peroxydisulfuric acid (often called piranha etch),

phosphoric/acetic/nitric acid etch, and buffered oxide etch. Samples were periodically removed from the solutions to measure the POSS thickness. Buffered oxide etch had the highest POSS dissolution rate at 67 nm/min. The dissolution rate for the others liquids were less than 6.7 nm/min. The films showed no visible damage or swelling after being submerged in any of the baths. A sample was also placed in concentrated HF, which resulted in the quick release and subsequent disintegration of the film. The silicon oxide cage/epoxy hybrid structure of POSS gives the cross-linked film improved resistance to chemical attack that otherwise would affect organic polymer films or silicon dioxide films.

The thermal stability of POSS was investigated by thermal gravimetric analysis (TGA). A small sample of an exposed film was heated at 1°C/min to 500°C. Figure 5.6 shows some weight loss of POSS film at 350°C, which is likely due to the organic content of POSS decomposing. The remaining silicon oxide, ca. 45%, decomposed at higher temperature. The mass loss at temperatures below 250°C is likely due to loss of residual solvent (70°C to 160°C range), and loss of water produced during the epoxy cross-linking within the film at temperatures above 170°C. The mechanical stability of the cross-linked 6 µm thick POSS films was examined starting at 250°C. Samples were examined after heating to 250°C and higher temperatures at 25°C intervals. Each sample was held at temperature for one hour in a nitrogen atmosphere. Cracks were visible in samples heated to 350°C, which corresponds to the degradation temperature in the TGA result.

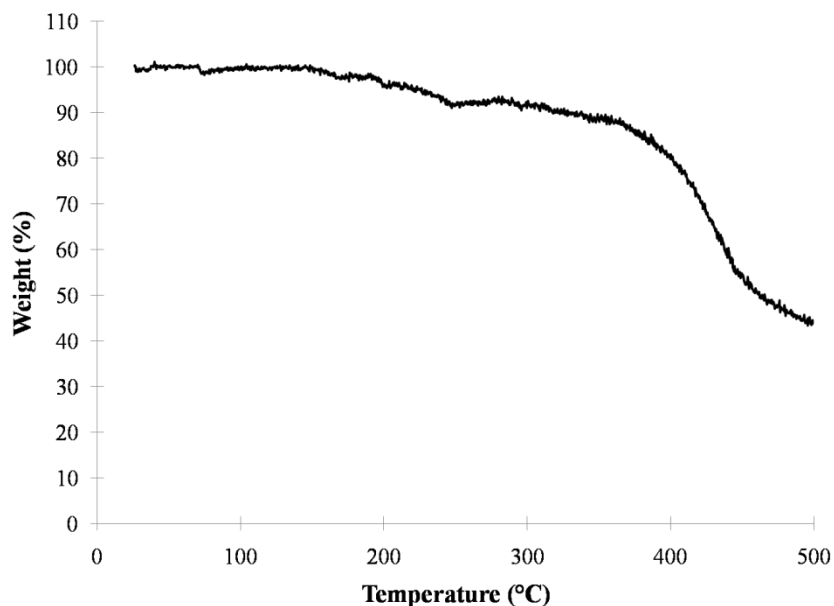


Figure 5.5: Thermal gravimetric analysis of POSS film to 500 °C at a ramp rate of 1 °C/min.

The hydrophilic/hydrophobic nature of the POSS films was investigated using contact angle measurements with a Rame–Hart CA goniometer. A 5 μm POSS film was post exposure baked and brought in contact with a 4 μL water drop and the contact angle was measured. The measured contact angle was 85.0 ± 1.5 degrees. The film was then cured at 240°C and the measurement was repeated. The contact angle did not change showing a hydrophobic character. The contact angle of silicon dioxide is generally 25° or less [57]. The contact angle of silicon dioxide after treatment with silane coupling agents was measured. Treatment with trimethyl methoxysilane, phenyldimethyl ethoxysilane, and trifluoropropyl dimethylchlorosilane gave contact angles of 68°, 68°, and 83°, respectively [5].

The electrical permittivity of the POSS film would be of importance for most dielectric applications and expand its use as a material in microelectronics packaging. Dielectric measurements were performed by fabricating parallel-plate capacitors. The

bottom plate of the capacitors was a full-surface metal film of sputtered Ti/Au/Ti (300 Å/4000 Å/300 Å) using the Unifilm sputtering system. The top electrode consisting of Ti/Au/Ti (300 Å/4000 Å/300 Å) was patterned by photolithography and wet etching. Capacitance and conductance were measured at 10 and 100 kHz using a Hewlett Packard 4236 LCR meter on a Karl Suss probe station. No correction was needed for fringing fields around the perimeter of the capacitors due to the high capacitor area to thickness ratio (>1000). The POSS film's dielectric constant will be determined by the shape of the cage, and free volume created through the cage-to-cage cross-linking. The initial formulation provided a permittivity of 3.03. The loss tangent was calculated to be 0.124 and 0.019 at 10kHz and 100kHz respectively. The free volume in the cage structure gives it a dielectric constant well below that of full dense silicon dioxide, $\epsilon_r=4$. The dielectric constant of current packaging polymer dielectrics Avatrel 2000P is 2.55 [58] and SU-8 is 3.2 [59].

The elastic modulus and hardness of POSS was studied using nano-indentation. A 5 μm thick films was measured using a Berkovich tip after PEB. The film was found to have a reduced modulus of 4.9 GPa and a hardness of 0.56 GPa. POSS films were then cured to 205°C to 240°C and held for 2 hours in nitrogen atmosphere. The 205°C and 240°C cured POSS films had a modulus of 5.3 GPa, and 4.1 GPa, and hardness of 0.64 GPa and 0.41 GPa, respectively. The change in modulus is due to the epoxy cross-linking resulting in an increase in modulus followed by thermal degradation of the cross-link bonds above 205°C causing a slight drop in modulus. The POSS elastic modulus is comparable to SU-8, a photodefinable epoxy polymer used in MEMS structures, which had a modulus of 4.02 GPa [60].

The use of POSS as a hard mask in reactive ion etching for pattern transfer was investigated. The silicon dioxide nature of POSS results in low etch rate in an oxygen plasma compared to an organic polymer film. Polypropylene carbonate (PPC) was patterned using POSS as the etch-resistant mask. 5 μm thick PPC films with POSS-overcoat were etched in an oxygen plasma at 310 mTorr pressure and 250 W power. The etch gas was O_2 with 0 to 10% CHF_3 . The CHF_3 was used to assist in polymer etching and minimize the hydrocarbon residue. The film thickness was measured every 30 seconds during the etch process to determine etching rate. The corresponding POSS etch rates and selectivity are shown in Table 5.1. The PPC etch rate was 0.66 $\mu\text{m}/\text{min}$ etch rate using 94% oxygen and 6% CHF_3 . The etch selectivity, shown in Table 5.1, drops at higher CHF_3 concentrations because the fluorinated products attack the SiO bonds. High CHF_3 concentrations can be used to remove the POSS after polymer etching, if necessary. The POSS etch rate in the 94% O_2 with 6% CHF_3 plasma was compared to Avatrel 2000P and Avatrel 8000P etch rate, which can also be used for pattern transfer. The etch rate of Avatrel 2000P and Avatrel 8000P was 0.44 $\mu\text{m}/\text{min}$ and 0.35 $\mu\text{m}/\text{min}$, respectively. The selectivity of Avatrel 2000P and Avatrel 8000P with respect to PPC is 1.5 and 1.9, respectively, compared to 24 for POSS. The combination of high modulus, chemical and thermal stability, and high selectivity are desirable attributes making POSS an interesting permanent dielectric or temporary etch mask.

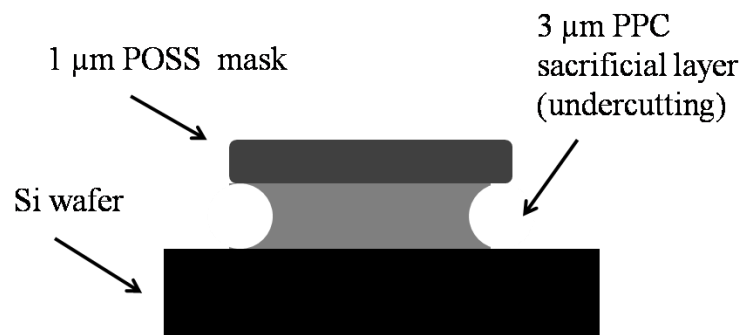
Table 5.1: POSS etch rates and selectivity in 250 W O₂ plasma with different CHF₃ concentrations. The selectivity is for a polypropylene carbonate etch rate of 0.66μm/min.

CHF ₃ concentration	POSS etch rate (μm/min)	PPC/POSS Selectivity
0% CHF ₃	0.003	220
1% CHF ₃	0.007	95
2% CHF ₃	0.02	33
4% CHF ₃	0.023	29
6% CHF ₃	0.027	24
8% CHF ₃	0.04	16.5
10% CHF ₃	0.05	13.2

POSS was used as the overcoat and pattern transfer material in air cavity fabrication. A thin film of PPC was patterned and etched using POSS as the pattern transfer mask, as shown in Figure 5.7(a). The PPC feature is 25 μm wide line and 3 μm thick. A 1 μm thick layer of POSS was coated on the PPC and imaged so as to serve as the etch mask. The PPC field region was clean after 5 min. etching in a 94% O₂, 6% CHF₃ reactive ion etch condition, as described above. The PPC undercut was 500 nm after the plasma etch.



(a)



(b)

Figure 5.6: (a) SEM image of a 3 μ m thick line of polypropylene carbonate with a 1 μ m patterned POSS mask after an O₂ plasma RIE. (b) A schematic of the patterned PPC/POSS line.

POSS was then used as the overcoat for the PPC/POSS structure in fabricating buried microchannels that could be used in MEMS packaging. The microchannels would take the shape of the PPC region in the PPC/POSS structure. Dimensions of 50 to 100 μ m wide, 1 cm in length, and 3 μ m tall were necessary for the microchannel structures. A 3 μ m film of PPC was spin-coated and a POSS pattern transfer mask was deposited over the sacrificial PPC. The sample was then plasma etched in 94% O₂, 6% CHF₃ for 5 minutes to transfer the pattern from the POSS to the PPC. The POSS etch mask was left

in place so as to provide additional support to the top of the cavity. Several overcoat materials on top of the POSS to encapsulate the cavities were investigated. The overcoat should have adequate mechanical support to maintain the cavity shape and allow the decomposition products to permeate the overcoat leaving a gas-cavity. Three overcoats were investigated: 2 μm Avatrel 2000P, 2 μm POSS overcoat, and 1 μm POSS with 2 μm Avatrel 8000P. The latter composite overcoat (POSS-Avatrel) used the POSS to protect the PPC from deformation from the solvent used in Avatrel 8000P. After the air cavity was formed, a thin layer of aluminum was evaporated on the POSS or Avatrel to improve the mechanical rigidity of the structure. A brief oxygen plasma etching of the POSS surface was done at low power to improve the adhesion of the final metal cap evaporated on the air cavity structure. The decomposition of the PPC could be performed in the same vacuum chamber as the aluminum evaporation, just before evaporation or in a separate chamber before evaporation. 1 μm of aluminum was used to hermetically seal the cavity. The microchannel cavities were cross-sectioned and observed under SEM. Figure 5.8 shows a cavity using Avatrel 2000P as the overcoat in the microchannels.

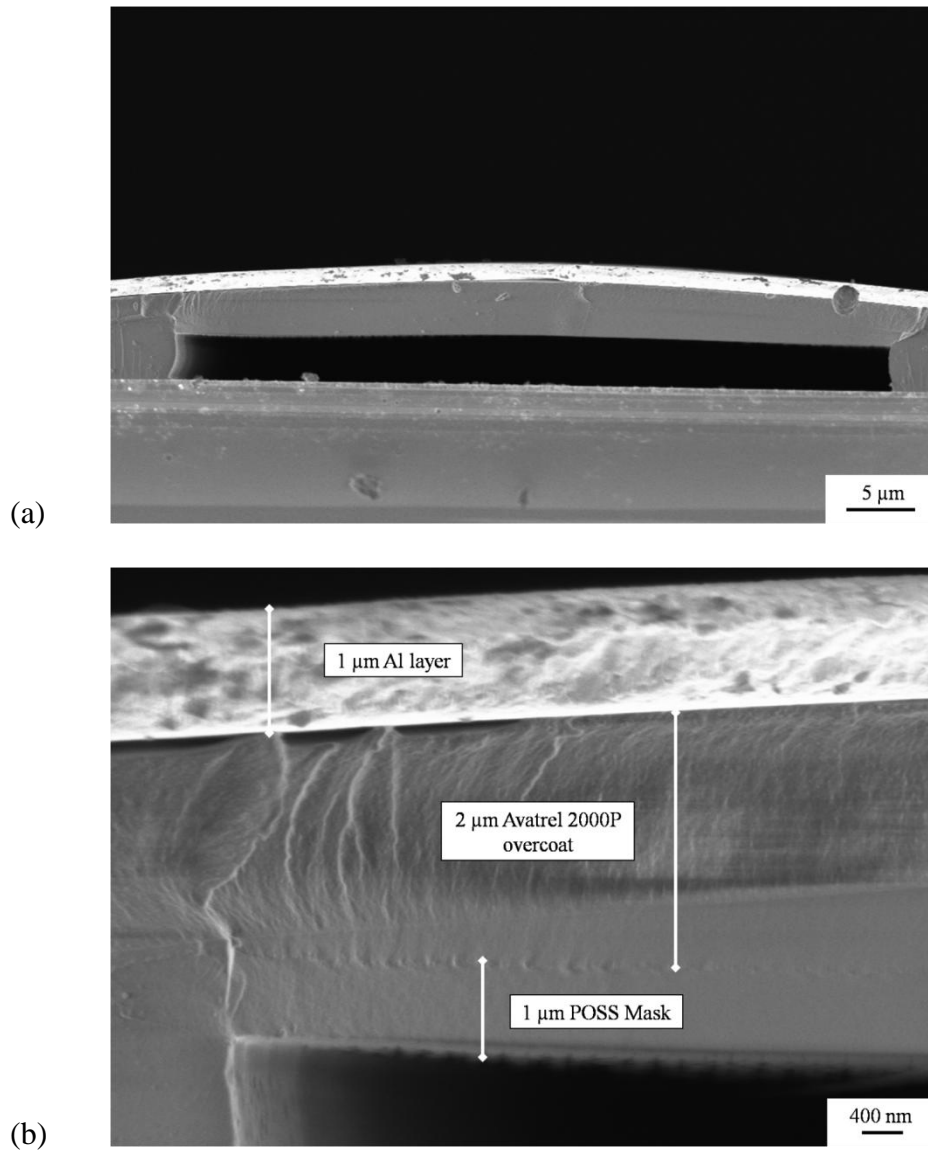


Figure 5.7: (a) SEM image of a cavity utilizing a POSS mask with an Avatrel 200P overcoat. The width of the cavity is 50 μm and has a height of 3 μm. (b) A close up of the corner of the cavity in (a). The POSS mask, Avatrel 2000P overcoat and aluminum cap have been identified and measured.

The cavity retained the shape of the PPC and showed no deformation of Avatrel/aluminum overcoat. The POSS mask was left in place after pattern transfer in Fig. 9(a), providing additional mechanical support for the top of the cavity. Figure 5.8(b) shows the corner of the cavity from Figure 5.8(a). All layers can be seen and have the correct thickness with cleanly defined cavity walls. Cavities using POSS as the pattern

transfer material and POSS/Avatrel 8000P overcoat showed similar results with respect to edge and shape definition. Figure 5.9 shows a cross-section of an all POSS overcoat MEMS packaging application for a resonator. The resonator cavity dimensions were 3 μm high, 60 to 300 μm wide, and 100 to 500 μm long and was made using a similar process as above. The two trenches in the wafer are to resemble a dummy setup of an actual resonator device. The overcoat maintains the shape of the cavity and clean decomposition of the sacrificial material shows that the cavity is visibly clean. This would allow the resonator to be free of debris. The cavities could be made to contain an inert gas, or vacuum, depending on the metal deposition conditions.

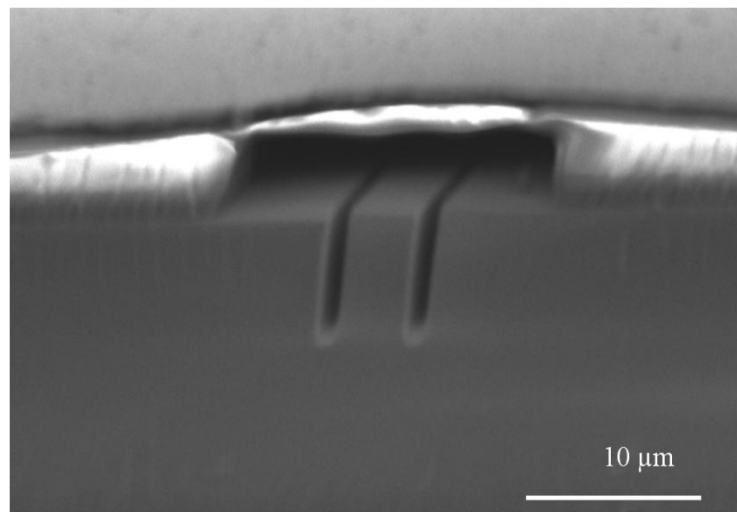


Figure 5.8: An all POSS overcoat cavity designed for a resonator. A 1 μm Al layer is on top of the 2 μm POSS overcoat. The trenches in the wafer show where the resonator would be located.

5.4 Conclusion

The epoxy POSS dielectric provides a resilient, strong inorganic/organic hybrid dielectric for use in microfabrication. The POSS dielectric uses simple processing steps for film fabrication and exhibits adequate optical properties and photodefineability. Its thermal and chemical stability allow for a tough, durable overcoat. A high plasma etch selectivity compared to organic polymers was demonstrated. The POSS dielectric was used to create microchannels with its RIE patterning capabilities. The microchannels used POSS as a protective chemical barrier and as a mechanical overcoat.

CHAPTER 6

POLYCARBONATES AS TEMPORARY ADHESIVES

6. 1 Introduction

Thin and ultrathin silicon substrates have received interest in recent years for device fabrication and packaging. Thin silicon substrates have improved heat dissipation, flexibility, reduced electrical resistance and 3-D stacking capabilities. However fabricating devices on thin substrates or thinning a fabricated device wafer requires a rigid carrier substrate to prevent damage to the device wafer. This rigid carrier substrate prevents fracture, warping, and folding of the device substrate. Temporary adhesives have become increasingly important for integrated circuit, solar cells, MEMS, and packaging applications due to low cost, adaptability, and low impact processing [61, 62]. Adhesive polymers used for the wafer-wafer bonding require adequate adhesion strength and easily deposited uniform films [63]. The polymer's stability both chemically and thermally are important to withstand processing such as wet/dry etching and deposition. While some current materials meet these requirements, many of these materials require undesirable high temperature and/or mechanical force for release [64]. After the release, the substrate may require costly, device damaging cleaning processes to remove residues.

Polycarbonates, currently being studied as sacrificial place holders in microelectronic build up processes, provide a unique alternative to current polymer adhesives [9, 10, 22]. These polymers thermally decompose into small volatile compounds with minimal to no residue. Polycarbonates can be uniformly coated through spin coating at various thicknesses for easy processing. The polymer formulations can be

designed for solvent and thermal resistance to maintain the film during processing. The release of the processed wafer can be completed in a standard furnace at the decomposition temperature of the selected polycarbonate. For this project polycarbonate formulations were characterized and studied as temporary adhesives.

6.2 Experimental and Material Selection

Four polycarbonates were chosen for testing as temporary adhesives: polyethylene carbonate (PEC), polypropylene carbonate (PPC), polycyclohexene carbonate (PCC) and a copolymer of polypropylene carbonate and polycyclohexene carbonate (PPC/PCC). The PPC was obtained from Novomer Inc. and the rest of the polycarbonates from Empower Materials Inc. The polymer PEC, Figure 6.1(a) had a molecular weight of 170k and a polydispersity index(PDI) of 3.5. Several PPC, Figure 6.1(b) polymers were tested with molecular weights between 150k and 260k with PDI between 2 and 3. Both PEC and PPC polymers were dissolved in gamma butyrolactone, GBL, at 20 wt.% for a casting solvent. A 3 wt.% by polymer idonium photo acid generator (PAG) was added to several formulations to adjust decomposition temperature by photo exposure or thermal decomposition of the PAG.

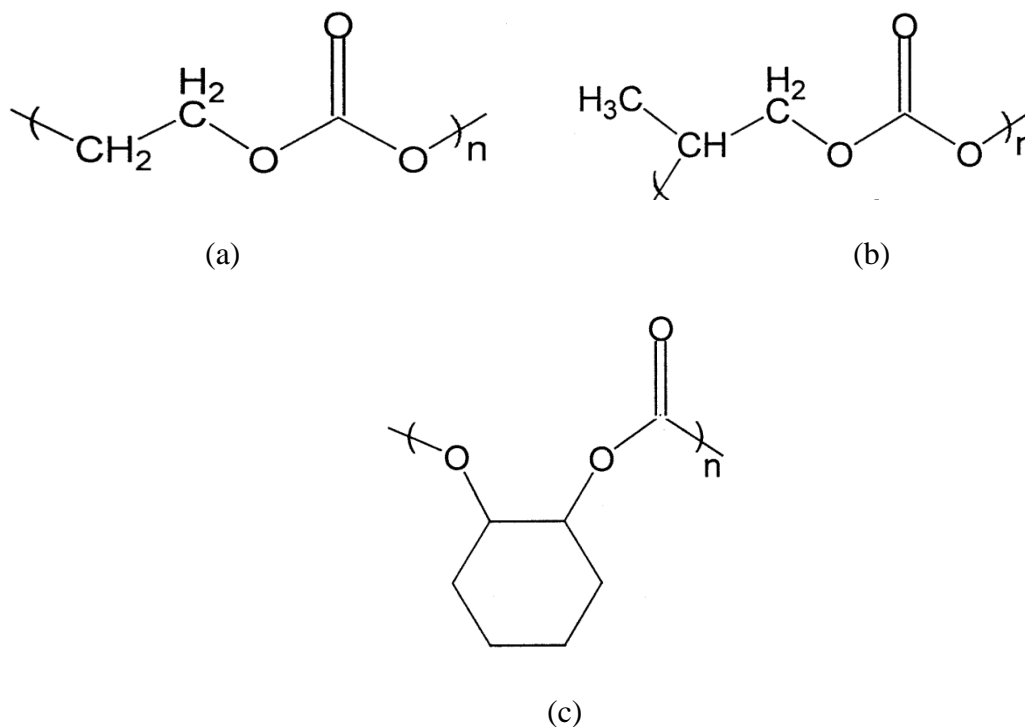


Figure 6.1: Structure of polycarbonates. (a) Polyethylene carbonate, PEC. (b) Polypropylene carbonate, PPC. (c) Polycyclohexene carbonate, PCC.

Since the higher temperature polycarbonates had not been investigated with previous air cavity research, some characterization was required. The PCC, Figure 6.1(c), and copolymer PPC/PCC were tested for decomposition products using gas chromatography – mass spectrometry. The copolymer ratio was determined by an H-NMR analysis compared to previous studies to PPC and PCC to determine the ratio for the copolymer. The materials were dissolved in solvents to test solubility for a casting solvent. The PCC polymer was dissolved to form a 12 wt.% solution in anisole. The copolymer was dissolved to a 11 wt. % in a 10:1 co-solvent of anisole and N-methylpyrrolidone, NMP. All polycarbonate formulations were tested for decomposition temperature and residue with a dynamic 1°C/min ramp thermal gravimetric analysis, TGA.

The bonding test was completed by spin coating the polymer on to silicon wafers or glass slides. The polymer was soft baked to remove the solvent and then bonded using a hydraulic heated press to the top substrate. Bonding parameters such as soft bake time, film thickness, pressure and temperature were optimized for bonding conditions. The adhesive strength of the polymers was tested using an ASM D429 Rubber – 90 degree peel test. The tests were conducted by bonding aluminum foil to silicon wafers at various film thicknesses, bonding temperatures, and bonding pressures. The aluminum foil was bonded to silicon wafers using the same hot press method. The samples were then diced into strips and clamped in an Instron, model 5842, where the aluminum is pulled 90 degree perpendicular to the wafer surface. Additional bonding test consisted of monitoring adhesion during the polishing two bonded wafers. The wafers were polished using a polisher at 350 rpm. Wafers were inspected for damage and undercut of the adhesive during the process. Wafers were released in a nitrogen purged tube furnace by decomposing the polycarbonate at the selected temperature for an hour.

6.3 Results and Discussion

In this study polycarbonates were studied for use as temporary wafer-wafer adhesives. Four polymers systems were characterized and tested for use. PPC and PEC were studied for low temperature use and PCC and the copolymer of PPC and PCC were tested for high temperature applications.

While PEC and PPC have been used in previous air cavity research, PCC and the copolymer are new sacrificial materials and require characterization. The polymers were put through a gel permeation column to determine the molecular weight of the materials.

The PCC material had an average molecular weight of 350,000 and polydispersity index of 5.5. The copolymer had an average molecular weight 300,000 and polydispersity index of 7. The large polydispersity index, PDI, is important to note and indicates a large distribution of molecular masses. The PPC and PEC have a low PDI and show a very tight control in polymerization. The high PDI of the PCC and the copolymer suggests that the materials may have more variance in decomposition temperature as well as some residue. Differential scanning calorimetry was used to determine the glass transition, T_g , of the materials. The copolymer and PCC showed glass transition temperatures of 107°C and 115°C respectively. The PEC and PPC have a T_g temperature of 25°C and 40°C respectively [65]. An increase in the T_g will help to stabilize the material from low temperature reflow or softening.

The copolymer was tested using H-NMR to determine the ratio of PPC to PCC. From previous research H-NMR analysis was completed for both PPC and PCC. PPC has the following chemical shift values, δ (ppm) from the proton nuclear magnetic resonance spectra (H NMR CDCl_3) are as follows: 1.34 (3H, CH_3), 4.17 (2H, CH_2), 5.00(H, CH) [66]. PCC has the following chemical shift values, δ (ppm) are: 1.00–2.30 (2H, CH_2), 4.6 (H, CH) [67, 68]. These peaks were the same ones present for the copolymer. The ratio can be determined by comparing the area of the 5.00 (H, CH) peak and the 4.6 (H, CH) peak. The 4.6 peak was divided by 2 to account for both CH sites of the cyclohexene monomer compared to one CH_3 site for the propylene carbonate. The ratio was determined to be 1:2.78 PPC to PCC.

Upon thermal decomposition, PEC and PPC have small volatile products of decomposition such as acetone and carbon dioxide [69]. The thermal decomposition of

PCC was analyzed with mass spectrometry. Above 250°C, the primary products consisted of volatile cyclohexane and carbon dioxide. As the decomposition temperature increased beyond 320°C, large organic products were released. The larger molecular weight groups could be due to ether linkage of the materials and other contaminants in the synthesis process. The decomposition of the copolymer resulted in the formation of similar products as with the PCC including some acetone and other small products from the PPC components.

Thermal gravimetric analysis was completed on each polymer to determine their decomposition temperature. The TGA was ramped at a constant 1°C/min, and the results seen in Figure 6.2. The PEC polymer decomposed at 165°C and PPC at 210°C. The copolymer and PCC showed very similar decomposition at 275°C. This shows that the PPC component of the copolymer will only decompose when the PCC component does. Since each polymer decomposes at a unique temperature, the material system can be selected in order to decompose at the desired temperature for each process of interest. The TGA could also be used to ascertain if significant residue would remain after decomposition. PPC and PEC showed no measurable residue in the TGA. The copolymer and PCC had a 2-5 wt. % residue remaining. This residue material could be washed away with N-methylpyrrolidone, NMP, or decomposed at higher temperature above 320°C.

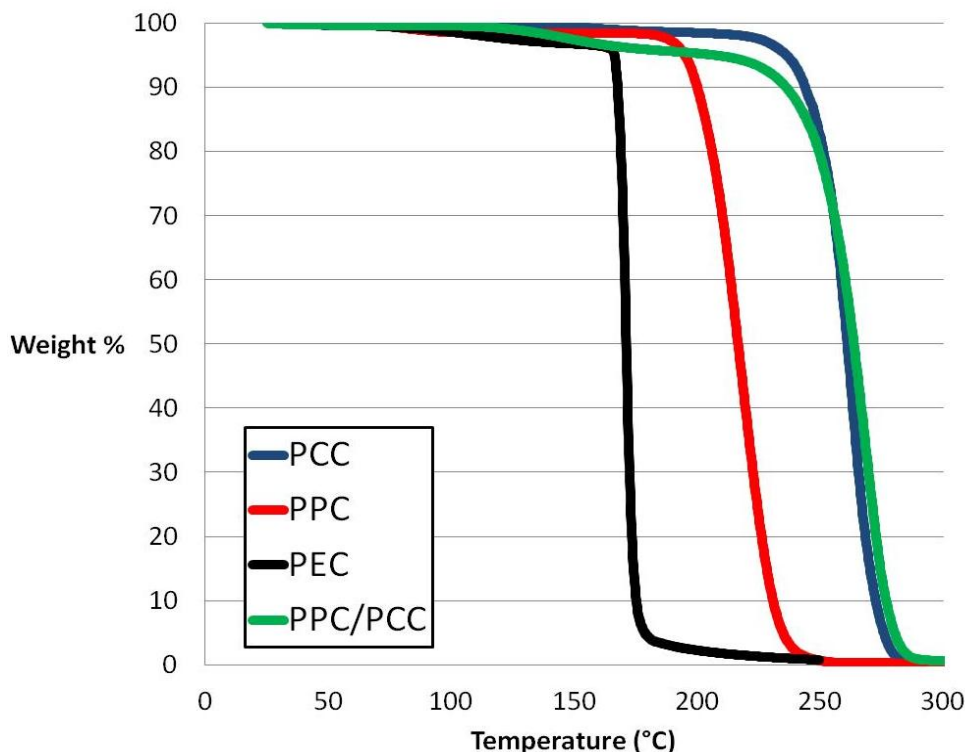


Figure 6.2: Dynamic thermal gravimetric analysis of polycarbonates ramped at 1°C/min.

Additives, such as a photo acid generator (PAG), can be added to PPC to lower decomposition temperature. The addition of PAG can provide thermal changes to lower the polycarbonate decomposition temperature by thermal or UV degradation of the PAG into an acid. This acid catalyzes the decomposition of the polycarbonate material [36]. Figure 6.3 shows a dynamic thermal gravimetric analysis (TGA) of pure PPC and a 3 wt% PAG loaded PPC. The PAG material thermally decomposes into an acid decreasing the decomposition temperature of the PPC. When exposed to ultraviolet radiation, the acid is generated at a lower temperature catalyzing the PPC decomposition at temperatures as low as 100°C. When PAG was added to the PCC, the polymer decomposed at 180°C with the unexposed case. This shows when a PAG is used the

polymer decomposition is controlled by the thermal or UV activation of the particular PAG and not the polymer.

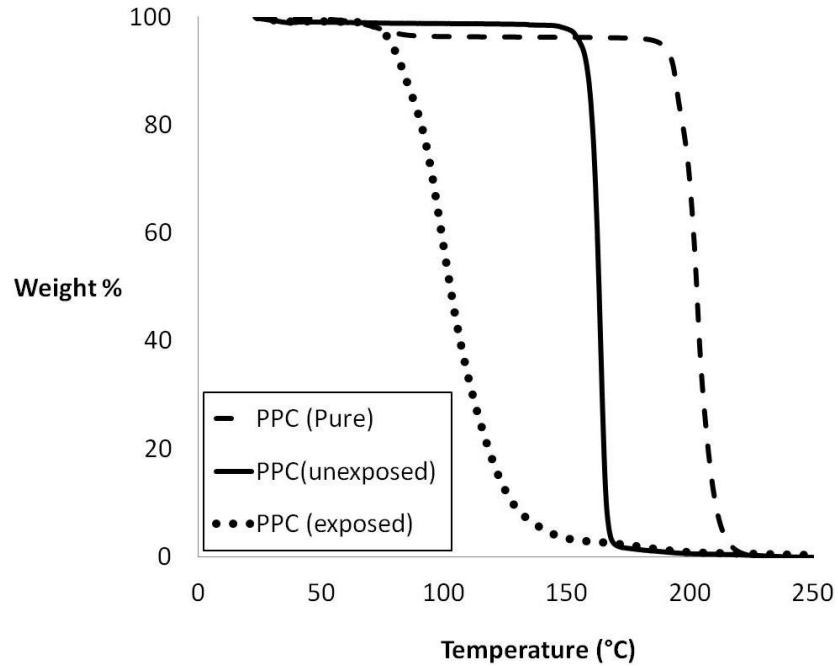


Figure 6.3: Dynamic TGA showing the effects of PAG on decomposition temperature.

Solubility testing was completed on the polycarbonates. The solubility test is important to determine which polymers would swell or dissolve in processing. Swelling, as a result of solvent uptake, may cause the polymer film to lift off from the wafers causing undercut and damage to the thin device. Polycarbonate films were exposed to solvent and observed over time. Table 6.1 shows the results of the solvent exposure to the film. The PEC and PPC experienced significant solvent uptake in many of the solvents used in microelectronic processing. The solvent uptake could prevent their use as adhesives in certain processes. PCC and copolymer were inert to a wider range of solvents preventing degradation when used as an adhesive.

Table 6.1: Solubility chart for polycarbonates. D= Dissolved, S=Swelled, and I=inert.

	Polycarbonates			
Solvent	PEC	PPC	PCC	PPC/PCC
Mesitylene	I	I	D	I
Isopropanol	I	I	I	I
Acetone	D	D	I	I
NMP	D	D	S	D
Anisole	D	D	D	D
PGMEA	D	D	I	S
GBL	D	D	I	S
Cylcohexanone	S	S	S	D
Propylene Carbonate	D	D	I	I
Methylene Chloride	D	D	D	D
Toluene	I	I	D	D
PGME	N	N	I	I
Diglyme	N	N	I	S
Benzotrifluoride	N	N	I	S
Ethyl Acetate	S	S	I	I
Xylenes	I	I	I	I

The solubility test was also completed to determine the appropriate casting solvent for the PCC and copolymer. The casting solvent should completely dissolve the material and have a low evaporation rate. If the evaporation rate is too high the solvent will evaporate during spin coating and produce uneven coats. The relative evaporation rate is given in comparison to an n-butyl-acetate standard, which has a value of 1 and is usually reported on the solvents MSDS. For instance, methylene chloride has an evaporation rate of 27.5. That is under the same conditions, methylene chloride will evaporate 27.5 times faster than n-butyl-acetate. Methylene chloride was able to dissolve all materials but is a poor choice for casting due to this evaporation rate. PPC and PEC use GBL, evaporation rate of 0.03, as a casting solvent and was tested with the previous

studies. Anisole was chosen as the best casting for PCC with an evaporation rate of 0.322. When anisole was used as solvent for the copolymer the polymer produced a film. The film was examined with a surface profilometer and found a periodic film roughness of 2000 angstroms. This roughness was removed by adding a 10% solvent loading of NMP that increased the solubility of the polymer. The roughness of the film decreased to less than 500 angstroms and was similar to the other polycarbonates. Once the polymers were dissolved, the solutions were spin coated on a wafer at various speeds and soft-baked until dry. The wafers had a visibly even-coat on the wafer except for the edge bead which covered the outermost 4 mm of the wafer coated at 500 rpm. The final film thickness, as measured at two locations on the wafer, is shown in Figure 6.4 for PCC and the copolymer.

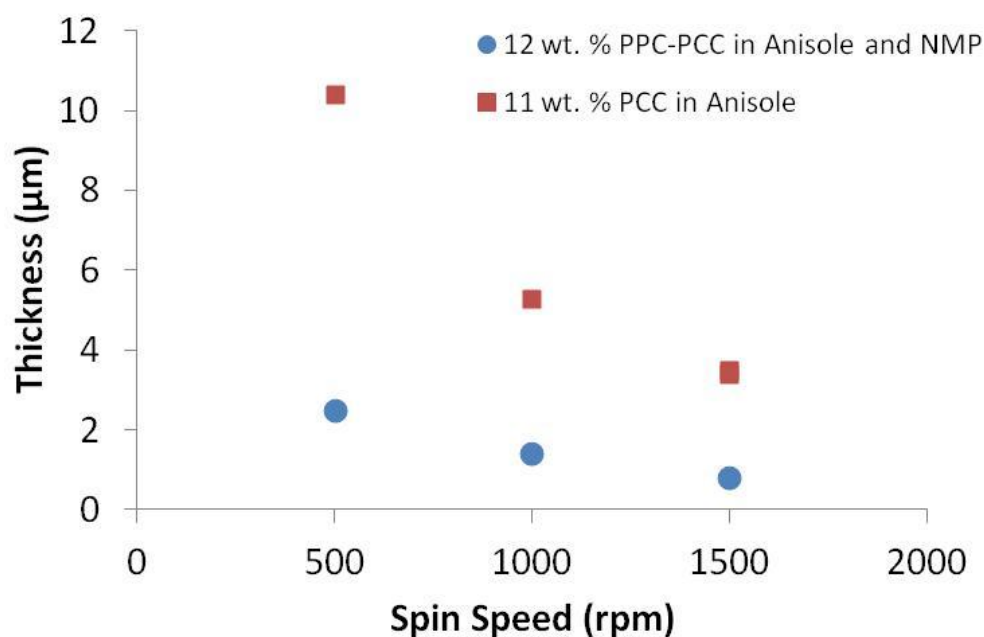


Figure 6.4: Spin speed curves for PCC and PPC/PCC formulations.

Once, formulations of the polycarbonates were specified, the corresponding films were optimized for substrate bonding. Films of each polycarbonate were spin coated on wafers. The samples were soft-baked to remove all the solvent. The soft bake time varies depending on thickness and casting solvents. If the soft bake is not long enough, the residue solvent will prevent adequate adhesion when bonding. Polymers dissolved in GBL required a soft bake for a minimum of 6-8 minutes at 100°C. The polymers dissolved in anisole had a faster evaporation rate and were soft baked for 1-3 minutes at 100°C. Variations in soft bake time were to account for different thickness of films with thicker films requiring longer soft bakes. The polymers were bonded to aluminum foil by being pressed in a heated press for 8 minutes. The bonding conditions were set to 135°C and 225 kPa. The samples were then diced into strips and clamped in an Instron, where the aluminum is pulled 90 degree perpendicular to the wafer surface.

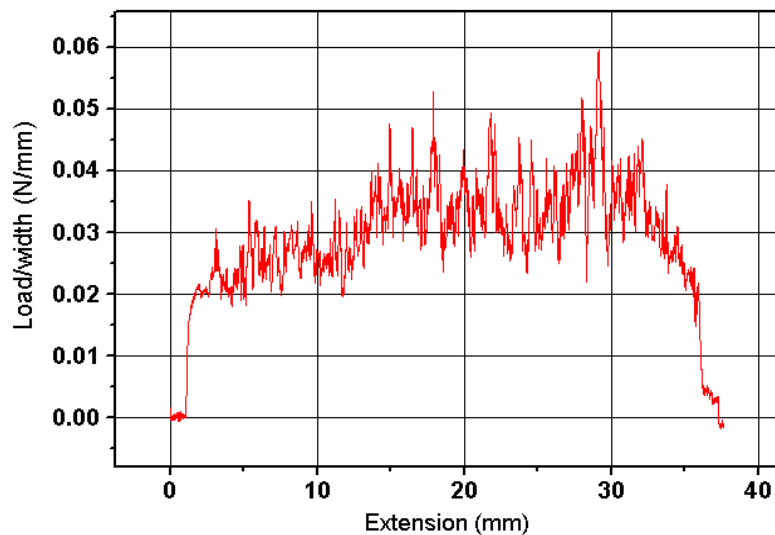


Figure 6.5: Result of a single PPC 90 degree peel test.

Since each sample had slight variance with each peel test, the average load of each test was recorded for 10-20 samples of each test. For instance Figure 6.5 shows the results from a typical peel test for a PPC film. The experiment determined an average peel strength of 0.03 N/mm. This run would then be repeated 20 times to confirm the result and determine any deviations. Table 6.2 shows the average result and deviation for each material.

Table 6.2: Average adhesive strengths for bonded polycarbonates and tapes.

Material	Adhesion strength (N/mm)
PEC	0.01± 0.005
PPC	0.03± 0.02
PCC	0.05± 0.02
PPC/PCC	0.05± 0.01
Furukawa Tape #1	0.05± 0.02 (unexposed)
Furukawa Tape #2	0.15± 0.03 (unexposed)
Scotch Tape	0.09± 0.02

In all cases, the aluminum foil debonded from the polycarbonate rather than the polycarbonate from the wafer. This suggests that the bond strength could be stronger than the measured adhesive strength. The polycarbonates bonding strength was compared to scotch tape and Furukawa UV tape. The Furukawa tape is a thermally bonded double sided tape. When exposed to UV light the adhesive decomposes allowing for a low force release. All polycarbonates show similar adhesion compared to the tapes. This is due to the fact that there is no chemical interaction between the polycarbonates and the wafer

surface. The adhesion is due to a low surface energy film brought into a uniform contact with a large surface.

The 90 degree peel test was used to optimize film thickness, bonding temperature and pressure. Films at thicknesses between 1 and 15 μm thick were tested for each polymer. Film thickness played no role in the adhesion strength. This is most likely due to the fact that the adhesion is a surface property. This allows thin film adhesives reducing material and space between the substrate and the handler wafer. Bonding temperatures were tested between 80°C and 180°C. Figure 6.6 shows the thermal optimization of PPC. The best adhesion showed the film should be well above the reflow temperatures of the polycarbonates. The reflow helps the polymer bond uniformly across the entire wafer surface. While an upper limit for bonding temperature was not determined, no advantage was found for higher temperature bonding.

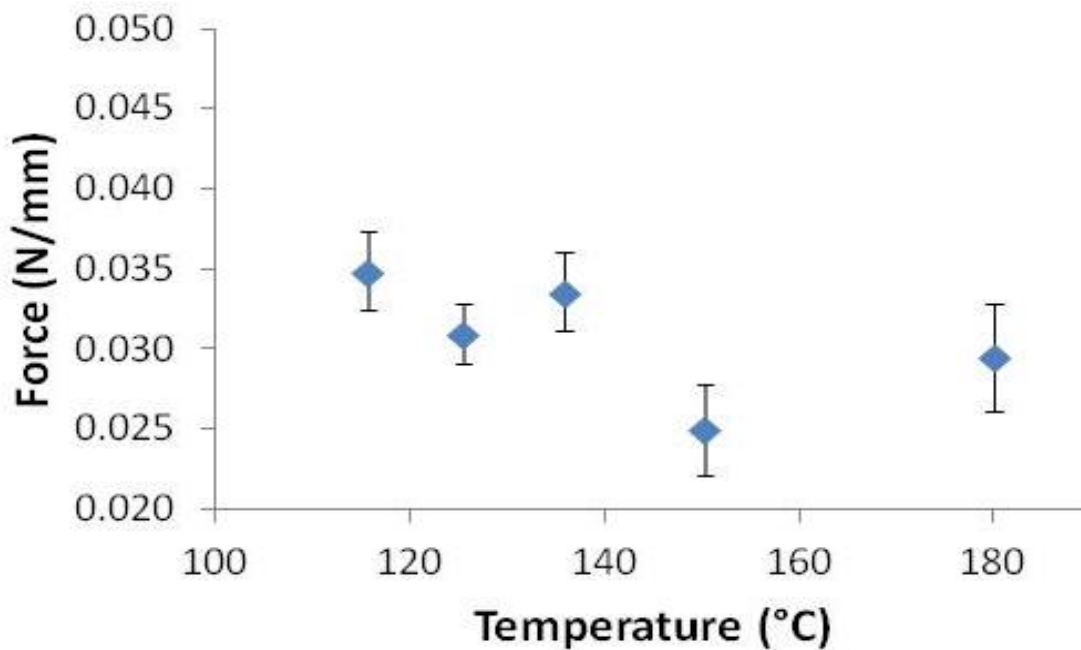


Figure 6.6: Peel test results from optimization of bonding temperature for PPC adhesive.

The bonding pressure tests were completed between 100 kPa and 600 kPa. Figure 6.7 shows the bonding pressure of PPC. The wafers did not successfully bond below pressures of 200kPa and could easily be removed by handling. Above 200 kPa, the bond strength proved adequate and did not increase with increased pressure.

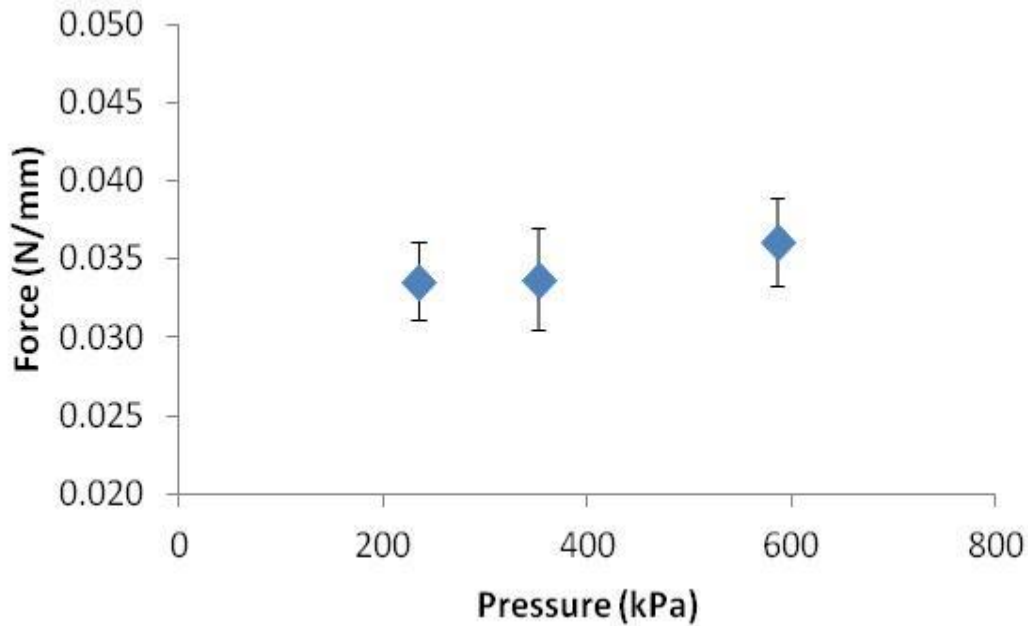


Figure 6.7: Peel test results from optimization of bonding pressure for PPC adhesive.

All polycarbonates showed similar bonding conditions to the PPC results above. This allowed the setting of optimal bonding conditions for all polycarbonate formulations. The optimal bonding conditions are 3-5 μ m thick films bonded at 135°C, 225 kPa for 8 minutes.

Once the optimum bonding conditions were set, the polycarbonate adhesives could be tested in a polishing system. Full wafers were bonded with each polycarbonate system. The wafers showed good adhesion and could not be separated by hand. The wafers were mechanically polished with a slurry at 350 rpm to remove 200-300 μ m of the

wafer. During the study no wafers were damaged or debonded during the polishing. The edges of the samples were optically investigated. The adhesives except for PEC showed no undercut of the material maintaining the full film and protecting the edge of the wafer. PEC showed an undercut of a few microns with material being etched out during the polishing process. The PEC bonded wafer was not damaged at this point but could be an issue with thinner substrates.

The debonding process was completed to demonstrate the ability to the release of the wafers. Debonding was completed in a nitrogen purged tube furnace. Samples were investigated for residue, damage, and remaining adhesion. The PPC and PEC samples were heated to 220°C for 2 hours to ensure complete decomposition. The wafers were released without any mechanical force. Inspection of the wafers shows no visible residue on the surface or damage. The PCC and copolymer were decomposed at 280°C for 2 hours. These wafers did not release freely and required a slight force of the hand to separate. Once separated the wafers showed a residue film dispersed over approximately 65% of each surface. When weighed and compared to the original weight of the film, the residue was approximately 2-5 wt. % of the adhesive applied. This correlates with TGA and mass spec results showing high molecular weight organic material remaining. The residue was easily removed with NMP solvent and a polishing cloth. A set of wafer/Al foil adhesive samples were decomposed and peeled to determine the adhesion strength of the PCC and the copolymer residues. The residue tests were compared to the exposed Furukawa tapes. Table 6.3 shows the result of the 90 degree peel test. The PCC and copolymer show an order of magnitude decrease in adhesion strength from the bonded samples. The adhesion also shows similar peel strength to the exposed tapes.

Table 6.3: Average adhesive strengths in wafer debonding for polycarbonate residues and UV exposed tapes.

Material	Adhesion strength (N/mm)
PEC	0
PPC	0
PCC	0.0035± 0.002
PPC/PCC	0.0035± 0.002
Furukawa Tape #1	0.024± 0.001 (exposed)
Furukawa Tape #2	0.004± 0.0005 (exposed)

6.4 Conclusion

Polycarbonates were tested for low cost temporary adhesives in wafer-wafer bonding. Polycarbonates were formulated for decomposition between 160°C and 270°C. Polycarbonates were characterized for spin coat deposition and optimal bonding conditions. Bonded wafers using the polycarbonates showed adequate adhesion for wafer thinning. Low temperature polycarbonates, PEC and PPC, showed modest resistance to chemical and thermal processing and free wafer release with no residue. High temperature polycarbonates demonstrated excellent chemical resistance, but slight adhesion upon release due to residue remaining after decomposition.

CHAPTER 7

ELECTROLESS DEPOSITION OF COPPER AND SILVER

7. 1 Introduction

Electroless deposition plays an important role in the microelectronic packaging industry. One particular area of interest is the electroless deposition of copper on epoxy based materials such as FR-4 board. The use of electroless metallization eliminates the need for costly vacuum processes, such as sputtering and evaporation. It would especially be valuable to electrolessly deposit metal on the overcoat for the MEMS package to improve the mechanical strength without the use of a sputtering system. A key to the performance and reliability of the electroless process is the adhesion between the deposited copper and the dielectric material. To ensure the materials have adequate adhesion, the substrate (e.g. epoxy board) is chemically etched to roughen the surface as to facilitate mechanical anchoring. The seeding of the surface with a metal catalyst activates the surface for deposition. Adhesion of the resulting copper layer is also achieved through intimate bonding of the catalyst layer to the dielectric surface. As the signal frequency increases, additional attributes are required. The high surface roughness of the epoxy board, which facilitates mechanical anchoring, causes electron scattering at high frequency.

Second, the current metal catalyst system, Sn/Pd colloids, has become expensive due to the cost of palladium. Non-palladium catalysts are of interest for the efficient catalysis and adhesion of electroless copper to organic and inorganic substrates.

The swell and etch process currently used to activate phenol-novolac epoxy used in printed wiring boards (PWB) provides an efficient, cost-effective method for creating a

catalyst-friendly surface. The swell and etch is completed in a three step process. The samples are placed in a swelling solvent which rearranges polar groups in the polymer into packets for etching [70]. The substrate is then etched in a potassium permanganate etch bath preferentially attacking these packets to form pores. A neutralizing bath is required to remove any trace amount of the etchant from the substrate before catalyst deposition. Figure 7.1 shows the proposed mechanism for this process which creates a porous surface for copper adhesion. A detailed study of the pore structure in the swell and etch process has been published [70-74].

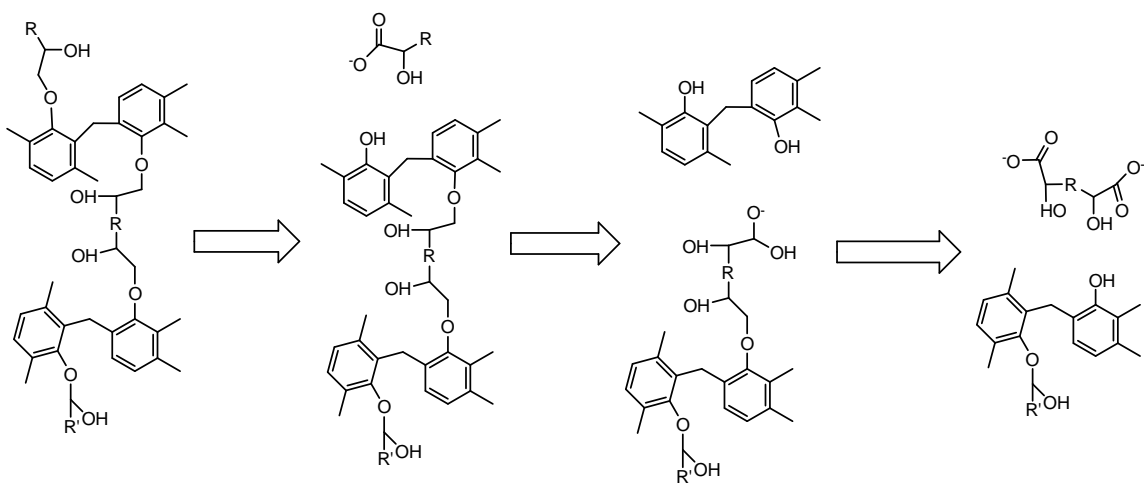


Figure 7.1: Mechanism of phenol-novolac etching prior to Sn-Pd activation [70].

Once the surface has been treated, the surface is activated by immersion in an acidic Sn(II)-Pd(II) chloride solution. The catalytic surface is composed of palladium particles produced through the reduction of Pd^{+2} to Pd, and oxidation of Sn^{+2} to Sn^{+4} [75-77]. The Pd activation process uses a colloidal tin solution, originating from the presence of Sn(IV) formed during the oxidation of Sn(II) [78]. Chloride ions are important in stabilizing the palladium/tin colloid in solution and on the epoxy surface [33]. The stannic chloride has been shown to form a stabilizing colloid around the Pd particles

which assists in adhesion of the copper film and uniformity of the catalyst. While there is no clear explanation of the mechanism or colloid adhesion, it is expected to be due to the electrostatic interactions of the negatively charged colloids with the positively charge surface created under acidic conditions [79].

Palladium-free catalysts have been investigated due to the rising cost of the metal. However, the key point of the process is how to form and adsorb the catalytic particles on the substrate with good uniformity and excellent adhesion, without increasing cost. Furthermore, the candidate materials should have a similar reduction potential so as to form the catalytic metal. The traditional reducing agent in electroless copper has been formaldehyde which can be catalyzed by many metals, including Au, Ag, Pt, Ru, Ni and Co [80-82]. Among them, silver is an interesting choice because it is a semi-precious metal with a reduction potential similar to Pd, and can be easily produced electrolessly, however at significantly lower cost (\$32/troy ounce for silver vs. \$575/troy ounce for palladium in November, 2011).

Inorganic substrates have attracted interest as dielectric materials due to their low dielectric constants and low CTE. The electroless deposition of silver on glass has been used to form adherent, smooth layers, especially in the production of mirrors. However, the approach has usually been to spray solution on to the surface in thin layers, and the process has not been used in microelectronics.

Thus, this investigation focuses on the deposition of thin silver layers on silicon oxide and POSS as the catalyst for the subsequent electroless copper deposition that could be used to improve packaging substrates. The electroless deposition on untreated silicon oxide could improve interposer technology such as metal deposition on vertical

sidewalls used in through silicon vias. The silicon oxide content in POSS, as described in Chapter 5, could be used in a similar manner as the silicon dioxide surface, to create a metalized dielectric. The goal is to create a catalytic surface for the electroless deposition of copper on both silicon oxide and POSS surfaces with good adhesion and without roughness which would interfere with the electrical conductivity at high frequency. The bath properties will be optimized to improve deposition rate and adhesion for use in inorganic packaging substrates.

7.2 Experimental and Material Selection

An FR-4 board was used as a substrate for Ag and Cu electroless plating before using silicon dioxide or POSS as the substrate to identify the optimum activation and plating conditions. A copper-cladded FR-4 board was used as the substrate. The Cu layer was etched in concentrated nitric acid, then rinsed in DI water and dried. The surface had rough finish with pores created from the previous swell and etch process. The deposition process consisted of Sn sensitization, Ag activation, and electroless plating. The samples were rinsed carefully in DI water between each step to avoid any cross-contamination of the solutions during the process.

Similar processing was then performed on the silicon oxide and POSS samples. A silicon oxide was grown on silicon wafers and followed by electroless deposition of copper. Once the electroless bath was optimized, the electroless copper process was used to deposit metal on the side walls of through silicon vias. The POSS samples were spin coated onto FR-4 boards and silicon wafers and then soft-baked on a hotplate at 85°C for 5 minutes to remove the solvent from the polymer film. A 1 kW Hg-Xe lamp with a

broad band filter over 350-380 nm was used for exposure with an optimal dose of 250 mJ/cm². The POSS film was sometimes reactive ion etched in an oxygen plasma at 310 mTorr pressure and 100 W power for 1 minute to remove the organic content near the surface. A chromic etch was also investigated on the POSS surfaces prior to the Sn sensitization to ensure the surfaces were clean and oxidized.

Substrates were characterized with a profilometer to determine surface roughness. Surface hydrophobicity was tested using water contact angle measurements with a Rame-Hart CA goniometer. A Thermo K-alpha XPS was used to analyze the metal seeding of the surface. Metallization was examined for plating quality and adhesion. Bath concentrations and time were adjusted to improve the metal quality. The metal was cross hatched and 3M tape tested for adhesion.

7.3 Results and Discussion

There are two goals to this effort. The first is the replace the palladium catalyst used in electroless copper deposition with a less expensive metal. The second goal is to achieve acceptable adhesion of the catalyst and subsequent electroless copper on smooth silicon dioxide, or primarily silicon dioxide surfaces. It is appropriate to simultaneously address the two goals since the initial catalyst deposited on the insulating surface is the primary route for bonding and adhering the electroless copper film to the insulator. Thus, creation of suitably active catalyst, such as for the oxidation of formaldehyde in electroless copper, with excellent bonding to the silicon dioxide containing surface is the central topic of this study. Silver was chosen as the metal of choice since it is easily

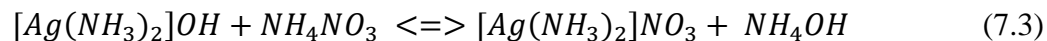
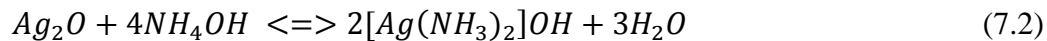
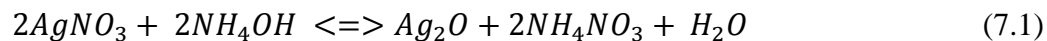
deposited electrolessly, can be deposited on glass surfaces with good adhesion, and is a Group IB metal (as copper is) and should provide a catalytic surface for copper.

Since the Sn (IV) colloid is an integral part of the formation and adhesion of the palladium catalyst to surfaces, a similar tin-colloid route was chosen with silver. A Sn/Ag catalyst seeding was tested on organic and inorganic substrates for potential use on organic (epoxy-based) boards and inorganic (silicon and silicon dioxide based) package substrates.

The electroless deposition was first tested on an FR-4 board, as a control followed by a POSS coated FR-4 board in an attempt to show that the Sn/Ag catalyst can be used to replace the Sn/Pd catalyst on organic and organic /inorganic hybrid surfaces. The FR-4 board was prepared for electroless deposition by etching the copper from a copper-clad board in nitric acid. One sample was seeded for electroless plating directly after stripping the copper and a second sample was spin-coated with POSS on the roughened epoxy surface, which will be discussed below. The seeding process consisted of the two-step activation process with the first step being tin sensitization followed by silver seeding. The tin bath served to seed the POSS surface with tin ions that anchor the silver-tin colloid to the POSS surface. The tin sensitization step consisted of a 30 min immersion in a bath consisting of 180 mL of de-ionized water, 2.4g of tin (II) chloride dihydrate, and 2 mL of hydrochloric acid. Other concentrations and immersion times were investigated. While some deposition of the catalyst, as measured by the subsequent deposition of electroless copper, almost always occurred, this formulation and immersion time were found to give the best coverage and most reproducible results.

The tin colloid on the FR-4 surface was used to reduce silver ion forming adherent islands on the surface to serve as the electroless copper catalyst. After immersion for 30 min in the tin chloride bath, the sample was rinsed with water and immersed in the silver nitrate bath. The silver/tin catalyst colloids are formed through the oxidation of tin (II) ions oxidize to tin (IV) and reduction of the Ag (I) to Ag. The silver bath consisted of 180 mL de-ionized water, 0.7 g silver nitrate, 10 g ammonium sulfate, 10 mL ammonium hydroxide, and 0.2 mL triton X-100. It is important that the components be mixed in the order listed here with the reducing agent, hydrazine sulfate, being added last so that an unstable mixture is not produced. The adhesion and surface coverage of the silver on the surface is a function of time in the bath. It was found that one minute is the optimal amount of time in the bath to produce a suitably thick, adherent film on the surface to serve as the catalyst for electroless silver or electroless copper plating.

Three different speed plating baths were investigated for each copper and silver, as described in Table 7.1 and 7.2. The deposition rate of the plating baths was changed by adjusting the concentration of the components. The concentration of the base (i.e.pH) is important because hydroxide is consumed in oxidation of the reducing agent. The concentration of metal ions is also important in the electrochemical reaction. Equations 7.1-7.4 show the reactions required for silver plating with hydrazine as the reducing agent [83]. In the reaction the silver nitrate and ammonium hydroxide are necessary to form the silver ammonia nitrate consumed in the deposition reaction, (Equation 7.4). By controlling the concentration of these two components, the speed of the bath can be controlled through the equilibrium reactions, 7.1-7.3.



The deposition rate generally has a strong influence on the density, grain size, and surface texture of the deposited metal. The deposition rate of the metal can also affect the adhesion of the metal to the surface. If the metal catalyst is the anchor for adhesion of the deposited layer to the surface, then slow growth, where the catalytic islands evolve into full surface films, is preferred. High densities of these catalytic islands are preferred. If the growth rate is too fast, a sufficient number of nucleation sites may not form on the substrate surface. These nucleation sites are key for adhesion of the film to the surface.

Table 7.1: Bath formulations for electroless silver.

	Water	AgNO ₃	NH ₄ (SO ₄) ₂	NH ₄ OH	Triton X-100	H ₆ N ₂ O ₄ S	Average Plating Rate
Ag-A	180 mL	0.2 g	10 g	15 mL	0.2 mL	0.25 g	40 nm/min
Ag-B	180 mL	0.4 g	10 g	15 mL	0.2 mL	0.25 g	20 nm/min
Ag-C	180 mL	0.7 g	10 g	20 mL	0.2 mL	0.25 g	10 nm/min

The electroless baths shown in Tables 7.1 and 7.2 had limited lifetimes after the hydrazine sulfate was added. The baths were active for several hours before spontaneous reaction of the reducing agent and metal ion occurred.

The slowest deposition rate silver bath, Ag-A, produced a 800 nm layer of silver in about 20 minutes. The medium speed silver bath, Ag-B, produced the same quantity of

metal in half the time, ca. 10 minutes. The fastest bath, Ag-C, was about twice the rate of Ag-B. An inadequate seed layer resulted in slower overall deposition rates.

The electroless copper baths shown in Table 7.2 were operated at 55°C. The overall reaction for copper plating, equation 7.5, also consumes the copper ions and the base allowing the same control for deposition rate [70].



The average deposition rates for Cu-A, Cu-B, and Cu-C were 60, 30, and 15 nm/min, respectively.

Table 7.2: Bath formulations for electroless copper.

	Water	CuSO ₄ * 5H ₂ O	EDTA	KOH	Triton X- 100	HCHO	Average Plating Rate
Cu-A	200 mL	0.25 g	0.63 g	0.86 g	0.2 mL	0.58 g	60 nm/min
Cu-B	200 mL	0.75 g	1.89 g	2.58 g	0.2 mL	0.58 g	30 nm/min
Cu-C	200 mL	1.26 g	3.16 g	4.3 g	0.2 mL	0.58 g	15 nm/min

The A and C bath for copper and silver were tested on the FR-4 board after silver activation. The films deposited for 45 minutes had a uniform thickness and matte finish, suggesting a somewhat rough surface. The speed of the bath (A and C) produced the same finish, and adhesion for silver and copper on the FR-4 board.

The adhesion of the electrodeposited films to the substrates was investigated using a traditional tape test, ASTM D3359. A cross-hatch of 1 mm squares was scribed into the sample to test the peel strength at the corners of the cross-hatched pattern. The film adhesion was found to be excellent with no film peel-up or damage of the electrodeposited film. The surface roughness was found to be 200 to 500 nm (room mean square value of peaks-to-valleys). Since the Sn/Ag catalyst with electroless plating passed

the same tape-test, just as the Sn/Pd catalyst did, we conclude that the Sn/Ag is an effective and adherent catalyst for electroless deposition on FR-4 boards.

The electroless deposition was then tested on epoxycyclohexyl POSS coated substrates. An epoxy POSS film was spin coated onto FR-4 boards, prepared as described above. The films were soft baked for 5 minutes and then exposed 365 nm radiation at a dose of 250 mJ/cm². The POSS film formed a smooth, hydrophobic surface. The organic component of the POSS likely contributed to its hydrophobic nature. An oxygen plasma was used to change the surface properties of the POSS. The reactive ion etch conditions include a pressure of 310 mTorr pressure and 100 W power for 1 minute. The reactive ion etch likely removed the organic component of the POSS at the surface leaving a predominantly silicon oxide surface. The POSS surface changed from hydrophobic with a water contact angle of 88° to hydrophilic with a water contact angle of 13°. The effect of oxygen plasma etching on the electroless seeding was investigated using the silver activation and plating process. The plasma etched sample showed uniform deposits over the entire sample whereas the unetched POSS surfaces showed little to no deposition. It was found that the silver bath with the slowest deposition rate, Ag-A, produced films with the highest adhesion. The samples produced using the fastest plating bath, Ag-C did not pass the tape test.

In an effort to improve the metal adhesion to the POSS surface, a variety of cleaning steps were investigated. It is possible that organic material remained on the POSS surface. Several different cleaning baths were tested including a (i) 3 vol% sulfuric acid bath, (ii) 1:1:2 vol. ratio of acetone, isopropyl alcohol, and water, and (iii) citric acid and peroxide bath. These baths generally improved the adhesion of the electroless metal,

especially if the samples were left in the cleaning solution for extended periods of time, e.g. 50 min. However, none of these cleaning solutions was fully effective at providing adequate adhesion to the POSS surface.

Based on the three cleaning baths described above, it was concluded that the surface contaminants responsible for blocking adhesion were not simply adsorbed on the surface since these baths did not dissolve away the contaminants. Thus, a stronger oxidant was chosen in attempt to improve the chemical bonding of the metal film to the POSS surface. Previously, dichromate has been used to oxidize surface films and etch epoxy boards to improve the chemical bonding of electroless metal to the surface [84]. The chromic acid etch consisted of 40 mL de-ionized water, 75 mL sulfuric acid, and 1.3 g potassium dichromate and was maintained at 70°C.

The sample treated with the chromic acid etch for 1 to 10 minutes showed similar adhesion to the POSS surface as those etched in 3 vol.% H₂SO₄ for an equivalent amount of time. However, the samples in chromic acid had a faster deposition rate on POSS and FR-4 board surfaces than when the samples were cleaned with sulfuric acid. This was determined by investigation of the back of the samples (POSS free). The FR-4 surface was uniformly plated and adherent when using the chromic acid and had no plating when the sulfuric acid bath was used instead.

Samples that were etched for 30 minutes in the chromic acid etch and silver plated produced undesirable results. A 2 µm silver film was deposited on the POSS substrate using bath Ag-C. The film appeared to be reflective and uniform. However when tape tested, the silver layer would uniformly peel up showing a second silver layer underneath it. The second silver layer appeared to be granular and adherent. Thermal annealing the

samples at 200°C for 8 hours did not improve adhesion of the silver layers to each other. It was assumed that this dual-layer silver was resulting because of the silver bath properties and not the catalyst process due to the adherent silver on the POSS surface. Attention was shifted to copper deposition to see if a similar effect would occur through the electroless deposition of copper.

The adhesion of the electroless copper to the POSS surface was investigated using oxygen plasma etching and chromic acid etching. All samples were then tin sensitized for 30 min, followed by silver activation for 1 min, and copper deposition in Cu-B at 55°C for 3 to 5 min. The tape test showed that the adhesion of the copper to the POSS surface was substantially improved. When the chromic acid etch time was increased to 30 min, the POSS surface was easier to activate. Copper films deposited for 4 min had uniform coverage and very good adhesion. Only small, isolated regions of the copper surface were removed in the tape test. It was found that samples which were allowed to dry for 24 h at room temperature showed excellent adhesion with no defects or removal of the copper during the tape test. Figure 7.2 shows the resulting copper sample and tape test. The copper was highly reflective compared to the film prepared on the FR-4 board indicating a smooth POSS base coat compared to the roughened FR-4 starting material.

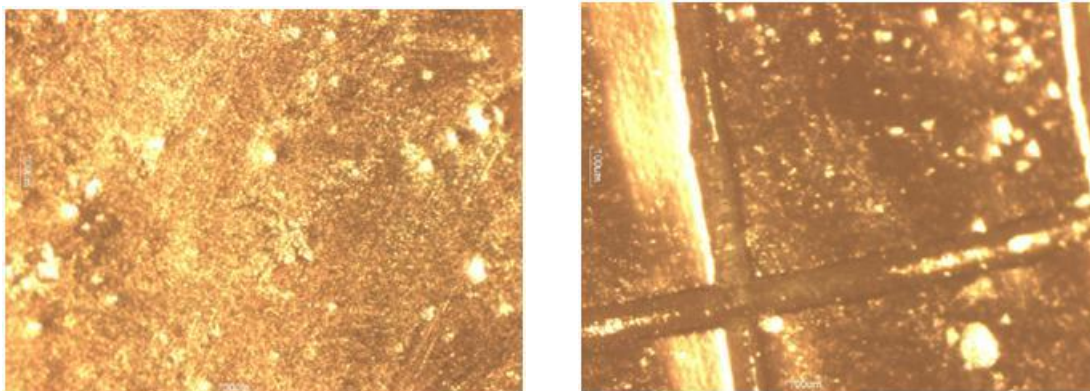


Figure 7.2: Electroless copper deposition on the treated POSS surface and a portion of the cross hatch test.

The surface properties of POSS were characterized to investigate the origin of the improvement in copper adhesion. POSS coated samples were taken through the activation process, but not electrolessly plated. The surface roughness was found to be 30 to 50 nm, a ten-fold improvement compared to the FR-4 surface. The deposition of adherent electroless copper on a smooth POSS surface is an important advancement for improving high frequency performance of interconnects on substrates. The etching processes used to create a suitable POSS surface do not roughen the surface like was needed for mechanical adhesion to an epoxy board. Thus, there is a greater degree of chemical bonding to the POSS surface. Thus use of hexavalent chromium as the adhesion promoting etchant has been reported previously by Laine-Ma et al [84]. They claimed a sulfuric acid/chromate etch had the best adhesion for surface conditioned epoxy board. The chromic etch was compared to mechanical abrasion, permanganate etch, and nitric acid etchants used. In their study maintaining a high chromic acid concentration, temperature and etch time were important to ensure the surface conditioning for adhesion of the copper film. The adhesion mechanism was assumed to be a combination of mechanical interlocking of metal particles and interfacial forces between the metal layer and the substrate [84].

However when used on the POSS surface in this study, the surface roughness does not increase as it did in the epoxy systems. This suggests interfacial forces between the metal and substrate and/or another chemical interaction is providing the improved adhesion of copper to POSS.

It is of interest to investigate the surface conditions created related to the improved adhesion. The POSS surface was analyzed using XPS determined chemical state of the surface just after catalyst activation. Untreated POSS was analyzed and, the original surface conditions contained 68% carbon, 11% silicon, and 23% oxygen. The etched/catalyzed POSS surface was found to contain 32% carbon, 25% silicon, and 38% oxygen. This shows a lower carbon content compared to untreated POSS due to the RIE and chromic etch removal of organic material. The surface also contained 3% Ag (zero valence state) and 1% Sn (IV). Sn(II) was not present. This is expected because Sn (II) is oxidized to Sn (IV) during the catalyst seeding process; however, any remaining Sn(II) oxidation may have occurred after the silver process was complete due to air oxidation. The chromium concentration was found to be ca. 0.25% in the form of Cr (VI). The chromium residue is undoubtedly from the chromic acid etch step. Based on the fact that a dramatic improvement in adhesion was realized with the addition of the chromic acid etch step without increasing the surface roughness, it is possible that the chromium moiety on the surface contributes to adhesion of the Sn/Ag catalyst itself, or it simply oxidizes the POSS in such a way so as to create chemical compositions which are more interactive with the Sn/Ag catalyst. Chromic acid is known to leave paramagnetic chromium (VI) on surfaces when cleaning glassware, which can be removed only with repeated soaks with nitric acid [85]. While a chromic etch has been successful for

improved epoxy etching and deposition for copper, the exact role of chromium residue in adhesion of electroless plating has not been reported in previous studies. It is also known that chromium metal acts as an adhesion-enhancing seed layer with other metals, such as copper, through the formation of chromium oxide linkages between the surface and the metal. The improvement in adhesion with a 24 h digestion period is also curious. It is possible that copper grain growth, adhesion layer oxidation/reduction, or surface dehydration could be taking place. Probing the interface between the electrolessly deposited copper and POSS for changes in the trace impurity levels is exceedingly difficult and has not yet yielded successful results in this study.

The electroless deposition of copper directly on a thermally grown silicon oxide layer was also attempted. There are advantages to electrolessly depositing copper on an oxide coated wafer, especially in cases such as through-holes used in through silicon vias, TSVs, and other applications. The deposition of metal on the sidewalls of high aspect ratio through-holes is difficult by sputtering or evaporation because of the line-of-sight nature of those processes. The ability to metalize sidewalls can improve processing for chip packaging and MEMS devices.

The electroless Cu deposition on silicon dioxide surfaces and in TSV-etched wafer involved the same four steps as used above: (i) cleaning, (ii) Sn sensitization, (iii) Ag activation, and (iv) electroless Cu deposition. The cleaning solution used was 3 vol% H_2SO_4 in water. The tin sensitization solution and silver activation baths were the same as discussed above. The Cu-B bath was used. It was found that baths with higher deposition rates, e.g. Cu-C, produced hydrogen gas at too high of a rate causing poor film uniformity. The deposition rate of the Cu-A bath was inconsistent on the silicon oxide

surface.

Wafers containing an array of 120 μm diameter TSVs were fabricated. After fabrication, plasma enhanced vapor deposition was used to deposit a 500 nm thick silicon dioxide layer. The samples were cleaned for 10 min on an inclined plane in the bath for better flow into the vias. The sample was rinsed and placed in the Sn sensitizer for 15 min. It was then placed in the Ag activation solution for 1 min followed by copper deposition in the Cu-B solution for 3 min. The 500 nm thick Cu was uniform and reflective. The inside of the holes were coated with copper as shown in Figure 7.3. Since plating occurred on both sides of the substrate the deposition was not limited by the depth of the TSVs or mobility of the bath to the sidewalls. The copper film showed modest adhesion to the top of the substrate when tape tested 24 hours after the deposition. Thus, the Sn/Ag activation step was effective for activating the silicon dioxide surface as well as producing an adherent coating to the substrate and TSVs.

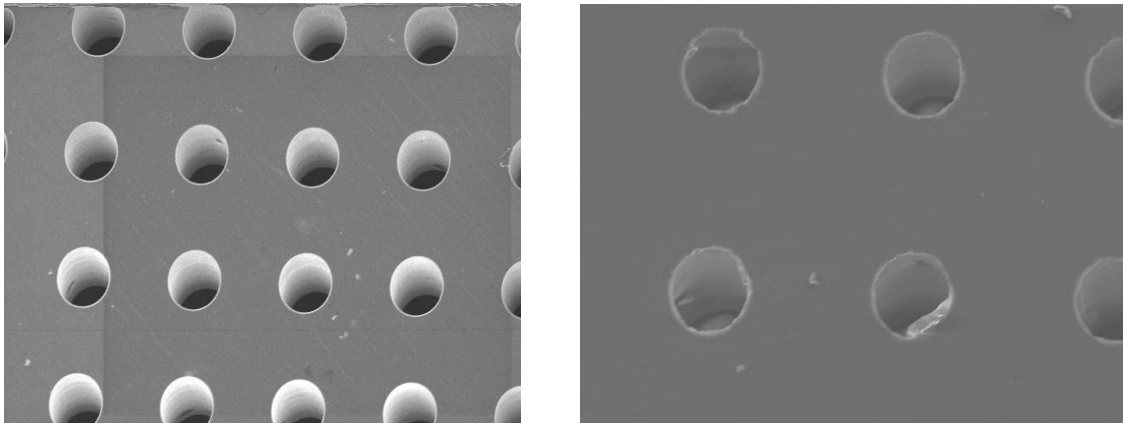


Figure 7.3: SEMs of electroless copper deposited on the sidewalls of TSVs. The copper on the top surface was polished off.

7.4 Conclusion

An improved electroless deposition process for silver and copper was developed. The Sn/Pd activation was replaced by a cost efficient Sn/Ag catalyst. The process was shown to be able to deposit silver and copper on epoxy, POSS, and silicon dioxide. The films were adherent on to a roughened epoxy board, POSS coated surfaces, and silicon dioxide. Silver deposition on POSS showed poor adhesion; however, the adhesion of copper on smooth POSS was dramatically improved by the addition of an oxygen plasma clean and chromic acid etch. Electroless copper deposition was demonstrated on untreated silicon oxide wafers for TSV sidewall deposition.

CHAPTER 8

MICROFABRICATION CHALLENGES AND SUMMARY

8.1 Feasibility and Challenges

This work, demonstrates improvements in materials and processing for air cavity technology for the particular application of MEMS packaging. The air cavity MEMS package project provided a demonstration of the technology at both the wafer and chip level, as well as a fundamental understanding of the mechanical requirements necessary for further advancement. Additionally, the materials and processing developed in this work have already been applied and improved other air cavity and microfabrication studies such as air clad coaxial interconnects [86], air gap polyimide foam used in mechanical sensors [87], and magnetically actuated micro peel test structures [88]. However, there are still issues to address concerning air cavity technology and materials which will contribute to MEMS packaging and other microfabrication processes. A discussion is provided of the feasibility and challenges of implementing materials and air cavity processing for these packaging technologies.

8.1.1 MEMS Packaging

The air cavity process has proven to be successful in packaging a capacitance resonator from this study as well as others from previous studies [9-11]. The addition of the POSS material provided a clean patterning method for the sacrificial material and a rigid overcoat. Molding conditions were then tested on empty cavities to test for collapse during chip packaging. This work provided insight to the mechanical structure of the

cavity and showed that such a process could potentially package a large variety of devices with different functions and sizes. However the results showed certain limitations in processing approaches. The ability to package large millimeter scale hermetic packages proved to be a very complex problem. The metalized cavities need to maintain smaller sizes, under 500 μm , for several reasons. The decomposition recipe used to prevent damage to the thin overcoat was set to decompose under 2 wt.%/min. This rate was sufficient for the decomposition products to diffuse out of the cavity and not cause pressure or damage to cavities up to 300 μm wide. However, larger cavities will need a slower decomposition rate (e.g. 1 wt.%/min.) due to the increased sacrificial material within the structure. This decreased rate will extend the thermal process to more than 8 hours which does not match commercial processes. A thicker overcoat film can help but may have undesirable film stress and additional processing.

When molding the metalized cavities, the adjustable parameters to prevent cavity collapse under pressure were the height of the cavity and the metal thickness. Since MEMS devices usually have mechanical components over most of the area under the package, traditional architectural support structures such as support beams and columns cannot be used in fabrication and requires the roof to be self-sustained. From the analytical bulge equation discussed in chapter 4, the half width of the cavity is scaled to the fourth causing the roof of large cavities becomes very sensitive to pressure.

$$P = \frac{2ht\sigma_0}{a^2} + \frac{4h^3Et}{3a^4(1-\nu^2)} \quad (4.1)$$

Changing the height of the cavity height and thickness are both required to account for the width's effect of the collapse. This is due to the height being the third power and the thickness to the first. For example, a 400 μm wide cavity's ideal requirements to prevent

collapse are a 15 μm tall cavity with a 20 μm copper overcoat. The increased height of the cavity makes uniform overcoat coverage of the cavity difficult causing defects at the edges. The metal choice is limited to copper due to higher modulus metals cracking with thick depositions which would result in a non-hermetic seal. The thickness causes high stress metal films with poor adhesion to the overcoat causing additional processing problems. Metal patterning with chemical etchant for the electrical connections tends to have poor results with the thick film as well. The novel in-situ decomposition/cure package was able to handle the larger cavities with fewer processing problems but cannot be metalized limiting certain devices. This shows the importance of proper design and mechanical testing of the air cavity for each type of MEMS device.

The testing of the package with regards to device operational requirements needs continuous investigation. The capacitance resonators used in this study had certain limitations and showed only a few working devices. The resonator could not be wafer-level tested before packaging and, required hermetic packaging. These devices could fail due to device fabrication, damaged devices, residue or device contact and/or lack of vacuum around the device. Since wafer-level testing, could not be completed, no determination could be made whether the mode of failure for a device was due to the package process or device fabrication. The working device yield due to packaging could not be determined for this reason. Once the wafer-level package was complete the devices had to be diced and wire bonded before testing. Since a few devices did work, it was concluded some cavities were able to hold a vacuum. However, due to device quality issues no long term or fatigue testing were done on these particular devices to see if the vacuum and device operation could be maintained. Long term testing will be

necessary to prove that a package can maintain its properties over the life time of the device.

The capacitance resonators were not designed for lead frame packaging and would have a poor signal output due to the long leads of the package. Therefore, empty cavity packages were substituted for the resonators when testing the chip level packaging. Since this was a novel testing of the air cavity in chip packaging, cavity collapse was the only tested failure. The chip level packaging will need to be tested for functioning devices as well as traditional package testing such as thermal shock, impact, and humidity testing. For future testing, piezoresonators would be an example of appropriate device for testing. These devices can be designed to be functional under fluid, air or vacuum with increasing quality depending on the density of the medium. This would allow package testing under both fluidic and hermetic systems. If degradation of the package would occur over time from hermetic to air, the quality factor of the device would drop but still operate. Devices could possibly be tested on the wafer-level allowing for package yield testing and optimization. The packages for these devices are of similar sizes to those tested and would be appropriate for lead frame packaging and testing of the hermitic and semi-hermetic types.

8.1.2 Packaging Materials and Processes

The study of the epoxy POSS film provided a rigid overcoat material for the air cavity and other microfabricated structures. The current material demonstrated POSS as a full film and not just an additive. However, there was little optimization of the POSS film. By using the epoxy POSS as the only cross-linked monomer, the mechanical

properties were optimized by maximizing silicon oxide content and cross link density. However, further work will be necessary to optimize it for other uses. One particular need is high-performance inorganic-based photosensitive dielectrics which can meet the packaging needs of future high-performance packages. In order for the POSS to be used in this application other properties will need to be further investigated and optimized. Investigation into the photolithography properties will improve the quality of patterning as well as introduce positive tone versions. Other properties such as the coefficient of thermal expansion and dielectric constant will need to be investigated and optimized as well. Once POSS films can be optimized for these properties they can easily be implemented into current packaging systems using organic dielectrics.

The temporary adhesives study demonstrated the use of polycarbonates for wafer-wafer bonding. These materials can be chosen based on chemical and thermal requirements to match the process of the device. This study investigated a general approach to the temporary adhesive problem. However, since each device process is unique; optimization and testing is necessary for each case. Another issue was the mechanically assisted release of the high temperature materials. This was due to the high temperature organic residue. The residue required a slight amount of force to separate the substrates as well as cleaning. Improvements to the synthesis and cleaning of the polycyclohexene carbonates can reduce this residue and make the material more viable for use as a temporary adhesive.

The electroless deposition of silver and copper was tested on silicon oxide and epoxy based substrates for packaging purposes. While the replacement of the palladium activation for silver proved useful, the adhesion testing on smooth surfaces is a difficult

problem. While some modest adhesion was present and successful for POSS and TSV applications, improvements must be made for commercial viability and board technology. As the source of the adhesion in electroless deposition is coming from these adhesive catalysts, the adhesion strength would be determined by the density of catalyst on the surface and the adhesion of each single catalyst to the substrate. Most of the research on surface catalyzing processes for improving the adhesion have been focused on the surface modification (control adhesion of each catalyst by changing interfacial energy) and optimization of bath formulation to obtain better adhesion and higher nucleation density. This includes the addition of surfactants, surface modification by chemical reaction or plasma treatment, and adsorption of adhesion promoters on the surface [89-91]. While mechanical roughening of the surface would improve adhesion this is undesirable. Further work will need to be conducted to improve chemical adhesion. The chromic etch of an RIE etched POSS surface was able to provide excellent copper adhesion. However it is unclear if the chromium plays a role in the adhesion or if it can be substituted with an environmentally friendly strong oxidizing solution. Since electroless deposition chemistry is very sensitive to changes, finding the correct bath chemistry can be challenging and require extensive work. Once working conditions are determined identifying the chemistry and physics behind that adhesion is vital for further advancement of the technology. Future work will look to optimize bath properties to improve adhesion of the Sn/Ag seeding to POSS and silicon dioxide for the electroless growth of metals on them.

8. 2 Summary and Conclusions

The scope of this work was to improve the air cavity technology for use in MEMS packaging applications. The air cavity process would allow a low cost packaging process for a wide range of MEMS devices. A novel tri-material system comprising of PPC/POSS/metal was used successfully fabricate air-cavities to package MEMS devices on the wafer-level. The sacrificial material was deposited in a manner to mask and planarize the topography of the MEMS device. The overcoat and decomposition recipe was optimized for a crack free overcoat after the decomposition. The air cavities are flexible in size and shape, mechanically robust, and debris-free. Nano-indentation was carried out to estimate the mechanical strength of the cavities. Further, a set of capacitive resonator devices were successfully packaged and characterized using this process.

Once an air cavity wafer-level package is completed the device can be packaged at the chip level using standard IC packaging processes. Compression/injection molding was carried out on cavities with different metal overcoats. Stronger and thicker metal overcoats offer better cavity-strength. Both FEM and analytical equations were able to predict the deformation behavior of the cavities under applied molding pressure. Metallized cavities up to 75 μm wide were able to withstand the transfer molding. A novel semi-hermetic package was created using an in-situ sacrificial decomposition/epoxy cure molding step for creating large cavity chip packages.

Through the optimization of the air cavity, new materials and processes were tested for general microfabrication. The epoxy POSS dielectric provides a resilient, strong inorganic/organic hybrid dielectric for use in microfabrication and packaging

applications. The POSS dielectric uses simple processing steps for film fabrication and exhibits adequate optical properties and photodefineability. Its thermal and chemical stability allow for a tough, durable overcoat. A high plasma etch selectivity compared to organic polymers was demonstrated. The POSS dielectric was used to create microchannels with its RIE patterning capabilities. The microchannels used POSS as a protective chemical barrier and as a mechanical overcoat.

Polycarbonates can be used for temporary adhesives in wafer-wafer bonding. This is a different application from their traditional sacrificial place holder in 3D structures but demonstrates similar processability. Polycarbonates were formulated for decomposition between 160°C and 270°C. Low temperature polycarbonates showed adequate adhesion, modest resistance to process chemistry, and a residue free release. High temperature polycarbonates showed similar adhesion, excellent chemical resistance, but slight adhesion due to residue upon release. The low cost temporary adhesives can be used for wafer thinning in MEMS, IC and solar cell devices.

An improved electroless deposition process for silver and copper was developed. The Sn/Pd activation was replaced by a cost efficient Sn/Ag catalyst. The process was shown to be able to deposit silver and copper on epoxy, POSS, and silicon dioxide. The films were adherent a roughened epoxy board, POSS coated surfaces, and silicon dioxide. Silver deposition on POSS showed poor adhesion, however, the adhesion of copper on smooth POSS was dramatically improved by the addition of an oxygen plasma clean and chromic acid etch. Electroless copper was demonstrated on untreated silicon oxide wafers for TSV sidewall deposition.

In summary, this work has led to the development and characterization of processes and materials to be used in MEMS packaging. The air cavity process showed significant promise as a versatile, cost efficient alternative to expensive, bulky wafer level MEMS packages. The air cavity process will allow MEMS devices to be packaged in a batch wafer process using photolithography processes. Several major issues facing the air cavity MEMS package have been investigated. First, a rigid POSS overcoat was investigated for improved cleanliness and mechanically rigid structures for the air cavity. Polycarbonates demonstrated adhesive properties for wafer thinning and handling. Metallization and mechanical studies allowed for the wafer-level package to be lead frame packaged using traditional IC packaging processes. These processes will continue to improve and reduce the cost for current and future MEMS packaging.

REFERENCES

1. Wu, X.Q. et al. (2003). "Fabrication of microchannels using polynorbornene photosensitive sacrificial materials." Journal of the Electrochemical Society, 150(9): p. H205-H213.
2. Jayachandran, J.P. et al. (2003). "Air-channel fabrication for microelectromechanical systems via sacrificial photosensitive polycarbonates." Journal of Microelectromechanical Systems, 12(2): p. 147-159.
3. Joseph, P.J. et al. (2005). "Improved fabrication of micro air-channels by incorporation of a structural barrier." Journal of Micromechanics and Microengineering, 15(1): p. 35-42.
4. Spencer, T.J. et al. (2007). "Air-gap transmission lines on organic substrates for low-loss interconnects." IEEE Transactions on Microwave Theory and Techniques, 55(9): p. 1919-1925.
5. Salas-Vernis, J.L. et al. (2004). "Hydrophobic/hydrophilic surface modification within buried air channels." Journal of Vacuum Science & Technology B, 22(3): p. 953-960.
6. Li, W.L. et al. (2003). "Sacrificial polymers for nanofluidic channels in biological applications." Nanotechnology, 14(6): p. 578-583.

7. Li, J. et al. (2006). "Microfabricated fuel cell with composite glass/Nafion proton exchange membrane." Journal of the Electrochemical Society, 153(2): p. A343-A347.
8. Kelleher, H. (2004). "Air-gaps via thermally decomposable polymers and their application to compliant wafer level packaging (CWLP), in chemical and biochemical engineering." Georgia Institute of Technology: Atlanta, Ga.
9. Joseph, P.J., et al. (2007). "Wafer-level packaging of micromechanical resonators." IEEE Transactions on Advanced Packaging, 30(1): p. 19-26.
10. Monajemi, P., et al. (2006). "Wafer-level MEMS packaging via thermally released metal-organic membranes." Journal of Micromechanics and Microengineering, 16(4): p. 742-750.
11. Rais-Zadch, M., et al. (2008). "MEMS switched tunable inductors." Journal of Microelectromechanical Systems, 17(1): p. 78-84.
12. (2008) "Global MEMS market forecast 2007 – 2012." I-Micronews.
13. Tummala, R.R. (2001). Fundamentals of Microsystems Packaging. New York: McGraw-Hill.

14. Tadigadapa, S. and K. Mateti. (2009). "Piezoelectric MEMS sensors: state-of-the-art and perspectives." Measurement Science & Technology, 20(9): p. 30.
15. McDonald, A.P.J. (July 2006) "MEMS resonators look to displace quartz resonators."
16. Madou, M. (1997). Fundamentals of Microfabrication. CRC Press.
17. Hsu, T.-R. (2008). MEMS and Microsystems: Design, Manufacture, and Nanoscale Engineering. Second ed. 2008, Hoboken, New Jersey: John Wiley and Sons.
18. Coulter, J.K., et al. (2008) Application of optimal and robust design methods to a MEMS accelerometer.
19. Ayazi, F. (2009). Integrated MEMS at Georgia Tech.
<http://www.ece.gatech.edu/research/integrated-mems/index.htm>.
20. Grace, R. (2010). Maher, M. A. Hearst Electronic Products,
http://www2.electronicproducts.com/PageSearch.aspx?FName=farc_sodtmems_nov2010.html.

21. Esashi, M., (2008). "Wafer level packaging of MEMS." Journal of Micromechanics and Microengineering, 18(7).
22. Fritz, N. et. al. (2011). "Lead frame packaging of MEMS devices using wafer-level, air-gap structures." NSTI-Nanotech 2011, 2, pp. 314-317.
23. Saha, R. et. al. (2010). "Three dimensional air-gap structures for MEMS packaging." Proceedings of the 2010 Electronic Components and Technology Conference, NV, pp. 811-815.
24. Gan, Z. et. al. (2009). "Getter free vacuum packaging for MEMS." Sensors and Actuators A: Physical, 149, pp. 159-164.
25. Monajemi, P. et. al. (2006). "Characterization of a polymer based MEMS packaging technique." 11th International Symposium on Advanced Packaging Materials: Processes, Properties and Interface, pp. 139-144.
26. Monajemi, P. et. al. (2005). "A low-cost wafer level MEMS packaging technology." IEEE International Conference on MEMS, pp. 634-637.
27. Rais-zadeh, M. et. al. (2007). "A Packaged micromachined switched tunable inductor." Proceedings of MEMS 2007, Japan, pp. 799-802.

28. Reed, H. A. et. al. (2003). "Compliant wafer level package (CWLP) with embedded air-gaps for Sea of Leads (SoL) Interconnections." Proceedings of the IEEE2001 International Interconnect Technology Conference, pp. 151-153.
29. Kopeliovich, D. (2011). "Methods of polymers fabrication." SubsTech Substances and Technologies.
<http://www.substech.com/dokuwiki/doku.php?id=polymers>.
30. (2009). International Technology Roadmap for Semiconductors, ITRS roadmap: packaging and assembly, 2009.
31. Wheeler, H. A. (1942). "Formulas for the skin effect." Proceeding of IRE, pp. 412-424.
32. Sawada, Y. et al. (2003). "Study of package warp behavior for high-performance flip-chip BGA." Microelectronics Reliability, 43, pp 465-471.
33. Tan, W. et al. (2010). "Effects of warpage on fatigue reliability of solder bumps: experimental and analytical studies." IEEE transactions on Advanced Packaging, 33, pp. 314-322.
34. Banerji, S. et al. (2005). "Warpage-induced lithographic limitations of FR-4 and the need for novel board materials for future microvia and global interconnect needs." IEEE transactions on Advanced Packaging, vol. 28, pp. 102-113.

35. Chen, S. et. al. (2008). "Copolymerization of carbon dioxide and epoxides with a novel effective Zn–Ni double-metal cyanide complex." Journal of Applied Polymer Science, 107, pp. 3871-3877.
36. Spencer, T.; Kohl, P. A. (2011). "Decomposition of poly(propylene carbonate) with UV sensitive iodonium salts." Polymer Degradation and Stability, 96, pp686–702.
37. Du, L. C. et. al. (2004). "Synthesis and degradation behavior of poly(propylenecarbonate) derived from carbon dioxide and propylene oxide." Journal of Applied Polymer Science, 92, pp. 1840-1846.
38. Spencer, T. et. al. (2011) "Stabilization of the thermal decomposition of poly(propylenecarbonate) through copper ion incorporation and use in self-patterning." Journal of Electronic Materials, 40(3), pp. 1350-1363.
39. Fritz, N. et. al. (2010). "Photodefinable epoxycyclohexyl polyhedral silsesquioxane," Journal of ElectronicMaterials, 39(2), pp. 149-156.
40. Bakir, M.S. et al. (2003). "Sea-of-leads (SoL) ultrahigh density wafer-level input/output interconnections for gigascale integration (GSI)." IEEE Transactions on Electron Devices, 50(10), pp 2039–2048.
41. http://www.defelsko.com/technotes/adhesion_methods.htm

42. Gere, J.M. (2006). Mechanics of Materials. sixth edition ed. Toronto: Thomson Learning.
43. Pourkamali, S. et. al. (2007). “Low-impedance VHF and UHF capacitive silicon bulk acoustic wave resonators- Part I: Concept and fabrication.” IEEE Transactions on Electron Devices, 54(8), pp. 2017-2023.
44. Pourkamali, S. et. al. (2007). “Low-impedance VHF and UHF capacitive silicon bulk acoustic-wave resonators—Part II: Measurement and characterization.” IEEE Transactions on Electron Devices, 54(8), pp. 2024-2030.
45. Vlassak, J and Nix, W. (1992). “A new bulge test technique for the determination of young modulus and Poisson ratio of thin-films.” Journal of Materials Research, 7(12), pp. 3242-3249.
46. Huang, R. et. al. (2010). “Stress, sheet resistance, and microstructure evolution of electroplated Cu films during self-annealing.” IEEE Transactions on Device and Materials Reliability, 10(1), pp. 47-54.
47. Choi, J. et al. (2003). “Organic/inorganic hybrid composites from cubic silsesquioxanes. Epoxy resins of octa(dimethylsiloxyethylcyclohexylepoxide) silsesquioxane.” Macromolecules, 36(15): p. 5666-5682.

48. Lin, H.M. et al. (2008). "Characterization of negative-type photoresists containing polyhedral oligomeric silsesquioxane methacrylate." Microelectronic Engineering, 85(7): p. 1624-1628.
49. Lin, E.K. et al. (1999). "Materials characterization of model epoxy-functionalized silsesquioxanes as potential underfill encapsulants." Advanced Packaging Materials: Processes, Properties and Interfaces.
50. Asuncion, M.Z. and R.M. Laine, (2007). "Silsesquioxane barrier materials." Macromolecules, 40(3): p. 555-562.
51. Palmieri, F. et al. (2006). "Multi-level step and flash imprint lithography for direct patterning of dielectrics." 2006: SPIE.
52. Hao, J. et al. (2007). "Photocurable silicon-based materials for imprinting lithography." 2007: SPIE.
53. Rajarathinam, V. et al. (2009). "Aqueous-develop, photosensitive polynorbornene dielectric: Properties and characterization." Journal of Electronic Materials, 38(6): p. 778-786.

54. Bai, Y.Q., et al. (2004). "Photosensitive polynorbornene based dielectric. II. Sensitivity and spatial resolution." Journal of Applied Polymer Science, 91(5): p. 3031-3039.
55. Bai, Y.Q., et al. (2004). "Photosensitive polynorbornene based dielectric. I. Structure-property relationships." Journal of Applied Polymer Science, 91(5): p. 3023-3030.
56. Helbert, J.N. (2001). Handbook of VLSI Microlithography - Principles, Technology and Applications. 2nd edition ed. William Andrew Publishing/Noyes.
57. Reinhardt, K.K. (2008). Werner, Handbook of Silicon Wafer Cleaning Technology. 2nd Edition ed. William Andrew Publishing.
58. Patel, K.S. et al. (2001). "Three-dimensional Dielectric Characterization of Polymer Films." Journal of Applied Polymer Science, 80, pp 2328–2334.
59. MicroChem Website (2008). http://www.microchem.com/products/pdf/SU-82000DataSheet2000_5thru2015Ver4.pdf.
60. Bhushan, B. (2004). Springer Handbook of Nanotechnology. Springer - Verlag.

61. Niklaus, F. (2006). "Adhesive wafer bonding." Journal of Applied Physics. 99, 031101, pp 1-28.
62. Pargfreider, S. et al. (2009). "3D integration with TSV: temporary bonding and debonding." Solid State Technology, March 2009. pp 38-43.
63. Puligadda, R. et al. (2007). "High-performance temporary adhesives for wafer bonding applications." Material Research Society Symposium Proceedings, 970.
64. Niklaus, F. et al. (2001). "Low-temperature full wafer adhesive bonding." Journal of Micromechanics and Microengineering. 11, pp 100-107.
65. Empower-Materials (2008). "Poly(alkylene carbonates) typical properties." http://www.empowermaterials.com/download/Technical%20Information/typical_properties.pdf.
66. Ree, M., et al. (1999). "A new copolymerization process leading to poly(propylene carbonate) with a highly enhanced yield from carbon dioxide and propylene oxide." Journal of Polymer Science: Part A Polymer Chemistry, 37, pp 1863-1876.

67. Jayachandran, J. et al. (2003). "Air-channel fabrication for microelectromechanical systems via sacrificial photosensitive polycarbonates." Journal of Microelectromechanical Systems, 12(2). 147-159.
68. Koning, C. et al. (2001). "Synthesis and physical characterization of poly(cyclohexane carbonate) synthesized from CO₂ and cyclohexene oxide." Polymer 42, pp3995-4004.
69. Gupta, M.G. et al. (2009). "Photoacid generators for catalytic decomposition of polycarbonate." Journal of Applied Polymer Science, 105, pp 2655–2662.
70. Siau, S. et al. (2004). "Influence of chemical pretreatment of epoxy polymers on the adhesion strength of electrochemically deposited Cu for use in electronic interconnections." Journal of the Electrochemical Society, 151(2). p. C133-C141.
71. Siau, S. et al. (2004) "Epoxy polymer surface roughness modeling based on kinetic studies of wet chemical treatments." Journal of the Electrochemical Society, 151(8). p. J54-J61.
72. Siau, S. et al. (2004). "Kinetic study of wet chemical treatments on the surface roughness of epoxy polymer layers for buildup layers - I. Sweller influence." Journal of the Electrochemical Society, 151(12). p. C816-C830.

73. Siau, S. et al. (2004). "Kinetic study of wet chemical treatments on the surface roughness of epoxy polymer layers for buildup layers - II. Oxidative treatment of the surface." Journal of the Electrochemical Society, 151(12). p. C831-C849.
74. Hayden, H. et al. (2009). "Adhesion enhancement between electroless copper and epoxy-based dielectrics." IEEE Transactions on Advanced Packaging, 32 (10), pp 758–767.
75. Cohen, R. L. et al. (1971). "Study of tin(II) sensitizer deposits on Kapton." Journal of the Electrochemical Society, 118, pp. 2042-2046.
76. Feldstein, N. et al. (1972). "Contact angle measurements of tin sensitizing solutions." Journal of the Electrochemical Society, 119, pp. 668-671.
77. Meek, R. L. (1975). "A Rutherford scattering study of catalyst systems for electroless Cu plating." Journal of the Electrochemical Society, 122, pp. 1478, 1481.
78. Feldstein, N. et al. (1972). "Some aspects of the chemistry of tin sensitizing solutions." Journal of the Electrochemical Society, 119, pp. 1486-1490.

79. Lan, J.-L. et al. (2008). "Mechanistic study of Ag/Pd-PVP nanoparticles and their functions as catalyst for electroless copper deposition." Journal of the Electrochemical Society, 155, pp. K77-K83.
80. Li, Y. et al. (2004). "Preparation of surface bound silver nanoparticles on polyimide by surface modification method and its application on electroless metal deposition." Applied Surface Science, 223, pp. 299-306.
81. Chen, D. et al. (2006). "Laser-induced site-selective silver seeding on polyimide for electroless copper plating." Applied Surface Science, 253, pp. 1573-1580.
82. Cha, S. H. et al. (2005). "The inhibition of silver agglomeration by gold activation in silver electroless plating." Journal of the Electrochemical Society, 152, pp. C388-C391.
83. Koura, N. (1990). "Electroless plating of silver." Electroless Plating: Fundamentals and Applications. pp. 441-461.
84. Laine-Ma, T. et al. (2009). "Electroless copper plating and surface characterization of thermoplastic PPO based printed circuit boards." Circuit World, 35(4), pp. 22-30.
85. (2011) "NMR-010: Proper cleaning procedures for NMR sample tubes." Wilmad-Labglass. http://www.wilmad-labglass.com/services/NMR_010.jsp

86. Rajarathinam, V. et al. (2011). "Imprint lithography enabling ultra-low loss coaxial interconnects." Microelectronics Engineering, 88, pp 240–246.
87. Dobrzynska, J. et al. (2011). "Polyimide foam-like microstructures: technology and mechanical properties." Journal of Micromechanics and Microengineering, 21.
88. Ostrowicki, G. et al. (2011). "Domed and released thin film construct - An approach for material characterization and compliant interconnects." IEEE Transactions on Device and Materials Reliability.
89. Kobayashi, Y. et al. (2001). "Deposition of silver nanoparticles on silica spheres by pretreatment steps in electroless plating." Chemistry of Materials, 13, pp. 1630-1633.
90. Esrom, H. et al. (2000). "Surface activation of polyimide with dielectric barrier discharge for electroless metal deposition." Surface and Coating Technology, 125, pp. 19-24.
91. Yang, G. H. et al. (2001). "Surface graft copolymerization of poly(tetrafluoroethylene) films with N-Containing vinyl monomers for the electroless plating of copper." Langmuir, 17, pp. 211-218.

